Biochemical and Biophysical Characterization of a Prephenate Dehydrogenase from the Hyperthermophilic Bacterium *Aquifex aeolicus*

Julie Bonvin

A Thesis

In

The Department

Of

Chemistry and Biochemistry

Presented in Partial Fulfillment of the Requirements

for the Degree of Doctor of Philosophy at

Concordia University

Montreal, Quebec, Canada

August 2008

Your file Votre référence
ISBN: 978-0-494-45651-4
Our file Notre référence
ISBN: 978-0-494-45651-4

Abstract

Biochemical and Biophysical Characterization of a Prephenate Dehydrogenase from the Hyperthermophilic Bacterium *Aquifex aeolicus*

Julie Bonvin, Ph. D.

Prephenate dehydrogenase is a key enzyme from the TyrA protein family responsible for catalyzing the NAD^+-dependent oxidative decarboxylation of prephenate to hydroxylphenylpyruvate, one of the terminal steps in the biosynthesis of tyrosine (Tyr). To gain structural and biophysical information on this protein, PD from the thermophilic bacterium *Aquifex aeolicus* was expressed as a His-tagged protein in *Escherichia coli* and was purified by nickel affinity chromatography. The enzyme is susceptible to proteolysis at the N-terminal region of the protein and the exact site of cleavage was determined by mass spectrometry. Crystallography trials on several N-terminally truncated variants performed by our collaborators at the University of Toronto indicated that only the PD variant missing the first 19 amino acids (Δ19PD) yielded quality diffraction crystals. The biochemical and biophysical properties of the full-length PD were compared to Δ19PD also expressed recombinantly in *E. coli*. The enzyme functions as a cyclohexadienyl dehydrogenase, accepting prephenate (effectively) and L-arogenate (poorly) as substrates. Both forms of the enzyme are thermally stable and show maximal activity only at high temperatures, although Δ19PD is less stable but more active than the full-length protein. Low concentrations of the denaturant guanidinium hydrochloride (Gdn-HCl) activate the activity of Δ19PD, but at higher concentrations activity is lost concomitant with a multi-state pathway of denaturation which proceeds

through unfolding of the dimer, oligomerization, then unfolding of monomers. Measurements of steady-state fluorescence intensity and its quenching by acrylamide in the presence of Gdn-HCl suggest that of the two tryptophan (Trp) residues per monomer, one is buried in a hydrophobic pocket and does not become solvent exposed until the protein unfolds, while the less buried Trp is at the active site. These findings are in accordance with the crystal structure of Δ19PD.

Site-directed mutagenesis and steady-state kinetic analyses of variant proteins were used to probe the roles of conserved residues. In accord with the crystal structure of the enzyme bound with NAD^+ plus product and product analogues, His147 acted as a catalytic hydrogen bond acceptor while Ser216 was responsible for coordinating NAD^+ and His147 to facilitate hydride transfer. Arg250 and His217 were responsible for binding prephenate in the active site. Additionally and most importantly, His217 in *A. aeolicus* PD and the homologous residue in *E. coli* CM-PD (His257) was shown to be critical for inhibition of activity by Tyr. Two assays were developed to assess Tyr binding to wild-type and variant enzymes. Our results are placed in context of crystal structures of PD bound with Tyr and indicate how TyrA proteins can accept hydroxyphenylpuruvate and Tyr in the active site of the enzyme.

Acknowledgements

First, I would like to thank my thesis supervisor, Dr. Joanne Turnbull (Jojo), for her dedication to my training, her support and patience throughout all these years. I also want to thank her for always pushing me, sometimes really hard, to meet her high scientific standards, which I hope to adhere in my future scientific career. I thank the members of my Research Committee, Drs. M.J. Kornblatt and P. Joyce, for their help and suggestions during my Ph. D. studies. I want to thank all the members of the Turnbull's lab encountered during these years and a lot of other graduate students from our department and from other departments (Zack, Michaela, Steve, Maggy, Cathy, Ernesto, Jason...). A special thank to John (mon petit bazo), who was first a classmate, then a colleague and who finally became an exceptional friend. He was always present when I needed him, and I'm sure always will. I sincerely want to acknowledge the never-ending presence and the incredible laziness of Mushu, my loved cat, who spent my entire Ph. D. laying down on the myriad of publications spread on my floor. He probably became the most intelligent cat, but he is so humble that he does not show it; we should all think about it. Special thanks for my friends from France (Anne, Van (la vieille), Dam and Yo) who had the patience to wait for me to come back, after all those years. To You, "Pouet-Pouet", my love, who left this life a little bit too early. Finally, I want to thank all my family: Alexandre, Dany et Guy, for their love, support and encouragement.

Table of Contents

List of Figures

List of Tables

List of Abbreviations

Å	angstroms
ACN	acetonitrile
AD	arogenate dehydrogenase
ADT	arogenate dehydratase
ANS	1-anilino-8-naphthalene sulfonic acid
AUC	analytical ultracentrifugation
CD	circular dichroism
CM	chorismate mutase
CM-PD	chorismate mutase–prephenate dehydrogenase
CM-PDT	chorismate mutase–prephenate dehydratase
Da	Dalton
DEPC	diethylpyrocarbonate
DMSO	dimethyl sulfoxide
DNA	deoxyribonucleic acid
DSC	differential scanning calorimetry
DTT	dithiothreitol
EDTA	ethylenediamine tetra-acetic acid
ESI	electrospray ionization
FA	formic acid
FPLC	fast protein liquid chromatography
FT	Fourier transform

Gdn-HCl	guanidinium hydrochloride
H-bond	hydrogen bond
HCCA	α-cyano-4-hydroxycinnamic acid
HEPES	4-(2-hydroxyethyl)-1-piperazineethanesulfonic acid
HPLC	high performance liquid chromatography
HPP	(4-hydroxyphenyl)pyruvate
HPpropionate	4-hydroxyphenyl propionate
IMAC	immobilized metal affinity chromatography
IPTG	isopropyl-β-D-thiogalactopyranoside
IR	infrared
KdsA	3-deoxy-D-*manno*-octulosonic acid 8-phosphate synthase
LB	Luria broth
MALDI	matrix-assisted laser desorption ionization
MS	mass spectrometry
MW	molecular weight
$NAD(P)^+$	oxidized form of nicotinamide adenine dinucleotide (phosphate)
NAD(P)H	reduced form of nicotinamide adenine dinucleotide (phosphate)
NATA	N-Acetyl-L-tryptophanamide
NAYA	N-acetyl-L-tyrosinamide
NMR	nuclear magnetic resonance
NTA	nitrolotriacetic acid
PAGE	polyacrylamide gel electrophoresis
PCR	polymerase chain reaction

PD	prephenate dehydrogenase
PDT	prephenate dehydratase
PMSF	phenylmethylsulfonyl fluoride
PRE	prephenate
TCEP	tri(2-carboxyethyl)phosphine hydrochloride
TFA	trifluoroacetic acid
Tris	tris(hydroxymethyl)aminomethane
SDS	sodium dodecylsulfate
U	units
UV	ultra violet
VT	variable temperature

Contributions of Authors

Most of the work presented in Chapters 2 and 3 are published in *Protein Science* (J. Bonvin, R. Aponte, M. Marcantonio, S. Singh, D. Christendat and J.L. Turnbull, 2006, 15:1417-1432, sup. mat.1-4) or have been recently submitted to the *Journal of Biological Chemistry* (W. Sun, D. Shahinas, J. Bonvin, W. Hou, J. Turnbull and D. Christendat). Chapter 2 constitutes my experimental input to the publication in *Protein Science*. I performed all the experiments, helped write the paper and reformatted its contents to highlight my contributions. R. Aponte worked out a purification scheme for the full-length *A. aeolicus* PD enzyme, examined its thermal stability and supplied the preliminary kinetic parameters of the enzyme at one temperature. M. Marcantonio, honours undergraduate student, conducted the first CD experiments on Δ19PD. I repeated the work and incorporated any additional unpublished findings into Chapter 2. Chapter 3 constitutes my experimental input to a manuscript that has been submitted to *JBC*. However, plasmid DNA for Δ19PD WT, His147Asn, Glu153Ala, Ser126Ala, Asp247Ala was supplied by W. Sun while W. Hou supplied the plasmid DNA for R250Q and H217N and the kinetic values for the R250Q variant. All of the crystallographic work (including interpretation) was contributed by the Christendat lab; J. Turnbull helped with the interpretation. I wrote this chapter. For Chapter 4, J. Manioudakis supplied the His257Ala protein and kinetic parameters of the enzyme. T. Lee performed initial Tyr inhibition studies on His247Ala. I repeated these experiments and performed all other experiments in the chapter, provided interpretation of the data and wrote the chapter (manuscript in preparation).

Chapter 1

General Introduction

1.0 AROMATIC AMINO ACID BIOSYNTHESIS

The aromatic amino acids, L-tyrosine (Tyr), L-tryptophan (Trp) and L-phenylalanine (Phe) are of critical importance for the growth and maintenance of all living organisms. These amino acids act both as products and precursors. In the former case, they can be used for protein synthesis, whereas in the latter case, they can be substrates for enzymes in the downstream pathways. They also produce aromatic metabolites which are involved in primary biological processes, making them indispensable for survival. This includes compounds such as flavonoids (*1*), quinones (*2, 3*), cyanogenic glycosides (*4*) and alkaloids (*5, 6*). In archae, eubacteria, plants and fungi, the three aromatic amino acids are synthesized *via* the shikimate pathway. This pathway, which links the metabolism of carbohydrates to the biosynthesis of aromatic compounds, was elucidated mainly through the work of Davis (*7*) and Sprinson (*8*). It encompasses seven metabolic steps initiated by the condensation of erythrose-4-phosphate and phosphoenol-pyruvate to give a 7-carbon compound, 3-deoxy-D-*arabino*-heptulosonate 7-phosphate (DAHP) (Fig. 1.1). This step is catalyzed by the highly regulated 3-deoxy-D-*arabino*-heptulosonate 7-phosphate synthases (DAHP synthases) of which there are three isoenzyme forms: DAHP synthase (Phe), (Trp) and (Tyr) (*9, 10*). Each form is classified according to the amino acid which serves as a feedback inhibitor. The pathway ends with the synthesis of the branch point intermediate of the pathway, chorismate, which serves in turn not only as a precursor for the biosynthesis of the three aromatic amino acids, but also a number of other aromatic compounds such as vitamins, quinones or folates (*11, 12*).

Figure 1.1: The shikimate pathway. The shikimate pathway consists of seven enzyme-catalyzed steps. Metabolites symbols: DHAP, 3-deoxy-D-*arabino*-heptulosonate 7-phosphate; DHQ, 3-dehydroquinate; SH, shikimate; EPSP, 5-enolpyruvateshikimate 3-phosphate and CHO, chorismate.

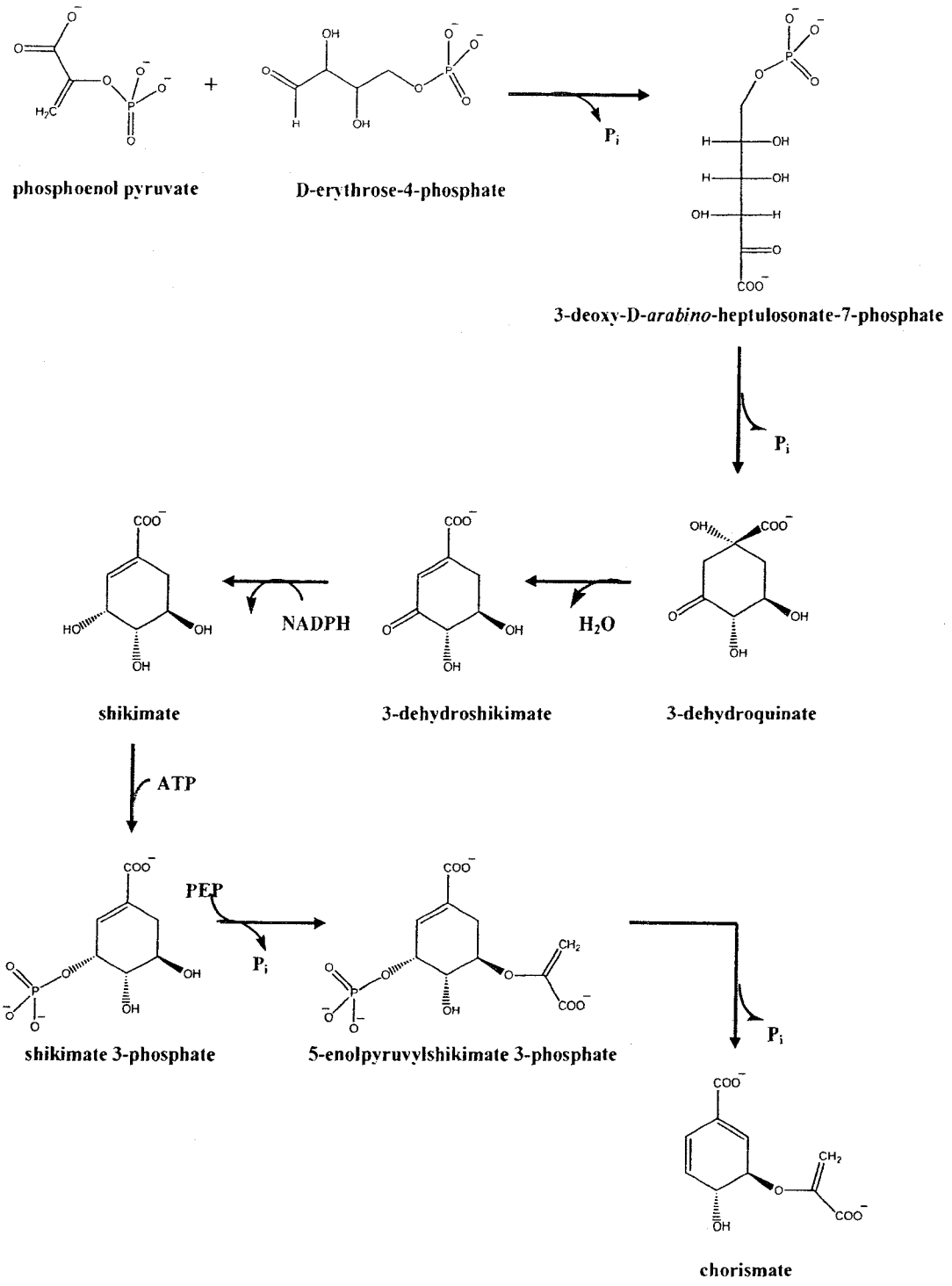
phosphoenol pyruvate
D-erythrose-4-phosphate
P_i
3-deoxy-D-*arabino*-heptulosonate-7-phosphate
P_i
shikimate
NADPH
3-dehydroshikimate
H_2O
3-dehydroquinate
ATP
shikimate 3-phosphate
PEP
P_i
5-enolpyruvylshikimate 3-phosphate
P_i
chorismate

Chorismate is then converted to L-Tyr or L-Phe via the "common pathway" (Fig. 1.2). In this pathway, chorismate undergoes a Claisen rearrangement to prephenate, catalyzed by chorismate mutase (CM), then prephenate is either oxidatively decarboxylated by the NAD^+-dependent prephenate dehydrogenase (PD) to form *p*-hydroxyphenylpyruvate (HPP) or is dehydrated and decarboxylated by prephenate dehydratase (PDT) to phenylpyruvate (PP). These aromatic precursors are then transaminated appropriately to either L-Tyr or L- Phe. The biosynthesis of the third amino acid, L-Trp, also originates from chorismate but involves six steps from a separate pathway (Fig. 1.3). The first two and last two reactions are catalyzed by enzyme complexes, namely the anthranilate synthase-phosphoribosyl transferase complex and the tryptophan synthase complex, respectively.

Both the shikimate and the "common" pathways are not present in mammals, consequently, these enzymes are attractive targets for the design of inhibitors which can act as herbicides, fungicides and antimicrobial agents (*13, 14*). One of the best known examples is the herbicide, glyphosate (Roundup®), which inhibits 5-*enol*pyruvyl shikimate 3-phosphate synthase (*15*). Moreover, these enzymes are well recognized in bioengineering as targets for aromatic amino acid and secondary metabolites production (*16*). The use of metabolic engineering to produce Phe and Trp has gained considerable attention due to the commercial value of these aromatic amino acids (and their synthetic intermediates) in the food, pharmaceutical and agricultural industries. For example, the Trp biosynthetic pathway has been exploited in *E. coli* for the production of aromatic compounds such as bio-indigo (*17, 18*) and shikimic acid (*19*); Trp is also used as

Supprimé : <sp><sp>

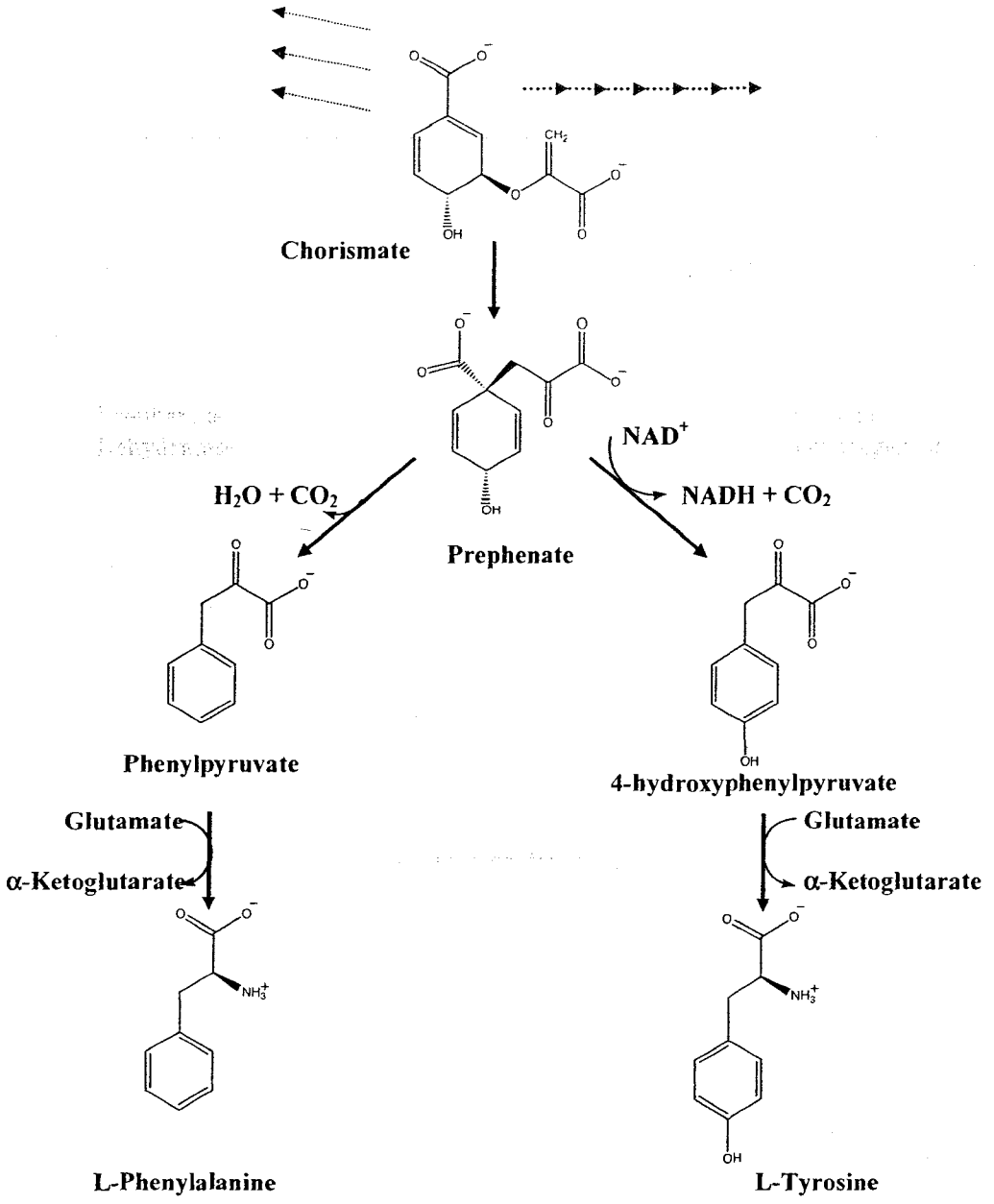

Figure 1.2: Aromatic amino acid biosynthesis in *E. coli via* the "common pathway".

Intermediates are shown in black and enzyme in grey.

Figure 1.3: Tryptophan biosynthesis. The pathway consists of six enzyme-catalyzed steps. **1**, anthranilate synthase, **2**, anthranilate phosphoribosyltransferase, **3**, phosphoribosylanthranilate isomerase, **4**, indole-3-glycerol-phosphate synthase, **5-6**, tryptophan synthase enzyme complex. PRPP: 5-phosphoribosyl-α-pyrophosphate

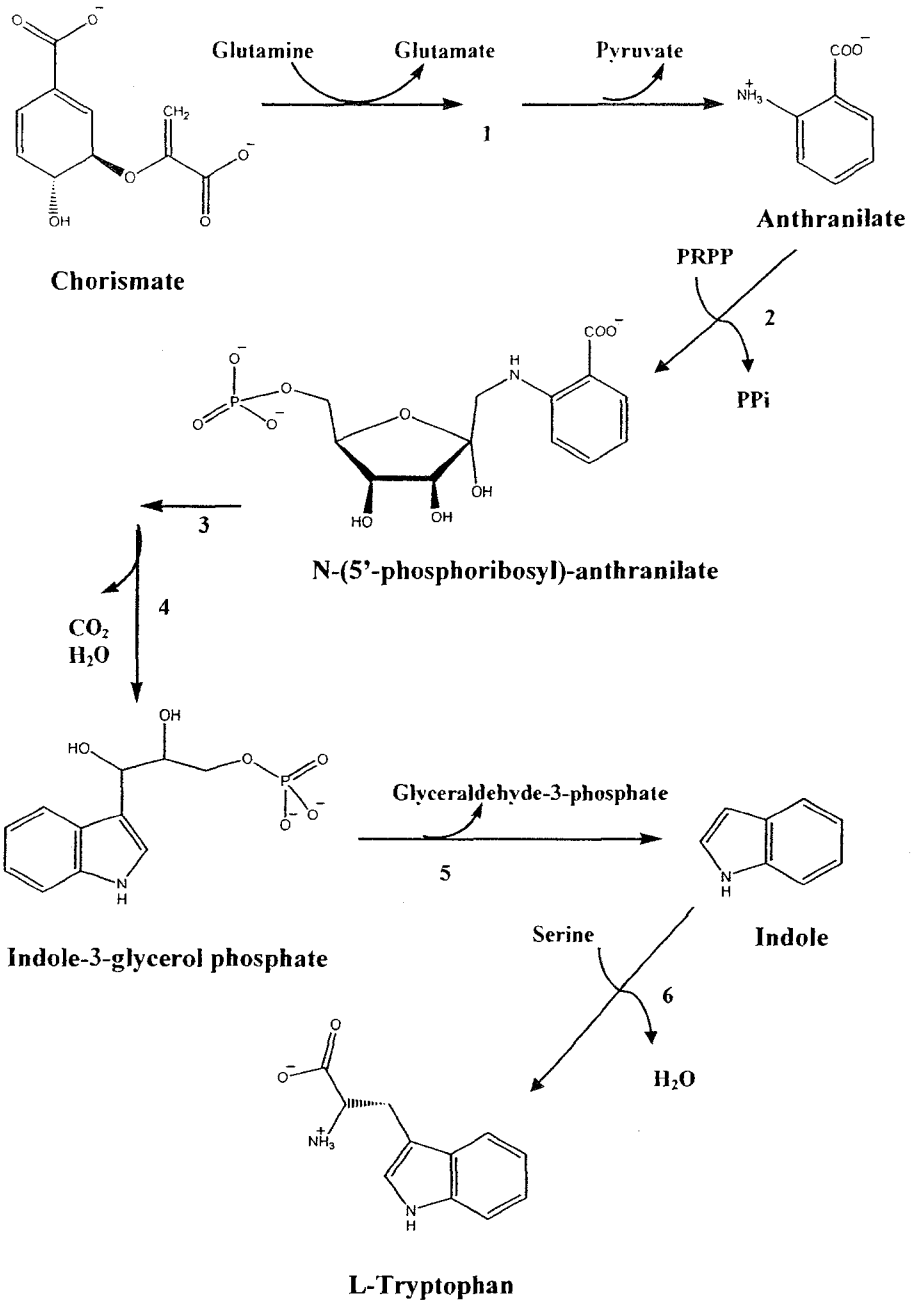
Glutamine
Glutamate
Pyruvate
1
Anthranilate
Chorismate
PRPP
2
PPi
3
N-(5'-phosphoribosyl)-anthranilate
4
CO_2
H_2O
Indole-3-glycerol phosphate
Glyceraldehyde-3-phosphate
5
Indole
Serine
6
H_2O
L-Tryptophan

an animal feed. Similarly, Phe is one of the major constituents of the sweetner aspartame, also known as NutraSweet® (*20*). In the past, Tyr was supplied mainly by chemical synthesis and protein hydrolysis since only small volume applications were required. More recently however, Tyr has been identified as a valuable precursor in the synthesis of melanin (*21*), anti-Parkinson's drugs L-dopa (*22, 23*) and 3,4-dihydroxyphenyl-L-alanine (*19*) and biodegradable polymers (*24*). In order to support the demands for large scale production of Tyr and intermediates in the common pathway, strategies to manipulate its biosynthetic route are now being explored (*25, 26*). Hence, there is considerable interest in understanding the catalytic mechanism and modes of regulation of aromatic amino acid-producing enzymes in a number of organisms.

The aromatic amino acid biosynthesis pathway is regulated at both the genetic and protein level. Many of the genes encoding the biosynthetic enzymes for aromatic amino acids are organized in operons. The operons are regulated by three regulatory genes *tyrR*, *trpR* or *pheR*. The protein products of these genes combine with the appropriate amino acid co-repressor, resulting in the formation of complexes that bind at the operator loci. Additional regulation is achieved through attenuation at the level of charged tRNA(s) (*27*), although, the major form of control is achieved through feedback inhibition by Phe, Tyr or Trp of enzymes at the start (DHAP synthase) and at the branch point in the biosynthetic pathways leading to these products. Interestingly, bacterial enzymes are controlled mainly by feedback inhibition while in higher plants regulation occurs at the genetic level and physiological feedback inhibition is absent (*28*). Accordingly, research efforts are now being directed towards engineering strains of organisms that lack *tyr*R and/or are resistant to feedback inhibition in order to modulate Tyr production (*29*).

1.1 ALTERNATE BIOSYNTHETIC ROUTES TO TYROSINE AND PHENYLALANINE

We have outlined previously how L-Tyr and L-Phe can be synthesized from HPP and PP, respectively (Fig. 1.2). However, an alternate pathway to Tyr and Phe production exists that utilizes L-arogenate as an intermediate (Fig. 1.4). L-arogenate possesses many of the same structural features as prephenate but it is a cyclohexadienyl amino acid: an alanyl group replaces the pyruvyl side chain at C-1. In the arogenate route, prephenate is first transaminated into L-arogenate which then is converted to L-Tyr or L-Phe by arogenate dehydrogenase (AD) or arogenate dehydratase (ADT). The arogenate pathway was discovered in cyanobacteria by Stenmark *et al.*(*30*) about 40 years ago. While kinetic assays failed to reveal prephenate dehydrogenase activity (*30*), they noted the consumption of an amino acid in addition to prephenate. This finding signified that transamination could occur prior to decarboxylation. Stenmark and coworkers then went on to isolate the novel dehydrogenase and named the aromatic compound pretyrosine. Only when it was discovered that pretyrosine could be a precursor of L-Phe was it renamed L-arogenate (*31*).

The ubiquitous combination of the two routes, the HPP/PP and the arogenate routes, results in widespread diversity in the biosynthesis of Tyr and Phe. In most plants and some bacteria (ie. cyanobacteria) both Tyr and Phe are synthesized using the arogenate pathway, while in *E. coli* and yeast, this pathway is reportedly absent (*32-36*). In cyanobacteria and several other microorganisms such as *Brevibacterium flavum*, the arogenate pathway is used to produce Tyr while Phe is synthesized from PP (*35, 37*).

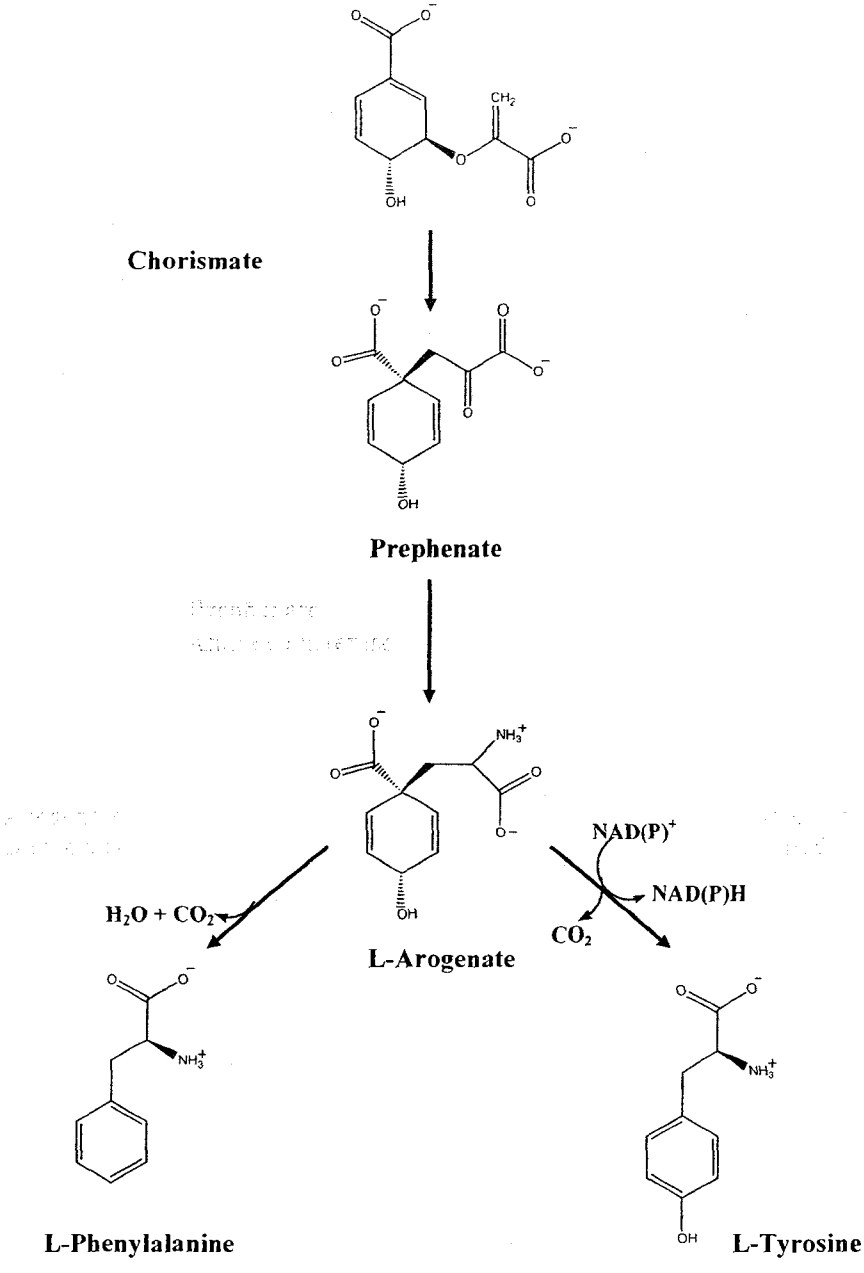

Figure 1.4: L-tyrosine and L-phenylalanine biosynthesis *via* the arogenate route

In other bacterial species, such as *Zymomonas mobilis* and *Pseudomonas aeruginosa*, the HPP and L-arogenate routes coexist (*38, 39*). Distinct enzyme combinations allow for considerable regulatory control over the type and amount of end products that accumulate in a pathway. For example in plants, arogenate is the sole branch point for the biosynthesis of Tyr and Phe, hence ADs must be "accurately" regulated to balance the flux of intermediates between these aromatic end products. Phe and its myriad of secondary metabolites are of great importance for plant survival. When required, 30% of the carbon fixed during photosynthesis is shunted to Phe for the synthesis of phenylpropanoids such as lignins, hydroxycinnamic amides, flavonoid phytoalexins, and pigments; much less carbon is incorporated into the production of Tyr. AD in plants is very sensitive to feed feedback inhibition by Tyr (*40, 41*) whereas ADT is stimulated by Tyr (*42*). In contrast, in *Synechocystis* where Tyr is synthesized by the arogenate route, AD is not at a branch point since Phe is synthesized via the PP route (*32-35*). Accordingly, AD from this organism is reported to be less sensitive to Tyr (*43*).

1.2 TYRA PROTEIN FAMILY

The TyrA protein family is dedicated to Tyr biosynthesis and consists of homologous dehydrogenases that are classified into three categories depending upon their specificities for the cyclohexadienyl substrate; prephenate dehydrogenases are specific for prephenate, arogenate dehydrogenases (AD) for L-arogenate and cyclohexadienyl dehydrogenases can accept both substrates. In addition to their specificity for the cyclohexadienyl substrate, these dehydrogenases may be specific for NAD^+ or $NADP^+$ or may use both (*36*). Absolute specificity for prephenate tends to be accompanied by

absolute specificity for NAD^+ and the reverse relationship is also observed, whereby absolute specificity for L-arogenate is usually accompanied by absolute specificity for $NADP^+$ (*44, 45*).

In all three domains of life, these proteins catalyze an irreversible oxidative step in Tyr biosynthesis. They share a catalytic core region of about 30 kDa and maintain a common scaffold of fundamental reaction chemistry (*46*). Many exist as monofunctional enzymes, but some are linked to other enzymes or fused to regulatory domain(s). To cite several examples, TyrA from *Z. mobilis*, *N. gonorrhoeae* or *Synechocystis* sp. are structurally the simplest proteins belonging to the TyrA family; they contain only a core catalytic domain (*36*). Interestingly, TyrA from *Z. mobilis* is insensitive to feedback inhibition. In the enteric lineage (ie. *E. coli*, *H. influenza*, *P. agglomerans*) however, *tyrA* is fused with *aroQ* (encoding chorismate mutase). Additionally, the *aroF* gene encoding enolpyruvylshikimate-3-P synthase is fused to *tyrA* in at least two clades of *Bacteria* such as *Ps. stutzeri*, *P. aeruginosa* and *Burkholderia pseudomallei*. Song *et al.* reported that in a single organism, *Rhodobacter sphaeroides*, *tyrA* is fused to $hisH_b$ which encodes an aromatic aminotransferase (*47*). Other examples are cited by Sun *et al.* (*48*). Another type of fusion partner found in several other organisms are regulatory domains. For example, the well-characterized TyrA from *B. subtilis* possesses a carboxy-terminal fusion domain denoted ATC, after the first letters of three of the proteins possessing this domain (Aspartate kinase-Chorismate mutase-TyrA), which is capable of binding small regulatory molecules. In *Archaea*, a putative regulatory domain, REG, has been identified (*47*).

The TyrA protein family has been extensively studied in a phylogenetic/bioinformatics context (two excellent review has been very recently published by Jensen and co-workers (*36, 45*)). While enzymes from a variety or organisms have been (tentatively) classified in terms of their substrate specificity and mode of regulation through *in silico* analyses, only a few TyrA proteins have been purified and characterized. These include arogenate dehydrogenases from *Synechocystis* sp. (*36*) and *A. thaliana* (*40, 49*), two cyclohexadienyl dehydrogenases (from *Z. mobilis* and *Ps. stutzeri*) and the genetically engineered monofunctional PDs from *E. coli* (*50*) and *E. herbicola* (*51*). Extensive biochemical and biophysical studies have been conducted only on the bifunctional *E. coli* enzyme CM-PD (*52, 53*) however, the findings of which have provided valuable insight into the catalytic mechanism of the PD enzyme.

1.3 THE BIFUNCTIONAL *E. COLI* ENZYME, CM-PD: THE STRUCTURAL RELATIONSHIP BETWEEN THE TWO ACTIVITIES

In *E. coli* the pathway for Tyr biosynthesis involves two sequential reactions catalyzed by the bifunctional enzyme chorismate mutase-prephenate dehydrogenase (CM-PD) (*54, 55*) known as the T-protein. L-Tyr, the end product of the pathway is a feedback inhibitor of both the mutase and dehydrogenase activities (*54*).

Solution studies indicate that the *E. coli* enzyme is homodimeric with a molecular weight of about 84 kDa (*56, 57*). The enzyme is considered bifunctional however, since both activities are associated with each of the polypeptide chains. Primary sequence alignment of CM-PD with the bifunctional enzyme CM-PDT leading to L-Phe indicates that of the 373 residues per monomer, the N-terminal 100 residues encode the mutase

domain while the remaining 273 residues are responsible for the dehydrogenase activity (*58*). The structural organization of the sites which catalyze the two activities within the bifunctional enzyme has not been firmly established.

Evidence supporting a unique site combining both activities comes from studies on the enzyme from *Aerobacter aerogenes* and *E. coli*. Subjecting the enzyme to a variety of treatments such as urea, heat, extreme pH, limited proteolysis (*59, 60*) or cysteine-modifying agents (*56, 61*) has led to the coordinate loss of both activities. Furthermore, inactivation by alkylation of both activities was prevented by prephenate, $NAD^{\pm}$, and NAD^{+} plus L-Tyr (*56, 61*). Further evidence stems from the results of studies of the inhibition of both activities with compounds that are clearly analogues of either chorismate or prephenate; these analogues bound with equal affinity to inhibit both CM and PD activities (*62*). Additionally, prephenate binds with similar affinity to the enzyme when acting as a substrate of the dehydrogenase reaction or as an inhibitor of the mutase reaction (*59*). Lastly, kinetic studies show that the two reactions are catalyzed with comparable turnover number (*63*).

There is also evidence in favor of two distinct sites or of specific residues involved in catalyzing each of the two reactions. The two enzymes display markedly different pH rate profiles (*64*) and both activities are inhibited to different degrees by L-Tyr (*56, 65*) and by the dicarboxylic acid malonic acid and several of its derivatives (*56*). Additionally, site-specific inhibitory compounds have been identified. A putative transition-state analog (*endo*-oxabicyclic diacid) of CM has been shown to competitively inhibit the mutase reaction without affecting dehydrogenase activity (*56*), while *trans*-2,3-pleiadanedicarboxylic acid reportedly inhibited PD without impairing the mutase

activity (*66*). This hypothesis has been supported by Christendat and Turnbull (*67*) whose peptide mass mapping experiments revealed the selective modification of mutase or dehydrogenase residues. Additionally, they demonstrated through site-directed mutagenesis studies that an amino acid substitution introduced in the CM domain (Lys37Gln) could totally eliminate mutase activity without affecting the dehydrogenase activity (*52*). Similarly, substitutions in the PD portion of the enzyme abolished only dehydrogenase activity (His197Asn) (*52*) or prephenate binding (Arg294Asn) (*53*).

Kinetic evidence also supports the idea that if the enzyme possesses two active sites, they must be in close proximity or in some way structurally dependent. Results of the inhibition of the enzyme by malonate or citrate by Christopherson (*62*) indicated that the binding of either analogue with prephenate was mutually exclusive but that malonate (or citrate) and chorismate could be on the enzyme at the same time, thus suggestive of overlapping active sites. Some prephenate from chorismate is converted directly to HPP, as would be expected if prephenate was channeled from one active site to the other (*68*). Lastly, further mutagenesis studies in the Turnbull lab have identified protein variants whose single substitutions (Lys178Arg, His189Asn, Cys215Ala, Arg286Ala) impaired both CM and PD activities (*52, 67*).

There have been efforts to separate the activities of the T-protein into discrete monofunctional domains. Jensen and coworkers initially reported the successful expression of a PD derived from *E. herbicola* CM-PD, but only when a large portion of the mutase domain remained intact (*69*). More recent work by Ganem and colleagues (*50*) and by our lab (Bonvin, unpublished data) showed that independently expressed CM and PD domains of the *E. coli* enzyme have reduced activity and are highly unstable or

insoluble, highlighting the structural interrelationship of the different regions of the polypeptide chain. In contrast, the related bifunctional enzyme CM-PDT involved in Phe biosynthesis, has been shown to possess two distinct non-interacting catalytic sites (*70-72*) and a separate inhibitory Phe binding domain (the ATC domain) at the C-terminal portion of each polypeptide (*73*). All of these domains found within CM-PDT can be separately expressed and are fully functional (*70, 74*). Additionally, Zhang et *al.* genetically linked the genes encoding the CM and Phe binding domains (*75*). Kinetic analysis of the fusion protein showed that Phe activated CM activity (although did not inhibit as expected), indicating nevertheless that allosteric control could be transmitted through the domain contacts.

1.4 CHORISMATE MUTASE MECHANISM

CM catalyzes the only pericyclic Claisen rearrangement reaction reported in nature (*76*). While the reaction can occur in the absence of the enzyme, the mutase accelerates the reaction by over a million-fold (*77, 78*) Both the uncatalyzed (*79, 80*) and enzyme catalyzed rearrangements (*77, 81, 82*) are thought to proceed via a chair-like transition state following selection of chorismate's less stable diaxial form.

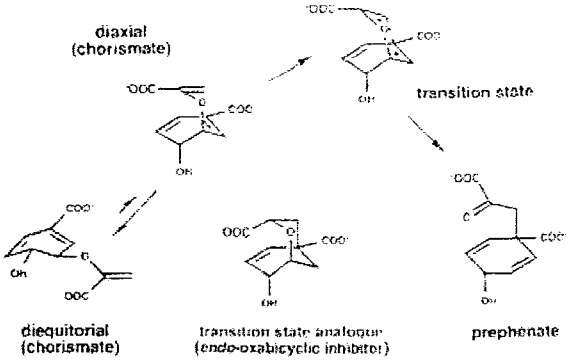

Figure 1.5: Rearrangement of chorismate through a transition-state complex. Adapted from Christendat *et al.* (*67*). Proton NMR studies indicate that 10 to 20% of chorismate is found in the diaxial conformer in equilibrium with the more stable diequatorial form.

Numerous isotope effect studies have been performed, which show that in the non-enzymatic reaction, bond-breaking precedes bond-making (*83*) although in the presence of CM, it was hypothesized that a conformational change might initiate the chemical rearrangement. While several chorismate analogues have been synthesized to delineate the structural features required for catalysis (*84*), an *endo*-oxabicyclic diacid inhibitor (*85*), with its bridged ether oxygen and *endo* conformation of the bridged carboxylate, appears to mimic the bicyclic structure of the transition state most effectively; the analogue binds about 300 times more tightly to the *E. coli* enzyme than chorismate (*56*).

Several natural monofunctional CMs have been crystallized such as those of *B. subtilis* (*79*), *S. cervisiae* (*86*), *T. thermophilus* (*87*), *C. thermocellum* (*88*), *M.*

tuberculosis (*89*), as well as the engineered mutase domain of the bifunctional *E. coli* CM-PDT (*72*), the "mini-mutase", complexed with the mutase transition-state analogue. CMs generally belong to one of two structurally distinct classes denoted AroH and AroQ (see Fig. 1.6). The less abundant AroH class comprises mainly trimeric α/β proteins while the protein scaffold of the more abundant AroQ class, which is adopted by the *E. coli* "mini-mutase" (*72*), is mainly α-helical and dimeric. The dimeric yeast CM is larger and more elaborate than *E. coli* CM, and contains a regulatory domain where allosteric effectors can bind (*86*). In both classes an active site is shared at the subunit interfaces. With expection, the dimeric *M. tuberculosis* CM is part of the AroQ protein family that exhibits a novel fold topology and houses a separate active site within each of the monomers (*89*). Interestingly, alignment of the primary sequences of all five mutases shows little similarity and their crystal structures reveal that they adopt unique folds, however the electronic environment and the geometry of the active site appears well conserved.

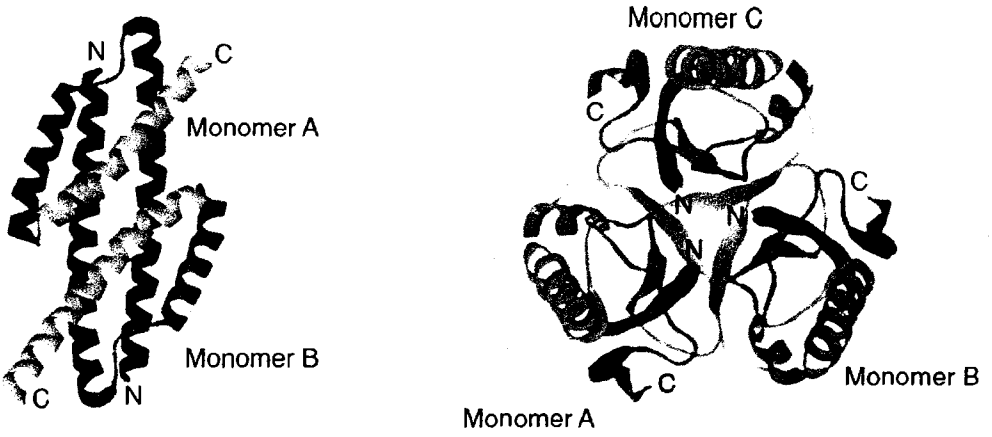

Figure 1.6: Ribbon diagram representations of the AroQ and AroH folds. The AroQ class (left) is completely helical and includes CMs from *E. coli* and *S. cerevisiae* The AroH class (right) is organized as a trimeric α/β-barrel fold; *B. subtilis* and C. *thermocellum* CMs are representative of this class.

The structures of CM from the *B. subtilis* (*90*), *S. cerevisiae* (*76*) and the *E. coli* "mini-mutase" (*72*) enzymes, in complex with *endo*-oxabicyclic acid, have provided the template for the design of extensive mutagenesis experiments, through site-directed approaches (*91, 92*) and by directed evolution (*93*). The results of mutagenesis in combination with the structural data revealed the importance of the active groups Lys39 and Gln88 in stabilizing the ether oxygen and of Lys39 and Arg11' in positioning the C-11 carboxylate

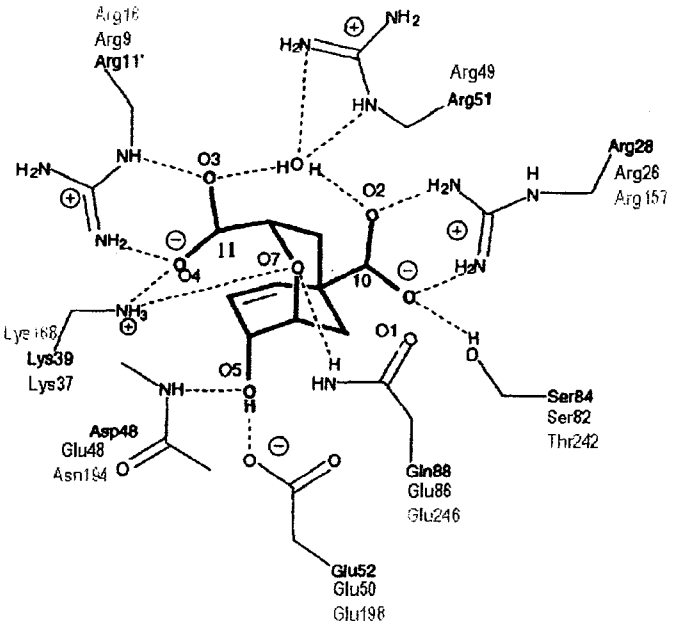

Figure 1.7: Schematic diagram of the crystal structure of the active site of yeast chorismate mutase and *E .coli* "mini-mutase" complexed with *endo*-oxabicyclic diacid. Residues from *E. coli* "mini-mutase" (black) and *S. cerevisiae* (green) were determined by X-ray crystallography while those from *E. coli* CM-PD (red) were elucidated through sequence alignments.

group in the highly charged region of the active site (Fig. 1.7). Undeniably Lys39 (Lys37 in *E. coli* CM-PD) is the key cationic residue. The activity of the mutase reaction from *E. coli* CM-PD is very pH dependent, indicating the participation of three groups (two protonated and one deprotonated) in substrate binding and/or catalysis; Lys37 may be one of these residues, poised to protonate the ether oxygen of chorismate in the transition state of the reaction(*64*). Additionally, pH-dependent activity profiles described for a variant (Gln88Glu) of the mini-mutase and for wild-type CM from yeast (contains Glu at position 246) indicated the importance of a protonated side chain at this position. There have been a number of chemical mechanisms proposed for the CM-catalyzed reactions: acid/base catalysis, a nucleophile-assisted dissociative mechanism (*80*), and transition state stabilization through conformational trapping. As expected, the catalytic mechanism of the CM-catalyzed reaction continues to be under intense study.

1.5 PREPHENATE DEHYDROGENASE MECHANISM AND ITS INHIBITION BY L-TYROSINE

The oxidative decarboxylation of prephenate to HPP in the presence of the cofactor NAD^+ is catalyzed by prephenate dehydrogenase. Since the subsequent product of this reaction is aromatic, this reaction is essentially irreversible. The non-enzymatic reaction has not been observed, nevertheless, under acidic conditions, prephenate can rapidly undergo decarboxylation to give phenylpyruvate. The acid-assisted decarboxylation occurs *via* a stepwise mechanism; protonation of the hydroxyl group of the prephenate leads to the formation of a resonance stabilized carbonium ion with subsequent decarboxylation. By contrast in the enzyme-catalyzed reaction,

decarboxylation and hydride transfer are concomitant (*94*). This mechanism was revealed through isotope effect studies performed by Hermes *et al.* (*94*). Using the substrate analogue deoxoprephenate, deuterated at C-4, they observed an isotope effect for the hydride transfer to NAD^- (*94*). Furthermore, using the natural abundance of ^{13}C in the substrate, they observed a carbon isotope effect for the cleavage of the C-C bond between the cyclohexadiene ring and the ring carboxylate. Interestingly, the carbon isotope effect obtained with the deuterium *versus* the hydrogen at position C-4 was smaller than with the natural ^{13}C indicating that both the deuterium and the ^{13}C isotope effects are in the same transition state; that is, deuterium made the ^{13}C-sensitive step more rate-limiting by slowing it down (*94*).

It has been determined by the analysis of initial velocity patterns using steady-state kinetic techniques that the *E. coli* PD reaction follows a sequential mechanism(*57*). Furthermore, product and dead-end inhibition studies have established that PD conforms to a rapid-equilibrium, random kinetic mechanism with two dead end complexes, enzyme-NADH-prephenate and enzyme-NAD-hydroxyphenylpyruvate (*63*). Isotope trapping with the enzyme-NAD^+ complex suggested that catalysis is the rate-limiting step since only a small proportion of the enzyme was trapped as [^{14}C]NADH (*63*). Similar reaction mechanism has been reported for CM-PD from *A. aerogenes* (*95*).

The pH dependence of the log *VEt* of the PD-catalyzed reaction showed that a single ionizing group (p*K* 6.5) was titrating in the rate profile and it had to be deprotonated for maximum activity (*64*). In contrast, the $\log(V/K)_{prephenate}$ pH profile displayed, in addition to the deprotonated group, a second ionizing group with a p*K* value of about 8.4 which must be protonated for maximum activity. This group was not

observed in the V profile and since prephenate does not possess a group titrating in this region, they proposed that this enzyme residue was involved in prephenate binding (*64*). Similar results for the $(V/K)_{prephenate}$ profile were obtained by Hermes *et al.* (*94*), who also identified through temperature and solvent perturbation studies that the deprotonated catalytic group was likely a histidine.

Studies by Christendat and Turnbull, using the results of sequence alignments, site-directed mutagenesis and pH-rate profiles, identified the conserved His197 as an essential catalytic residue. Replacement of the histidine by an asparagine reduced the dehydrogenase activity 5 orders of magnitude (*52*). Furthermore, the His197Asn substitution rendered the log V profile pH-independent suggesting that His197 might be the residue titrating in the acid limb that is essential for catalysis (*52*) or that the substitution had resulted in the change of the rate-determining step of the reaction. His197 acts as an hydrogen bond acceptor and is believed to polarize the 4-hydroxyl group of prephenate, lowering the activation barrier to facilitate decarboxylation and hydride transfer of prephenate to NAD^+ (*52*). The two chemical steps occur simultaneously, driven by the aromatic nature of the product and also because the ring carboxylate is likely near and/or in a hydrophobic pocket promoting decarboxylation (*53*).

Although attempts to identify the the prephenate binding residue with a pK value of about 8.4 have failed, Christendat and Turnbull noted Arg294 was critical for prephenate binding as suggested by the 120-fold increase in K_m for prephenate for an Arg294Qln variant (*53*). From their inhibition studies, they proposed that Arg294

interacted electrostatically with the ring carboxylate of prephenate (Fig. 1.8). They characterized

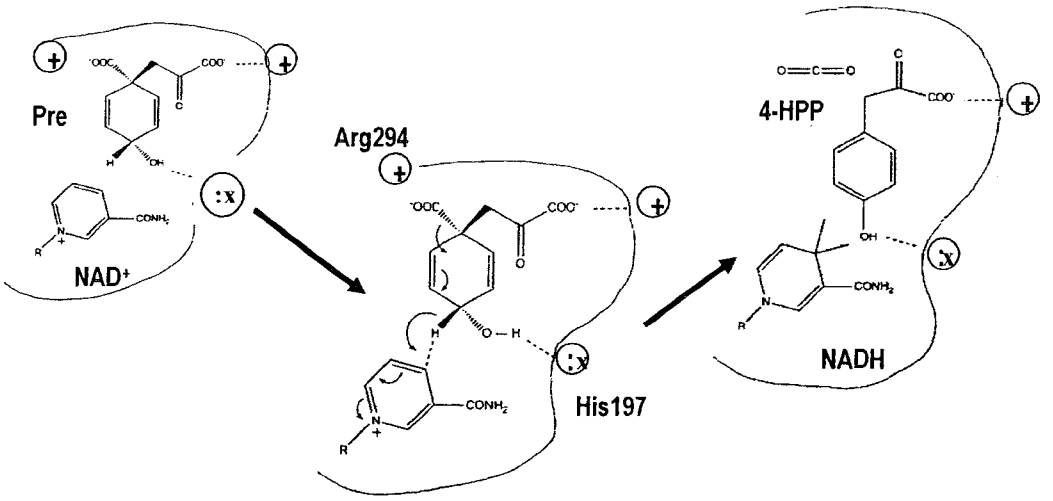

Figure 1.8: Proposed mechanism for the prephenate dehydrogenase-catalyzed reaction. A deprotonated group (:x), identified as His197 in *E. coli* CM-PD (His147 in *A. aeolicus* PD), helps polarize the 4-hydroxyl group of prephenate while an arginine, likely Arg294, is involved in prephenate binding.

Figure 1.9: Multiple sequence alignment of TyrA proteins. Sequences from monofunctional PDs (*A. aeolicus*, *B. subtilis*, *N. europaea*, *S. cerevisiae* and *M. tuberculosis*) and bifunctional CM-PDs (*E. coli* and *H. influenzae*). Conserved residues are indicated by an asterisk and are bolded and highlighted in gray. Sequences from *A. aeolicus*, *B. subtilis* and *M. tuberculosis* contain the R/KxxxR motif (underlined) described by Bonner *et al.* (*45*). The multiple sequence alignment was performed with ClustalW.

```
A. aeolicus     MAILSSMFNPSPPQGFCKKNIIKILKSLSMQNVLIVGVGFMGGSFAKSLRRSGFKGKIYG 60
E. coli         ------------------------------VVIVGGGGQMGRLFEKMLTLSG------- 22
H. influenza    --------------------FGFKTINSDIHKIVIVGGYGKLGGLFARYLRASG------- 34
B. subtilis     -------------------------MNQMKDTILLAGLGLIGGSIALAIKKNHPGKRIIG 35
N. europaea     ----------------------MAFPAISKLVVVGVGLIGGSFALALRRAGLVDRVVG 36
S. cerevisiae   -----------------MVSEDKIEQWKATKVIGIIGLGDMGLLYANKFTDAGWGVICCD 43
M. tubercul.    ----------------------------MRAAAAAGREVFG--YNRSVEGAHG------ 23
                                             : : *   :*

A. aeolicus     YDINPESISKAVDLGIIDEGTTSIAKVEDFSPDFVMLSSPVRTFREIAKKLSYILSEDAT 120
E. coli         -----------YQVRILEQHDWDRAADIVADAGMVIVSVPIHVTEQVIGKLPP-LPKDCI 70
H. influenza    -----------YPISILDREDWAVAESILANADVVIVSVPINLTLETIERLKPYLTENML 83
B. subtilis     IDISDEQAVAALKLGVIDDRADSFISGVKEAATVIIATPVEQTLVMLEELAHSGIEHELL 95
N. europaea     MGRSPENMQRALELGIIDEQTSDFAAALSG-ADFVLLAIPVKQTAGVMQQMAPHLKAHTI 95
S. cerevisiae   REEYYDELKEKYASAKFELVKNGHLVSRQS--DYIIYSVEASNISKIVATYGPSSKVGTI 101
M. tubercul.    --------ARSDGFDAITDLNQTLTRAAAT-EALIVLAVPMPALPGMLAHIRK-SAPGCP 73
                                             : :

A. aeolicus     VTDQGSVKGKLVYDLENILGKR---FVGGHPIAGTEKSGVEYSLDNLYEGKKVILTPTKK 177
E. coli         LVDLASVKN---GPLQAMLVAHDGPVLGLHPMFGPDSGSLAKQVVVWCDGR--------- 118
H. influenza    LADLTSVKR---EPLAKMLEVHTGAVLGLHPMFGADIASMAKQVVVRCDGR--------- 131
B. subtilis     ITDVGSTKQKVVDYADQVLPSRYQ-FVGGHPMAGSHKSGVAAAKEFLFENAFYILTPGQK 154
N. europaea     ISDVGSTKQNVVHAARANLGKRIERFIPAHPIAGTEFNGAEAAFPDLFQDKPVILTPLQE 155
S. cerevisiae   VGGQTSCKLPEIEAFEKYLPKDCD-IITVHSLHGPKVNTEGQPLVIINHRS--------- 151
M. tubercul.    LTDVTSVKCAVLDEVTAAGLQAR--YVGGHPMTGTAHSGWTAGHGGLFNRAPWVVSVDDH 131
                : .  * *                 :  *.: *.          .

A. aeolicus     TDKKRLKLVKRVWEDVGGVVEYMSPELHDYVFGVVSHLPHAVAFALVDTLIHMSTPEV-- 235
E. coli         -KPEAYQWFLEQIQVWGARLHRISAVEHDQNMAFIQALRHFATFAYGLHLAEENVQLEQL 177
H. influenza    -FPERYEWLLEQIQIWGAKIYQTNATEHDHNMTYIQALRHFSTFANGLHLSKQPINLANL 190
B. subtilis     TDKQAVEQLKNLLKGTNAHFVEMSPEEHDGVTSVISHFPHIVAASLVHQTHHSENLYP-- 212
N. europaea     NDQQIVDRVADLWQHCGASVSSMLPEQHDQLLAAISHLPHMLAFSLMQHIRTLSHTLSEG 215
S. cerevisiae   QYPESFEFVNSVMACLKSKQVYLTYEEHDKITADTQAVTHAAFLSMGSAWAKIKIYPWTL 211
M. tubercul.    VDPTVWSMVMTLALDCGAMVVPAKSDEHDAAAAAVSHLPHLLAEALAVTAAEVP------ 185
                        .       .         **      . . *

A. aeolicus     ----DLFKYPGGGFKDFTRIAKSDPIMWRDIFLENKENVMKAIEGFEKSLNHLKELIVRE 291
E. coli         -LALSSPIYR-LELAMVGRLFAQDPQLYADIIMS-SERNLALIKRYYKRFGEAIELLEQG 234
H. influenza    -LALSSPIYR-LELAMIGRLFAQDAELYADIIMD-KSENLAVIETLKQTYDEALTFFENN 247
B. subtilis     ----LVKRFAAGGFRDITRIASSSPAMWRDILLHNKDKILDRFDEWIREIDKIRTYVEQE 268
N. europaea     -DPLALLRFAGSSLNDMTRITASSPEMWRDICLENRAALLAQIEAYQQELSGLQQMLADH 274
S. cerevisiae   GVNKWYGGLENVKVNISLRIYSNKWHVYAGLAITNPSAHQQILQYATSATELFSLMIDNK 271
M. tubercul.    ----LAFALAAGSFRDATRVAATAPDLVRAMCEANTGQLAPAADRIIDLLSRARDSLQSH 241
                          .    *:      :   :            .            .

A. aeolicus     -AEEELVEYLKEVKIKRMEID---------------------------------------- 311
E. coli         -DKQAFIDSFRKVEHWFGDYAQRFQSESRVLLRQANDNRQ-------------------- 273
H. influenza    -DRQGFIDAFHKVRDWFGDYSEQFLKESRQLLQQANDLKQG------------------- 287
B. subtilis     -DAENLFRYFKTAKDYRDGLPLRQKGAIPAFYDLYVDVPDHPGVISEITAILAAERISIT 327
N. europaea     -DGESLEKLFAEARAIRQAWSAFRNQS------------------------------- 300
S. cerevisiae   --EQELTDRLLKAKQFVFGKHTGLLLLDDTILEKYSLSKSSIGNSNNCKPVPNSHLSLLA 329
M. tubercul.    GSIADLADAGHAARTRYDSFPRSDIVTVVIGADKWREQLAAAGRAGGVITSALPSLDSPQ 301
                         :       .
```

several substrate analogues, all lacking the ring carboxylate group at C-1 relative to prephenate, and found that the dissociation constant obtained with Arg294Gln for these substrate analogues were similar to those found with wild-type enzyme. Multiple sequence alignment with a number of prephenate dehydrogenase shows these residues are conserved as well as others (Fig. 1.9).

Any structural information for TyrA proteins was unavailable until very recently. In 2006 Christendat and coworkers (*48*) solved the first crystal structure of a TyrA protein, a monofunctional prephenate dehydrogenase from the hyperthermophilic bacterium *Aquifex aeolicus*. The structure of this enzyme in complex with NAD^+ has provided valuable insight into the location of the conserved residues in the active site. As expected, His147, the residue analogous to His197 in the *E. coli* enzyme, was positioned adjacent to NAD^+ and prephenate (the latter substrate modeled in the active site) to participate in catalysis. Similarly, Arg250, the residue homologous to Arg294 in the *E. coli* enzyme, was placed in the highly charged environment within in the active site of the enzyme, but the electron map density of this side chain was too poorly ordered to ascertain the residue's exact position. (*48*).

1.6 AROGENATE DEHYDROGENASES

In most plants, cyanobacteria, algae and several other microorganisms, both Tyr and Phe are synthesized from a common precursor, L-arogenate, *via* the arogenate route. As previously mentioned, in this pathway, prephenate is first converted to L-arogenate by a prephenate transaminase, then an arogenate dehydratase (ADT) or arogenate dehydrogenase (AD) converts L-arogenate into Phe or Tyr, respectively. Depending upon

the organism. ADs may be specific for NAD^+, $NADP^+$ or use both as co-factors(*36*). For the past 30 years, a large number of ADs have been studied and most work focused on substrates and cofactors specificities (*32, 33, 40, 49, 96-98*), feedback inhibition (*97, 98*), evolutionary perspective (*47, 99*) but only a few mechanistic studies were reported.

Recently, Legrand *et al.* published the crystal structure of AD from *Synechocystis* sp., complexed with its co-factor $NADP^+$ and with the substrate, L-arogenate, modeled in the active site (*43*). Examination of the crystal structure revealed that *Synechocystis* sp., AD and *Aquifex aeolicus* PD possess similar quaternary structure; both enzymes are homodimeric with each monomer housing a nucleotide binding domain and a dimerization domain (see Fig. 1.10). Furthermore, analysis of the PD and AD active sites reveals that functionally important residues are conserved. For example, the catalytic histidine, His147 in PD, and the important binding group, Arg250 in PD, are equivalently positioned in both structures. Moreover, the serine residues which are shown in modeled structures to bind to the C4-hydroxyl group of the cyclohexadienyl substrate are also spatially conserved. Other common active site residues include Gly151, Thr152, His205, Ser213, and His214 (numbering corresponds to the PD structure). The conservation of key functionally important residues indicates that L-arogenate may bind to the AD active site in a similar manner to that of prephenate in PD. In addition, analysis of sequence alignments of ADs shows that an Asp residue at position 138 (*E. coli* numbering) is a reliable indicator for NAD^+ specificity since $NADP^+$ is repelled by the negative charge of Asp. The Asn at the corresponding position in other ADs likely indicates $NADP^+$ specificity as demonstrated by Bonner *et al.* (*36*).

1.7 REGULATION BY FEEDBACK INHIBITION

TyrA proteins influence the flux of metabolites between Tyr and Phe; hence, the activities of these enzymes must be very well regulated. End-product inhibition of PD and AD provides major regulatory control in Tyr biosynthesis but the mechanism involved is still unclear. Some kinetic studies on *E. coli* CM-PD suggest that L-Tyr, the end product of the pathway, and HPP, the direct product of the PD reaction, act as competitive inhibitors with respect to prephenate (*100*); other studies suggest the presence of a distinct allosteric site for L-Tyr to interact (*101*). It is clearly documented in the *E. coli* enzyme that L-Tyr enhances the cooperativity between subunits in the binding of prephenate (*100*). Biophysical investigations have led to the interpretation that this enzyme interconverts from an active dimer to an inactive tetramer upon the binding of L-Tyr plus NAD^+ (*65*). Additionally, the effects of L-Tyr are dependent on the enzyme's interactions with NAD^+ and *vice-versa*. Recent work by Song *et al.* (*44*) *P. aeruginosa* have shown that some bacteria possess a C-terminal fusion domain, Aspartate kinase-Chorismate mutase-TyrA (ACT domain), that is responsible for the binding of the end product of the pathway. This domain exists in the monofunctional PD from *B. subtilis* as well as in the bifunctional CM-PDT from *E. coli*, but it is not found in *E. coli* CM-PD (*73*), although recent work by Stephanopoulos and Lüktke-Eversloh (*102*) suggests that two residues located at the C-terminus of *E. coli* CM-PD are involved in Tyr inhibition.

1.8 ALLOSTERIC REGULATION

Allosteric enzymes are widely distributed in living organisms and their interactions are important in many biological processes. The term *allostery* derived from

the Greek *allos*, "others", and *stereos*, "shape" and it is hypothesized that direct control of protein function through allosteric regulation is usually achieved *via* conformational changes of a given protein structure induced by the binding of an effector at another site than the orthosteric site. The conformational changes are transmitted through the bulk of the protein to the catalytic site and modulate the rate of the reaction with the substrate; as a consequence the v vs. S plot is no longer hyperbolic but sigmoidal. For the past fifty years, allosteric enzymes have captivated many famous researchers and have been extensively studied. In 1965, Monod and coworkers reviewed a dozen of allosteric enzymes and suggested that allostery control in proteins displays cooperative functional behavior along with feedback inhibition (*103*). Most of allosteric enzymes are oligomeric and are often found at key branch point in metabolism pathways. The Monod, Wyman and Changeux concerted model (*103*) (MWC model) was applied to understand kinetic results obtained with hemoglobin, aspartate transcarbamylase (ATCase), threonine desaminase and many other well known enzymes. In this model, binding of the effector brings about the change in all protein subunits. By contrast, Koshland, Némethy and Filmer (*104*) invoked a sequential (KNF model) rather than a concerted model, whereby a conformational change in one subunit does not necessarily induce a change in other subunits. Each subunit is allowed to change its tertiary structure on substrate binding permitting alteration of the chemical activities of its neighbors. In both theories, the enzyme subunits exist in a tense or relaxed conformation.

In the past, drug discovery scientists have focused on identifying compounds that interact directly with the orthosteric site to activate or block the enzyme of interest. This simplistic approach was significantly helped by computer assisted drug-design and has

resulted in excellent drugs, however those active site-directed compounds may not offer the selectivity required and could lead to undesirable side effects. Currently, pharmaceutical companies are focussing on allosteric sites since they offer the opportunities for discovering new drugs for enzymes for which designing an active site directed drug has been challenging. Furthermore, allosteric modulators are thought to be less harmfull since they are less likely to produce dangerous side effects.

As previously mentioned, kinetic studies on *E. coli* CM-PD suggest that the enzyme is allosterically inhibited by Tyr, although the exact mechanism of inhibition remains unclear (*101*). Hence, understanding the effects of Tyr on TyrA enzymes would help delineate the mode by which allosteric regulation is achieved and add to the body of knowledge which is being gathered on these fascinating enzymes.

1.9 THE MODEL CHOSEN: *AQUIFEX AEOLICUS* PD

Aquifex aeolicus was isolated from the thermal vents in Yellowstone National Park and the entire genome was sequenced by Deckert *et al.* (*105*). This organism belongs to the *Aquificaceae* which represent the most deeply branching family within the Bacterial domain and is one of the earliest diverging bacteria known. *A. aeolicus* is a microaerophilic, hydrogen-oxidizing, obligate chemolithautotroph (obtains its energy from inorganic compounds) organism. Organic substrates such as sugar, amino acids or meat extract cannot be used by *A. aeolicus* for its growth. As previously pointed out by Aponte (*106*), no gene for a monofunctional CM was identified, but a putative *tyrA* encoding a 311 residue PD was recognized. Additionally, the genome revealed the existence of a *pheA* gene encoding for a CM-PDT. Interestingly, *tyrA* from *A. aeolicus* is

found as an orphan gene since, contrary to the *E. coli tyrA* gene, it is not part of an operon. Sequence alignment of *A. aeolicus* PD and the PD domain of the bifunctional *E. coli* CM-PD revealed only about 18% sequence homology. Nevertheless, all residues which have been identified to be important for binding and/or catalysis in *E. coli* CM-PD are conserved in *A. aeolicus* PD (Fig. 1.9).

To date, all the efforts to obtain a three-dimensional structure of *E. coli* CM-PD have failed. Additionally, there had been no reported structure of any TyrA protein although, a host of monofunctional CMs have been successfully crystallized and their structures have been solved. The peculiar intrinsic physical properties of thermophilic enzymes (highly charged surface (*107-109*)) and increased packing density (*109, 110*) are known to render them better candidates for crystallization studies. Hence, our lab and our collaborators from U. of Toronto selected the monofunctional PD from the hyperthermophilic bacterium *A. aeolicus* to perform our biochemical, biophysical and crystallographic studies. An N-terminally deleted Δ19PD liganded with its cosubstrate NAD^+, yielded diffraction quality crystal and the three-dimensional structure was solved to a resolution of 1.9 Å (*48*). As depicted in Figure 1.10, the enzyme is homodimeric. Each monomer consists of a N-terminal domain, containing a Rossman fold and a C-terminal domain believed to participate in the dimerization (*48*) (Fig. 1.11). The X-ray structure revealed that the active site is at the located at the inter domain cleft of the two domains and that residues from both subunits contribute to a complete active site.

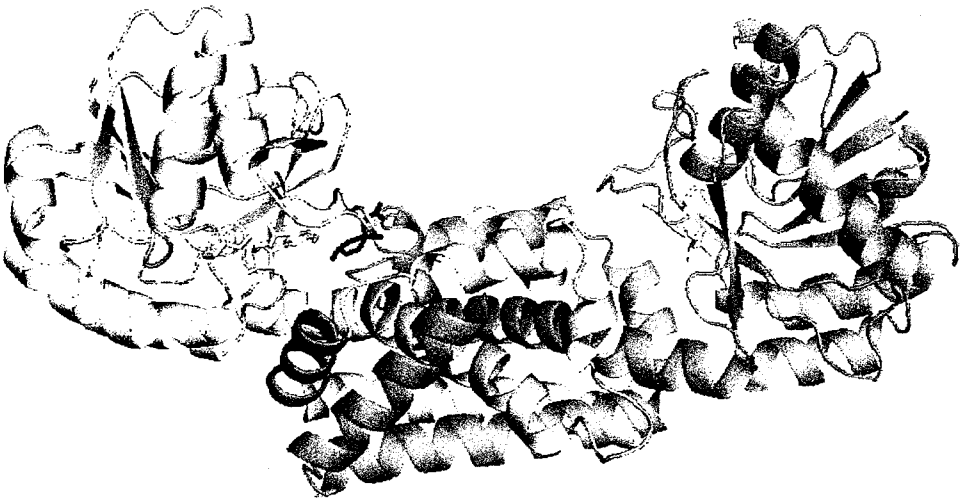

Figure 1.10: Structure of *Aquifex aeolicus* Δ19PD. Cartoon diagram of dimeric Δ19PD from co-crystallization studies with NAD^+ performed at pH 3.2. Monomer A and B are shown in pale green and green, respectively. The figure illustrates the two domains associated with each monomer: the N-terminal domain (dinucleotide-binding domain) and the C-terminal domain (dimerization domain). NAD^+ is represented as yellow sticks. Prephenate, modeled in the active site, is represented as blue sticks. The atomic coordinates and structure factors of Δ19PD in complex with NAD^+ are available in the Protein Data Bank, accession number 2g5c. Diagram was produced with PyMOL (http://pymol.sourceforge.net/) (*111*).

Figure 1.11: Cartoon diagram representation of the structure of one monomer of *Aquifex aeolicus* Δ19PD in complex with NAD^+. The N-terminal and the C-terminal domains are colored in pink and in blue, respectively. The N-terminus of Δ19PD is in green while its C-terminus is colored in red. The NAD^+-binding site is contained within the N-terminal domain. NAD^+ interacts with the residues of the loop between β1 and α1 which comprises the highly conserved motif (GXGXXG), signature of the NAD(P)-dependent oxidoreductases. The active site is located at the interdomain interface of the two domains. However, the majority of the prephenate binding pocket is contained within one subunit and includes regions of β6, α8 and α10 and the coil regions between β5 and α5 and between β6 and α6. A connecting loop between β6 and β7 caps the active site. Prephenate, modeled in the active site, is represented in blue sticks and NAD^+ in yellow sticks. Chain D of Δ19PD, shown here, was resolved from residue 30 to residue 307. The figure was generated using PyMOL.

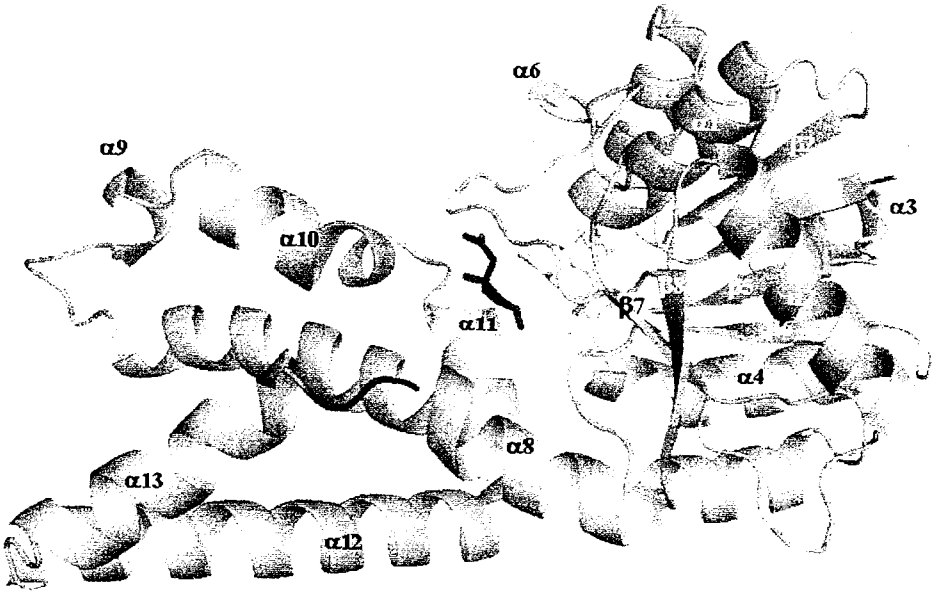
α6
α9
α3
α10
β7
α11
α4
α8
α13
α12

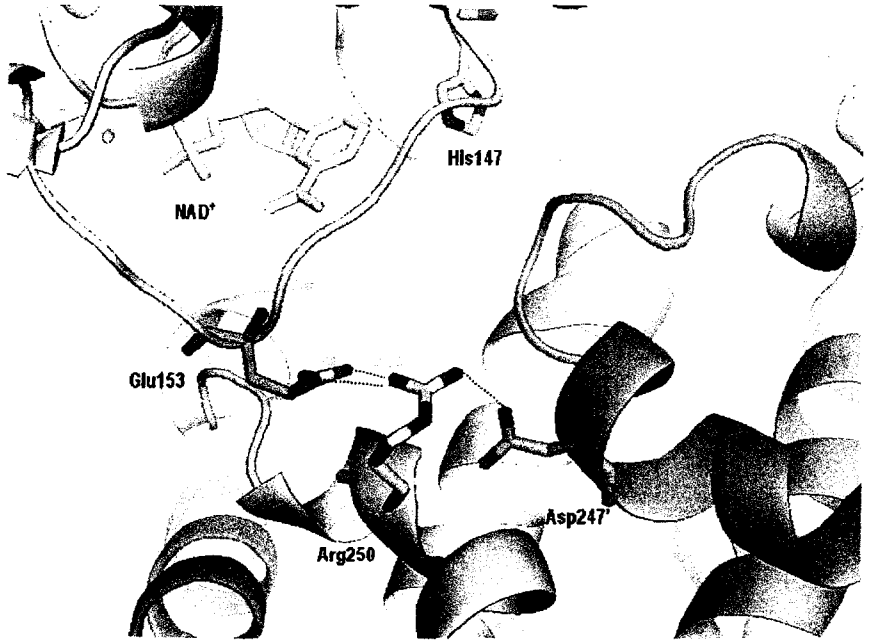

Figure 1.12: Selected active site residues of *Aquifex aeolicus* Δ19PD in complex with NAD^+. The active site, formed at the interdomain interface of the NAD^+-binding domain and C-terminal domain, contains residues which are shared between monomers; Glu153 and Arg250 from one subunit (gray-green) and Asp247' from the other subunit (green). These residues form an ionic network believed to help prephenate access into the active site. His147, conserved through all species, is the catalytic residue. Hydrogen bonds are represented as dots.

1.10 SCOPE AND ORGANIZATION OF THESIS

In chapter two, full-length PD and an N-terminally truncated protein variant (Δ19PD) expressed recombinantly in *E. coli*, were purified to homogeneity with Ni-NTA affinity chromatography. Circular dichroism and fluorescence spectroscopies were employed to assess the stability of Δ19PD to Gdn-HCl denaturation, and together with size exclusion chromatography, allowed elucidation of the pathway of unfolding in the presence of the denaturant. Additionally, the quenching of intrinsic fluorescence emission was used to gain structural insight into the environment of two Trp residues in the protein. Concomitant with these biophysical studies, Δ19PD in complex with NAD^+ yielded crystals that diffracted to a high resolution and our results are correlated with this structure. This chapter also demonstrated the benefits of mass spectrometry in identifying proteolytic fragments of PD which facilitated the construction of the crystallizable form of the enzyme, Δ19PD.

In chapter three, the temperature dependence of the reactions catalyzed by PD and Δ19PD were assessed as well as their ability to utilize L-arogenate as a substrate. Additionally, the importance of putative active site residues involved in the catalytic mechanism of Δ19PD was assigned from the results of the kinetic analysis of site-directed variants. Our findings are correlated with the most recent structure of Δ19PD in complex with NAD^+ plus HPP (manuscript submitted).

In chapter four, the inhibition of wild-type and variant forms of Δ19PD by L-Tyr was examined. This is achieved using kinetic analysis, thermodynamic radiolabeled Tyr binding experiments and fluorescence spectroscopy using anilino-naphtalene sulfonic

acid (ANS) as a probe of conformational changes induced by ligand binding. Our findings for the recombinant PDs from *A. aeolicus* are compared with results obtained with the bifunctional CM-PD from *E. coli.* We identified a residue which is critical for feedback inhibition by L-Tyr for both TyrA proteins. Additionally, our results are interpreted in light of the crystal structure of *A. aeolicus* Δ19PD in complex with NAD^+ plus L-Tyr as well as a structure of *E. coli* PD modeled from a structural template of *H. influenza* PD.

Chapter 2

Purification and Biophysical Properties of Full-Length PD and the Crystallizable Variant Δ19PD

2.0 INTRODUCTION

In previous studies, PD from *Aquifex aeolicus* was expressed in *Escherichia coli* with a removable N-terminal hexa-His tag by cloning of the *tyrA* gene into a pET-15b expression vector. The fusion protein was then purified by nickel affinity chromatography. Results of the overexpression, purification and the preliminary biophysical and kinetic characterization of PD have been reported by Aponte (*106*). Both Aponte and our collaborator D. Christendat noted unexpectantly that the His-tagged monomer purified as full-length and shortened forms. Aponte proposed that the truncated form of the enzyme resulted from an *in-vivo* N-terminal proteolytic cleavage as judged by SDS-PAGE analysis of fractions eluting from the Ni-NTA affinity column, although the exact site of cleavage was never firmly established. The biochemical or structural relevance of the proteolysis was not clear at this time. The behavior of the full-length PD on Ni-affinity and size exclusion resins indicated that the recombinant protein could form dimers in solution. Aponte also established that PD was resistant to chemical denaturation, however, the strength of the dimer interaction or the pathway of unfolding was never investigated fully.

In this chapter we report the development of a reliable protocol for ESI-MS analysis of PD and its degradation products which allowed the exact identification of the proteolytic cleavage site at the protein's N-terminal region. The overexpression and purification of Δ19PD, an N-terminal deletion construct, are described and its biophysical properties are compared with those of wild-type PD. We show that Δ19PD is very resistant to thermal and chemical denaturation and have established the pathway of unfolding of Δ19PD as directed by the chemical denaturant guanidine hydrochloride

(Gdn-HCl). Lastly, Δ19PD yields diffraction quality crystals. Thus, in this chapter our biophysical findings are correlated with those of the recently solved crystal structure of the enzyme(*48*). Material in this chapter has been published in *Protein Science* (*112*).

2.1 EXPERIMENTAL PROCEDURES

2.1.1 Materials

Prephenate (sodium salt) was obtained as previously described by Dudzinski and Morrison (*113*) while chorismate (free acid) was isolated from *Klebsiella pneumonia* (*114*). Thrombin and NAD^+ were obtained from Roche. High purity of the substrates was confirmed by either mass spectrometry or NMR. Concentrations of stock substrate solutions were determined using published extinction coefficients (*115*) and/or enzymatic end-point analysis. N-Acetyl-L-tryptophanamide (NATA), N-acetyl-L-tyrosinamide (NAYA) and 1-anilino-8-naphthalene sulfonic acid (ANS) were purchased from Sigma, and concentrations of stock solutions were determined spectrophotometrically (*116*). All acids and organic solvents for mass spectrometry were HPLC grade. Trifluoroacetic acid (TFA) and α-cyano-4-hydroxycinnamic acid (HCCA) were obtained from Sigma. C_{18} ZipTip cartridges were from Millipore Corp. Trypsin powder, for in-solution tryptic digestion, was sequencing grade modified and was purchased from Roche. Ni-NTA or Superflow™ chromatography resin was supplied by Qiagen; a binding capacity of 7.5 mg of hexa-His protein/mL of resin was assumed. Dialysis membrane (12-14 K cutoff) was from Spectrapor and ultrafiltration units (30 K or 10 K cutoff) were obtained from Amicon and were washed according to manufacturers instructions. All other chemical reagents were obtained commercially and were of the highest quality available.

E. coli strains DH5α (Life Technologies Inc.) [supE44 ΔlacU169 (ϕ80 lacZ ΔM15) hsdR17 recA1 endA1 gyrA96 thi-1 relA1] and BL21(DE3) Gold (Stratagene) [F^- dcm^+ Hte ompT hsdS(r_B^- m_B^-) gal λ (DE3) endA Tet^r] were used for plasmid production and for protein expression, respectively. The expression plasmid (Δ19PD) encoding residues 20-311 of the *A. aeolicus* VF5 PDH protein (gi:15282445) and a hexa-histidine tag at the N-terminus were prepared as described elsewhere (*117*). Dr. A. Edwards at the Ontario Cancer Institute, University of Toronto, kindly donated the helper plasmid pMagik encoding three rare tRNAs (AGG and AGA for Arg, ATA for Ile). Recombinant *E. coli* CM-PD was expressed and purified as described elsewhere (*53*) and was generously provided by J. Manioudakis.

2.1.2 Production and Purification of Recombinant PD and Δ19PD of *A. aeolicus*

Recombinant *A. aeolicus* PD and Δ19PD were overexpressed in *E. coli* BL21(DE3) Gold cells and purified according to the protocol of Aponte (*106*) but with minor modifications. Briefly, *E. coli* BL21(DE3) Gold cells harbouring pMagik and the expression plasmid (pRA-PD-3 or pΔ19PD) were grown in 50 mL of LB medium supplemented with 100 μg/mL ampicillin and 50 μg/mL kanamycin at 30°C for 15 h with shaking, and diluted into 1.5 L of the same medium. After growth to an OD_{600} of 0.6, 0.4 mM 1-thio-β-D-galactopyranoside was added. The cells were incubated further with shaking for an additional 5 h at room temperature and then overnight at 18°C. Cells were harvested by centrifugation and resuspended in 15 mL/L culture of ice-cold buffer A (50 mM Tris(hydroxymethyl)aminomethane hydrochloride (Tris-HCl), 0.5 M NaCl, 5% glycerol (v/v) at pH 7.5) supplemented with 5 mM imidazole, Complete™ (Roche

protease inhibitor cocktail, one tablet per 50 mL suspension), 1 mM benzamidine, and 0.5 mM phenylmethyl sulfonyl fluoride (PMSF). The cells were disrupted by two passages through a Thermo Spectronic French Press at 18,000 psi (instead of one cited by Aponte (*106*)), with additional benzamidine added after the first passage. Insoluble material was removed by centrifugation at 100,000*g* for 40 min at 4°C. The cell-free extract was incubated in an 85°C water bath for 10 min and centrifuged again, and the supernatant was directly applied to a 15 mL Superflow™ Ni-NTA column (Qiagen) at a flow rate of 1 mL/min equilibrated with buffer A containing 5 mM imidazole. Nickel resin was washed extensively with 400 mL of buffer A containing 30 mM imidazole (three times the volume used by Aponte (*106*)) and bound protein was eluted with buffer A containing 300 mM imidazole. Fractions were supplemented with 1 mM EDTA and 0.5 mM dithiothreitol (DTT). Those containing PD activity were pooled, and thrombin was added at a final protein:thrombin ratio of 1000:1 (w/w). To increase efficiency of thrombin, the sample was first dialyzed (Spectrapore, 12 K cutoff) for 2 h at room temperature, then overnight at 4°C against buffer A with 0.5 mM Tris(2-carboxyethyl) phosphine hydrochloride (TCEP-HCl). The sample was reapplied onto the Ni-NTA column. In the initial experiment, unbound PD was then rechromatographed on a 1 mL Hi-Trap™ benzamidine FF column (Amersham Bioscience) to remove any trace amounts of thrombin. However, this addition step afforded no advantage and was later omitted. PD was concentrated to 2-10 mg/mL (Amicon Ultra-15), and stored at -86°C in buffer A containing 5 mM DTT (storage buffer) and 1 mM benzamidine. Δ19PD was purified as described for PD, except thiol reducing agents were omitted in the purification procedure. PD and Δ19PD were detected in fractions by enzymatic assay and SDS-15% PAGE with

Coomassie Blue staining. Both forms of the enzyme were further purified by size exclusion chromatography (section 2.1.5.3) prior to spectroscopic studies.

2.1.3 SDS-Polyacrylamide Gel Electrophoresis

Denaturing SDS-PAGE was performed with either a 12% or 15% polyacrylamide gel following the method of Laemmli (*118*). Protein samples were diluted 1:2 (v/v) into 2 times SDS sample loading buffer (1.5 M Tris-HCl, 4% SDS, 20% glycerol (v/v), 0.002% Bromophenol Blue, pH 6.8) and incubated in a boiling water bath to 3 min then kept on ice 2 min prior to loading on a gel. The gel was electrophoresed at 80 V as samples migrated through the stacking gel, and then the voltage was increased to 180 to 200 V as the samples migrated to the resolving gel. Electrophoresis continued until the Bromophenol Blue tracking dye migrated off the resolving gel. Bio-Rad broad range molecular weight proteins standards were used to estimate the molecular weight of proteins in the samples. Protein was visualized by staining the gel with Coomassie Brilliant Blue R-250.

2.1.4 Determination of Enzyme Activity and Protein Concentration

The oxidative decarboxylation of prephenate in the presence of NAD^+ was followed at 340 nm as described by Turnbull *et al.* (*119*). The reactions (total volume 1 mL) were monitored continuously by using a Varian Cary 50 spectrophotometer equipped with a thermostated cuvette holder.

Standard activity assay for *A. aeolicus* PD and Δ19PD was measured at 55°C in a reaction buffer of 50 mM HEPES, 150 mM NaCl, (pH 7.5), at saturating concentrations

of NAD^+ (2 mM) and prephenate (1 mM). Buffer was incubated at 55°C (2 min), followed by the addition of an appropriate amount of enzyme (2 min) and NAD^+ (30 s), and then the reaction was initiated with prephenate. At each step, components were mixed by inversion of the cuvette. All substrates were at room temperature prior to their addition. *E. coli* CM-PD activity was assayed as described previously (*119*).

Reaction rates were calculated from the linear portion of the progress curve using the software supplied by the spectrophotometer. Values of steady-state kinetic parameters k_{cat} and K_m were obtained by fitting initial velocity data to the appropriate rate equations using nonlinear least-squares analysis provided by Grafit Software version 5.0 (Erathicus Software) or the programs of Cleland (*120*) (see also Chapter 3). Substrate saturation curves were fitted using the Michaelis-Menten equation. Specific activity was calculated from the amount of enzyme required for the conversion of 1 μmol of product per minute per mg of protein at the desired temperature.

Protein concentration was estimated using the Bio-Rad Protein Assay Kit (Bio-Rad Laboratories) with bovine serum albumin (Sigma) as a standard.

2.1.5 Molecular Weight Determination

2.1.5.1 Mass Spectrometry

2.1.5.1.1 Determination of Subunit Molecular Weights

Subunit molecular weight of PD and Δ19PD was determined by electrospray ionizing mass spectrometry (ESI-MS). Sample preparation was adapted by J. Manioudakis from a protocol for the analysis of membrane-associated proteins (*121*). An aliquot of 100 μL of enzyme (50 to 100 μg) in storage buffer was resuspended with 300

µL of methanol and 100 µL of chloroform. The sample was gently vortexed, then 200 µL of MilliQ water was added and the solution was vortexed again. The sample was centrifuged for 2 min at 14,000*g*, the top layer (methanol/water) was discarded and the protein precipitate (above chloroform layer) was washed twice with at least 300 µL of methanol, centrifuging each time after washing and decanting the aqueous layer. The resulting precipitate was solubilized by vortexing in 0.5-1 mL of a solution of 30% methanol and 0.2% formic acid (FA) (v/v). The solution was centrifuged immediately prior to injection. Analysis was carried out on a Waters Micromass Q-ToF-2 mass spectrometer operating in positive-ion mode following direct infusion of samples into the Z-spray ion source. Instrument parameters were as follows: source block temperature, 80°C; capillary voltage, 3.6 kV; cone voltage, 45 V; ToF 9.1 kV; MC, 2.1 kV. Data analysis and deconvolution were performed using MassLynx 4.0 software (Waters Micromass). Calibration of the instrument was checked with [Glu]-fibrinopeptide B (MW 1570.5) (Sigma). Mass shifts of ± 2 mass units for PD are within the expected experimental error.

2.1.5.1.2 Matrix-Assisted Laser Desorption/Ionization Mass Spectrometry Analysis of Tryptic Generated Peptides from *A. aeolicus* PD

In-solution tryptic digestion: An aliquot of thrombin-treated PD (5 mg/mL in storage buffer) was buffer exchanged with a NAP-5 column in 50 mM ammonium bicarbonate at pH 7.4 and concentrated to 5 mg/mL using a Millipore ultracentrifugation filter device (30 K cutoff). Trypsin was added to the sample to a final protease to protein ratio of 1:20 (w/w). Samples were incubated 16 h at 37°C and the reaction was stopped

by addition of 50 µL of 1 M HCl. Desalting of the samples was performed using reverse phase C_{18} Millipore ZipTip® tips ($ZipTip_{C18}$). $ZipTip_{C18}$ was pre-equilibrated with 60% acetonitrile (ACN) and 0.1% trifluoroacetic acid (TFA) (v/v) and washed three times with 5% ACN/0.1% TFA (v/v). The diluted sample was drawn into the tip to allow peptide binding, and the resin was washed five times (~50 µL total volume) with 5% ACN/0.1% TFA. The peptides were eluted from the $ZipTip_{C18}$ in a wash of 1.5 µL of 60% ACN/0.1% TFA. A saturated matrix solution was prepared in 40% ACN/0.1% TFA. One µL of the desalted protein solution was mixed with 1 µL of HCCA matrix and then 1 µL of the mixture was deposited on the sample probe. Samples were dried at room temperature prior to MS analysis.

In-gel tryptic digestion: Purified PD (before thrombin treatment) was dialyzed overnight (10 K cutoff) at 4°C against storage buffer with trypsin (20:1, w/w). An aliquot (~15 µg) of the protein sample resulting from the overnight digestion was resolved by SDS-PAGE and visualized by Coomassie Blue staining. The band containing the protein of interest was excised from the gel and destained completely with 50% ACN in 25 mM NH_4HCO_3. The excised gel pieces were cut into smaller particles (<1 mm^2), placed in eppendorf tubes, washed with several aliquots of 100 µL of ACN and dried completely in a SpeedVac at room temperature. Gel particles were rehydrated with 25 µL of 0.5 µg/µL trypsin in a solution of 25 mM NH_4HCO_3. The gel pieces were covered by 30 µL of 25 mM NH_4HCO_3 to keep them immersed throughout the digestion. Protein was digested for 16 h at 37°C then the reactions were stopped by adding 5 µL of 5% TFA. Tubes were shaken gently for 10 min, centrifuged to remove debris and the liquid was collected. The

supernatants were diluted, desalted and concentrated using C_{18} ZipTips (see below) and subjected to MALDI-MS analysis as described in the previous paragraph.

Sample analysis: Analysis was carried out on a MALDI-ToF mass spectrometer (Micromass Manchester, England) with a flight tube length of 1.0 m (linear mode) equipped with a N_2 UV laser (337 nm wavelength) and was set to deliver pulses at a rate of 5 Hz, with 25 shots per scan for linear mode. Peptides were analyzed in positive ion mode with a pulse voltage varying from 1800 to 2000 V. Theoretical maximum resolution in reflectron and linear modes is 10 000 and 100, respectively. Each spectrum represents the average of a minimum of 10 scans. MALDI-ToF-MS spectra were analyzed using the MassLynx 4.0 software (Waters Micromass). Calibration of the instrument was checked using a peptide mix containing angiotensin 1 (MW 1296.5), renin (MW 1759.0) and adrenocorticotropic hormone (MW 2465.7).

2.1.5.2 Analytical Ultracentrifugation

Native molecular weight and shape of PD and Δ19PD were determined by sedimentation velocity experiments performed at 30°C in a Beckman XL-I analytical ultracentrifuge and an An60Ti rotor using absorbance detection. Purified thrombin-cleaved enzymes were exchanged into a buffer containing 50 mM potassium phosphate buffer, 0.3 M NaCl and 0.5 mM TCEP (pH 7.5) using a NAP-5 size exclusion column (Amersham), diluted in the same buffer to give a final OD_{280} of 0.65 (PD) and 0.97 (Δ19PD), and loaded into 1.2 cm path-length double sector charcoal-filled epon centerpieces. Samples were spun at 35,000 rpm and 30°C for 10 h. Absorbance (280 nm) was collected in continuous mode with a step size of 0.005 cm and five replicate readings

at each point. Values for the sedimentation coefficient (s) and an average molar mass were calculated from the velocity and shape of the sedimenting boundary by fitting the time-dependent concentration profiles calculated with the Lamm equation (*122*) to the measured data. Calculations were performed on 200 scans for each protein using the program Sedfit (Sedfit). The program Sednterp (*123*) was used to calculate buffer density and the protein partial specific volume (1.0153 and 0.74, respectively, at 20°C, neglecting contributions due to TCEP) and to normalize the obtained sedimentation coefficient values in water at 20°C, $S_{20,w}$.

2.1.5.3 Analytical Size Exclusion Chromatography

The native molecular weight of *A. aeolicus* PD and Δ19PD was determined at ambient temperature by a Pharmacia Akta FPLC system fitted with a Superdex G-200 column (HR 10/30, Pharmacia). Chromatography was performed with mobile phases containing 50 mM potassium phosphate, 150 mM NaCl (pH 7.5) at a flow rate of 0.75 mL/min and injection volume of 500 µL. Elution was monitored at 256, 280 and 290 nm, and fractions (1 mL each) were assayed for enzyme activity. Bio-Rad gel filtration protein standards included vitamin B_{12} (1.35 kDa), equine myoglobin (17 kDa), chicken ovalbumin (44 kDa), bovine γ-globulin (158 kDa) and thyroglobulin (670 kDa). Void volume and total bed volume were evaluated with Blue Dextran and DTT, respectively. When further purification was required prior to spectroscopic analysis, Δ19PD and PD were subject to gel filtration chromatography as described above. When chromatography was conducted in the presence of Gdn-HCl-containing buffers, PD or protein standards (0.1 mg/mL) were incubated for 20 h at ambient temperature in a buffer of 50 mM

potassium phosphate, 150 mM NaCl and various Gdn-HCl concentrations (pH 7.5), and then isocratically separated in the same buffer at a flow rate of 0.4 mL/min.

2.1.6 Denaturation Studies

2.1.6.1 Circular Dichroism

Far-UV CD spectra of PD, Δ19PD and CM-PD (21 μM and 18 μM monomer, respectively) were recorded on a Jasco-710 spectropolarimeter in either a 0.05-cm or 0.1-cm path-length circular cell connected to a thermostated circulating water bath. Protein was exchanged into 50 mM potassium phosphate, 75 mM NaCl (pH 7.5) (PPS buffer), using a NAP-5 column and then diluted to the appropriate concentration in the same buffer. For studies with CM-PD, 25% glycerol (v/v) was added to the buffer. Spectra were recorded at 25°C by averaging 10 wavelength scans from 260 to 200 nm (1 nm bandwidth) in 0.2-nm steps at a rate of 50 nm/min, and 0.25 s response. The ellipticity at 222 nm (1 nm bandwidth) was measured from 25 to 95°C by using the instrument software controlled temperature ramping program and the following parameters: ΔT of 20°C/h, 0.2°C step resolution, and 1 s response.

Equilibrium denaturation of Δ19PD induced by Gdn-HCl was followed by measuring the ellipticity of the sample at 222 nm in a 0.1-cm path-length cell at 30°C. Samples at each Gdn-HCl concentration were obtained by mixing PPS and 8 M Gdn-HCl in PPS (pH 7.5) in the appropriate ratio and adding enzyme to 2.8 μM. Samples (1 mL) were equilibrated at ambient temperature for 20 h in capped Eppendorf tubes, and then ellipticities were measured from 210 to 230 nm using the instrument parameters listed above. The values at 222 nm (average of five readings) were corrected for background

signal from the buffer. The accurate concentration of 8 M Gdn-HCl in PPS was calculated from its refractive index (*124*).

2.1.6.2 Steady-State Fluorescence

Gdn-HCl-induced unfolding of Δ19PD was followed by fluorescence at 30°C using an Aminco Bowman Series 2 Luminescence Spectrometer equipped with a temperature-controlled cell holder. Excitation wavelengths were set to 280 nm or 295 nm, and emission scans were recorded from 300 to 400 nm. Excitation and emission slits were set to 4 nm. Measurements were performed in PPS buffer (reaction volume 2 mL) using a 1 cm x 1 cm cuvette. Incubation of Δ19PD (3 μM monomer) in Gdn-HCl-containing PPS were performed as outlined for CD experiments. Fluorescence intensities were compared with that of a solution containing NATA (6 μM) and NAYA (30 μM) having the same concentration of Trp and Tyr as the protein solution. Emission spectra were corrected for buffer blank and for the inner filter effect (*125*) using the equation 2.1:

$$F_{corr}=F_{obs} \times \text{antilog}[(A_{ex}+A_{em})/2] \qquad (2.1)$$

F_{obs} and F_{corr} represent observed fluorescence intensities and those corrected for the inner filter effect respectively. Absorbance readings (A), (cell plus sample blanked on air), were determined both at excitation (ex) and emission (em) wavelengths.

To determine if denaturation was reversible, 30 μM Δ19PD in 0 M, 3 M and 5 M Gdn-HCl were incubated for 20 h at room temperature. An aliquot of the denatured sample was then diluted 10-fold then incubated at room temperature for 2 h. Fluorescence

spectra and enzyme activities were recorded for each sample and compared to a protein incubated for the same time in the absence of denaturant. Measurements at 20, 24 and 36 h gave the same values.

2.1.6.3 ANS Fluorescence Experiments

Δ19PD (3 μM monomer) prepared in different concentrations of PPS-buffered Gdn-HCl (as described above) were incubated with 30 μM 1-anilino-8-naphthalene sulfonic acid (ANS) in the dark at 30°C. The total reaction volume was 2 mL. Fluorescence emission spectra were recorded from 400 to 600 nm with excitation at 370 nm and using bandwidths of 4 nm using an Aminco Bowman Series 2 Luminescence Spectrometer equipped with a temperature-controlled cell holder. The net fluorescence enhancement due to ANS binding to the protein was obtained by subtracting appropriate blank spectra of ANS in the corresponding denaturation buffer and corrected for inner filter effects as described above. ANS did not alter enzyme activity.

2.1.7 Determination of Dissociation Constants for Substrates

Values for the dissociation of NAD^+ or prephenate from the complex with Δ19PD were determined at 30°C by monitoring the quenching of protein intrinsic fluorescence. Excitation and emission wavelengths were set at 295 nm and 333 nm respectively, with bandwidths of 4 nm. Enzyme, NAD^+, and prephenate were prepared in PPS buffer. Titrations were performed by the progressive addition of NAD^+ (0.2-20 μM) or prephenate (2-480 μM) to PPS (2 mL) containing 0.24 μM or 1.6 μM monomer. Samples were mixed by gentle inversion and the reaction was allowed to equilibrate for 2 min

prior to recording measurements. The fluorescence data were corrected for inner filter effects, as well as for dilution and background fluorescence. A dissociation constant was determined by fitting the data to the Michaelis-Menten equation or the quadratic equation (*126*) (Equation 2.2) using Grafit 5.0:

$$\Delta F = \Delta F_m(([L_t]+[E_t]+K_d)-(([L]_t+[E_t]+K_d)^2-4[L_t][E_t])^{0.5})/(2[E_t]) \quad (2.2)$$

ΔF is the difference in fluorescence intensities in presence and absence of the titrant, ΔF_m is the maximum change in fluorescence intensity, $[L_t]$ is the total concentration of titrant, $[E_t]$ is the total enzyme concentration and K_d is the dissociation constant.

2.1.8 Fluorescence Quenching

The titration of Δ19PD with acrylamide and KI were performed at 30°C in PPS buffer. Excitation and emission wavelengths were set at 295 nm and 340, respectively, with bandwidths of 4 nm each. Sodium thiosulfate (100 μM) was added to solutions of KI to prevent I_3^- formation, which interferes with Trp fluorescence. Defined amounts of quencher (2-5 μL) were added from a stock of 5.0 M to a 2 mL (3 μM monomer) protein solution. Acrylamide and KI did not significantly inhibit enzyme activity (<5% loss of activity) at the amounts used in the quenching experiments. To determine if substrates protected against quenching, 3 μM monomer was incubated either with NAD^+ or prephenate (also in PPS) prior to the addition of acrylamide or KI. The effect of Gdn-HCl on fluorescence quenching was examined at 30°C by the addition of acrylamide to a reaction mixture containing 3 μM monomer and 0-6 M Gdn-HCl in PPS. Samples were

incubated for 20 h at room temperature prior to measurements. Emission spectra represented the average of three scans (2 nm/s), and were corrected for background and protein dilution, and when appropriate, the inner filter effect (*125*).

Fluorescence quenching data were analyzed by the Stern-Volmer equation 2.3 where static quenching is neglected (*127*):

$$F_o/F = 1 + K_{SV}[Q] \tag{2.3}$$

F_o and F are the fluorescence intensities in the absence and presence of the quencher, respectively; [Q] is the concentration of the quencher; and K_{SV} is the collisional Stern-Volmer constant, which is a direct measure of the quenching efficiency. In a protein containing multiple Trp residues, the presence of different classes of Trp residues is reflected by a downward curvature in the Stern-Volmer plot. The fraction of total fluorophore accessible to the quencher in a heterogeneous system was determined using equation 2.4, a modified Stern-Volmer plot (*127*):

$$F_o/(F_o-F) = 1/f_a + 1/[Q]K_Q f_a \tag{2.4}$$

K_Q is the modified quenching constant and f_a is the fraction of the initial fluorescence accessible to the quencher. Values for K_Q and f_a can be determined from a plot of $F_o/(F_o-F)$ versus 1/[Q].

2.2 RESULTS

2.2.1 Protein Purification and Subunit Composition of Full-Length PD

The recombinant form of PD from *A. aeolicus* expressed in *E. coli* contained a 20-residues N-terminal extension that included a hexa-His tag to facilitate purification by Ni-NTA affinity chromatography and a thrombin recognition site. Although it was expected that the 311 amino acid His-tagged PD purified to homogeneity would yield a single band on a denaturing polyacrylamide gel, previous work reported by Aponte (*106*) and later by Sun *et al.* (*48*) showed that purified His-tagged PD yielded two distinct bands representing full-length (~37 kDa) and shortened (~34 kDa) forms of the protein (*106*). We have reproduced these studies by Aponte on the expression and purification of PD and obtained the same results. Figure 2.1 lane 2 shows that the His-tagged PD, purified according to the procedure outlined in material and methods is resolved as a doublet by 15% SDS-PAGE. Moreover, treatment of the sample from lane 2 with thrombin yielded protein (lane 4) that appeared by Coomassie staining as a single band of about 34 kDa. This pattern was also observed by Aponte; the longer form appeared to be converted into the shorter form prompting the assumption that the cleavage site was at the thrombin recognition sequence. Also in keeping with the previous studies by Aponte(*106*) and Sun *et al.* (*48*), it was observed that the smaller sized protein flowed through the Ni-NTA column whereas the larger species bound to the column (data not shown), indicating that the lower molecular species is a C-terminal fragment that lacked the N-terminal hexa-His tag. Thus, under native conditions, PD appeared to chromatograph on affinity resin as a heterodimer (a monomer each of full-length His-tagged and shortened non-tagged forms).

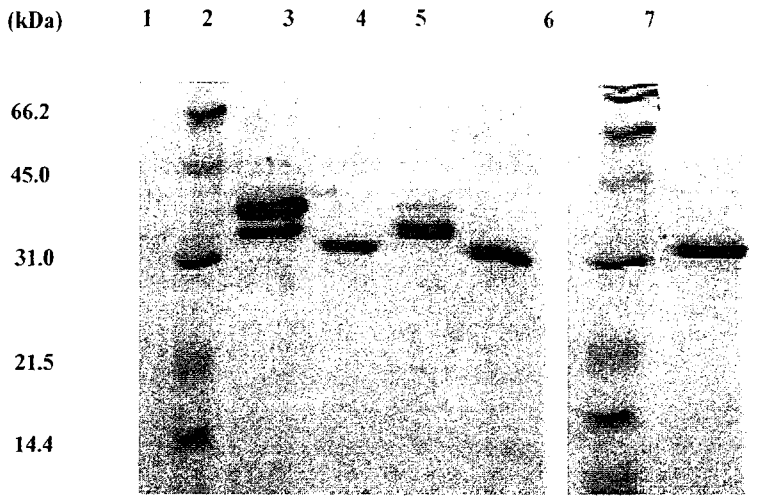

Figure 2.1: SDS-polyacrylamide gel electrophoresis of purified *A. aeolicus* PD.

Lanes 1 and 6, broad range protein molecular weight makers (Fermentas). Lane 2, pooled fractions of His-tagged PD after Ni-NTA affinity chromatography. Two distinct bands representing full-length (~37 kDa) and shortened non-tagged (~34 kDa) forms of the protein are observed. Lane 3, His-tagged PD treated with trypsin (final ratio 20:1 (w/w)). Lane 4, His-tagged PD treated with thrombin (final ratio 1000:1 (w/w)). Lane 5, His-tagged PD treated with both thrombin and trypsin. Lane 7, aged thrombin-cleaved PD (one year at 4°C in storage buffer).

Interestingly, treatment of either full-length or thrombin-treated PD with the protease trypsin (lanes 3 and 5, respectively) or prolonged storage of the protein at 4°C (lane 7) resulted in further cleavage of the monomer to a 32 kDa fragment as judged by SDS-PAGE analysis.

Development of a reliable protocol for ESI-MS analysis of PD confirmed the identity of each protein. In addition, the results supported the idea that the shortened form was produced by cleavage at the N-terminal region of PD. Figure 2.2 shows a schematic representation of the expression and primary sequence of PD. For clarity, amino acids are numbered for PD from 1-311, beginning with PD's authentic Met as annotated from the database; the residues of the tag are not numbered. For heterodimeric PD, analysis showed that the His-tagged subunit was post-translationally modified as it lacked the first Met at the tag's N-terminus (expected $[M+H^+]$, 36 881.6 Da; observed, 36 880.5 Da). The smaller 34 kDa subunit commenced at Ser5 in PD (expected $[M+H^+]$, 34 419.9 Da; observed, 34 419.5 Da) and indicated that the shortened form was generated by cleavage at a site downstream of the thrombin recognition site. As expected results for the purified thrombin-treated PD verified cleavage at the thrombin recognition site, between Arg and Gly within the N-terminal tag (expected $[M+H^+]$, 35 130.8 Da; observed, 35 130.6 Da) (Fig. 2.3 A). The sample also contained the 34 kDa product as a minor species (~15%) (Fig. 2.3 B). In summary, the shortened form of the recombinant PD was not produced by cleavage at the thrombin recognition site as suggested by Aponte (*106*), nor was it produced by translation starting at positions 1, 7, 30, 38 or 41 of PD (the latter two would result in truncation of the NAD^+-binding domain). Moreover, none of the peaks resolved

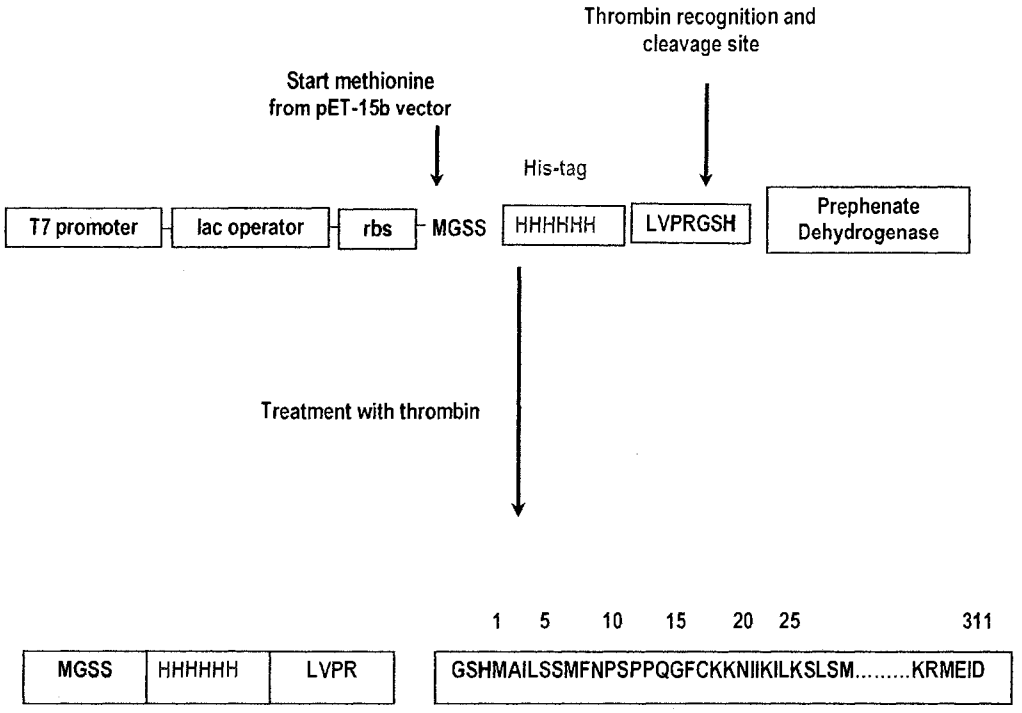

Figure 2.2: Schematic representation of the organization of the expression/cloning region of pET-15b vector containing *A. aeolicus tyrA*. Amino acids are numbered from 1 to 311, starting at PD's authentic methionine. Amino acids from the tag are not numbered.

by ESI- MS matched mass values predicted for cleavage within the protein's C-terminal region.

We found that purified thrombin-treated PD (1-10 mg/mL) remained stable and fully active when stored at -86°C. As mentioned previously however, the enzyme was susceptible to further N-terminal degradation if kept for extended periods of time at 4°C, or if purified in the absence of insufficient amounts of protease inhibitors. For example, when either His-tagged or thrombin-cleaved PD stored at 4°C for one year was subjected to ESI-MS, a major single peak was observed at 32 313 Da. ESI-MS data for His-tagged PD is shown Figure 2.3 C while SDS-PAGE analysis of the same sample is shown Figure 2.1 lane 7. This peak matched the mass predicted for a shortened protein resulting from the proteolytic cleavage at the N-terminus of the recombinant PD at Lys23 (expected $[M+H^+]$, 32 315.4 Da; observed, 32 313.0 Da). Additionally, SDS-PAGE analysis of purified PD treated with trypsin (Figure 2.1 lanes 3 and 5) revealed further cleavage at the protein's N-terminal region, although ESI-MS analysis on this stable fragment was not performed to confirm the exact site of cleavage.

Additional evidence strengthening our hypothesis of a truncation at the N-terminal region of PD comes from the results of MALDI-ToF-MS analysis of *in-solution* and *in-gel* tryptic digestions. Table 2.1 summarizes the calculated masses of the peptides from *in-silico* digestion of PD along with the peptides observed by MALDI-ToF-MS analysis. It is worth noting that these experiments were conducted prior to ESI-MS

Figure 2.3: Deconvoluted electrospray ionization mass spectra of PD (A) intact *A. aeolicus* thrombin-treated PD, expected $[M+H^+]$ of 35 130 Da. **(B)** Minor species of a shortened form of PD, observed $[M+H^+]$ of 34 419 Da. **(C)** A year-old sample of His-tagged PD showing a major peak at $[M+H^+]$ of 32 313 Da and corresponding to a cleavage at Lys23. The enzymes (2-5 μM monomer) were prepared as described in section 2.1.5.1.1 then resuspended in 0.5-1 mL of a solution of 30% methanol/0.2% formic acid (v/v) immediately prior to direct injection.

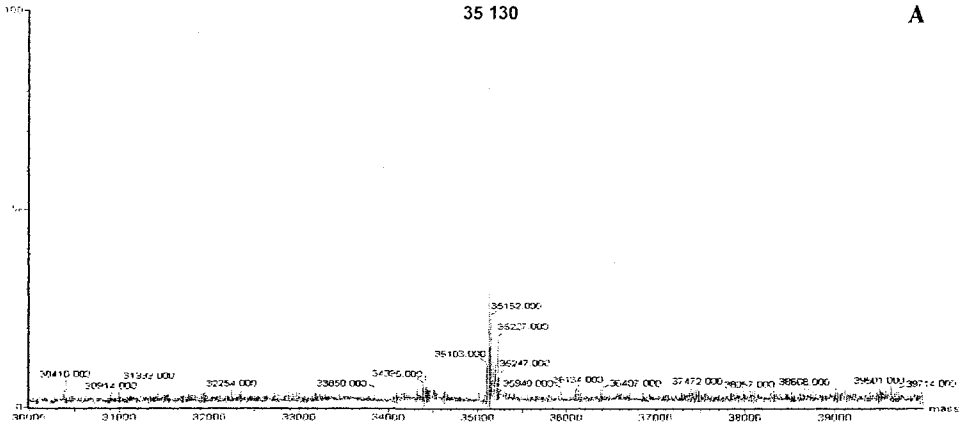
35 130
A
35152.000
35227.000
35103.000
36247.000
30410.000
30941.000
31997.000
32254.000
33850.000
34365.000
35940.000
36134.000
36407.000
37472.000
38608.000
39540.000
39714.000
mass

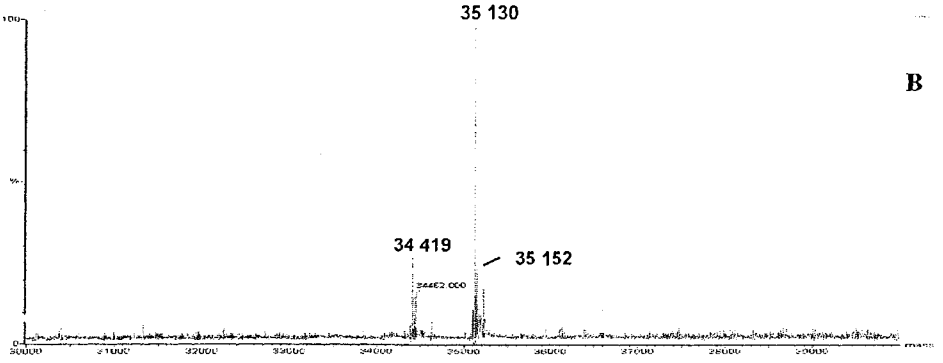
35 130
B
34 419
35 152
34462.000
mass

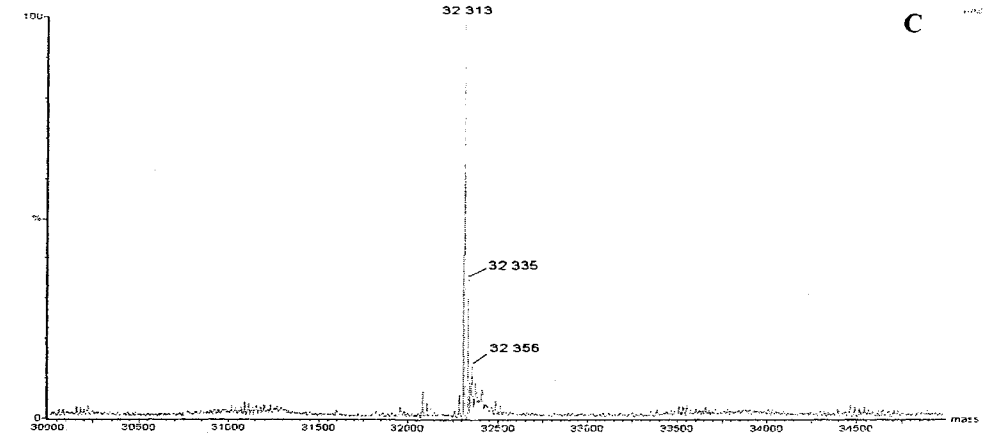
32 313
C
32 335
32 356
mass

analysis of the protein during which time the development of a reliable protocol for direct injection was underway.

The combined results from *in-gel* and *in-solution* tryptic digestion resulted in 73% coverage for thrombin-treated PD, with 13 peptides detected out of the 17 that would be theoretically generated by trypsin activity with no miscleavages. Using HCCA as the matrix, the detection range of the MALDI cannot resolve fragments with high or low molecular weights (above 5 kDa and below 700 Da, respectively). Additionally worth noting, the high percentage coverage could only be obtained by analyzing multiple samples of PD, each trial yielding about 10-20% sequence coverage but presumably exposing different regions of the protein.

As shown in Figure 2.4, the predicted C-terminal fragments were detected but none of the peptides belonging to the N-terminal region were observed, confirming that the truncation might have occurred between residues 1-30. Surprisingly, MALDI-ToF-MS analysis of several *in-solution* tryptic digests failed to reveal the fragment comprising PD's amino acid 1-21 (see Table 2.1). Additionally, residues 192-242 were not detected. Presumably, this large peptide fragment could not be resolved using the HCCA matrix. A similar although not identical pattern was also reported by Christendat's lab (*48*); only peptides commencing at position 61 in the primary sequence could be identified. Based on the findings from MALDI-ToF-MS and the results from secondary structure prediction, six protein variants lacking the first 19, 25, 28, 36, 52 and 55 amino acids were constructed and expressed by Christendat and coworkers for crystallography trials (numbered here from PD's Met starting site) and one of them, Δ19PD, yielded crystals diffracting to a high resolution (*48*).

2.2.2 Purification and Monomer Molecular Weight Determination of Δ19PD

The expression and purification of Δ19PD was performed as described for PD with minor modifications (see section 2.1.2). The results of the purification are summarized in Table 2.2 and Figure 2.5 and indicated that heat treatment (Fig. 2.5, lane 3) and affinity chromatography (Fig. 2.5, lane 6) were effective purification steps. The yield of Δ19PD is routinely ~14 mg/L of culture, and neither the His-tagged nor thrombin-treated forms showed heterogeneity during purification. The mass of Δ19PD was verified by ESI-MS (expected $[M+H^+]$ of His-tagged and thrombin-treated forms, 35 078.5 Da and 33 196.5 Da, respectively; observed, 35 077.1 Da and 33 196.3 Da, respectively) (Fig. 2.6), and was checked routinely throughout our studies. We noted, as with PD, that with prolonged storage at 4°C in the absence of sufficient amount of fresh protease inhibitors, Δ19PD also degraded to a Δ23 fragment (expected $[M+H^+]$, 32 315.4 Da; observed 32 313.0 Da). Some studies presented in this thesis have been performed only on PD, while others on both PD and Δ19PD. Detailed spectroscopic studies were pursued on the homogeneous, crystallizable Δ19PD form.

Table 2.1: MALDI-ToF MS analysis of thrombin-treated *A. aeolicus* PD proteolytic fragments generated by trypsin

Position[a]	Calculated[b] $[M+H]^+$	Observed[c] $[M+H]^+$	Peptide Sequence
192-242	5694.8326		VWEVGGVVEYMSPELHDYVFGVVSHLPHAVAFALVDTLIHMSTPEVDLFK
1-21	2236.0347		**GSH**MAILSSMFNPSPPQGFCK
30-50	2142.1085	2142.325	SLSMQNVLIVGVGFMGGSFAK
113-131[d]	2054.0651	2054.589	KLSYILSEDATVTDQGSVK
114-131	1925.9702		LSYILSEDATVTDQGSVK
90-105	1824.8836	1824.652	VEDFSPDFVMLSSPVR
74-89	1602.8584	1603.102	AVDLGIDEGTTSIAK
158-171	1573.7380	1573.457	SGVEYSLDNLYEGK
61-73	1498.7424	1498.502	IYGYDINPESISK
145-157[d]	1368.7382	1368.996	RFVGGHPIAGTEK
294-304	1351.6627	1351.971	EAEEELVEYLK
134-144	1276.7147	1276.528	LVYDLENILGK
146-157	1212.6371	1212.811	FVGGHPIAGTEK
257-263	904.4345	904.746	SDRPIMWR
264-270	878.4618	878.145	DIFLENK
276-282	793.4090	793.294	AIEGFEK
173-179	771.4974		VILTPTK
243-249	725.3617	725.263	YPGGGFK
283-288	711.4148	711.214	SLNHLK

[a] Amino acids are numbered commencing after the fusion protein's thrombin cleavage site (LVPR**GSH**).
[b] The average singly protonated mass of the tryptic product is shown as calculated using PeptideMass provided by Expasy Proteomics Server. Results display peptides with a MW higher than 700 Da. (http://ca.expasy.org/tools/peptide-mass.pl).
[c] Tryptic digestion was performed as outlined in section 2.1.5.1.2 and peptides were analyzed by MALDI-ToF mass spectrometry.
[d] Peptide resulting from one miscleavage.

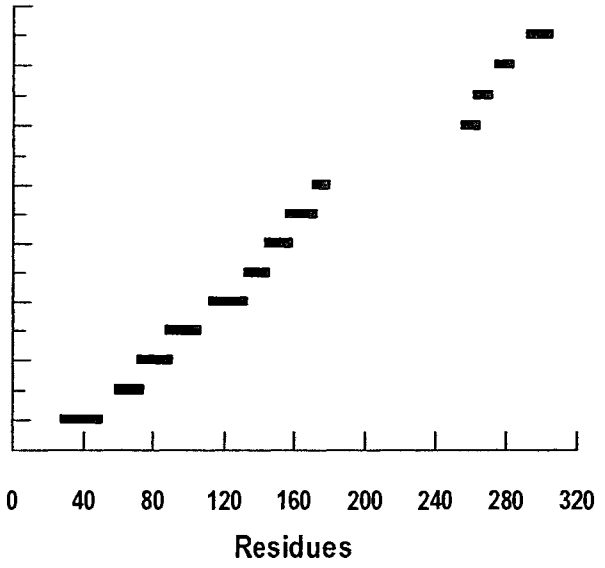

Figure 2.4: Sequence coverage obtained by MALDI analysis of peptides generated by tryptic digestion of thrombin-treated *A. aeolicus* PD.

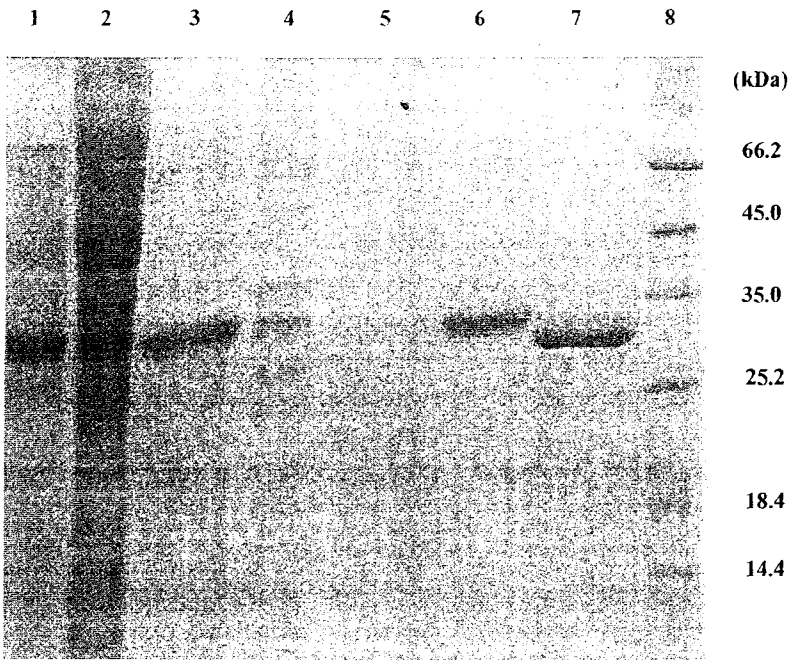

Figure 2.5: SDS-polyacrylamide gel electrophoresis of purified *A. aeolicus* Δ19PD. Lane 1, cell lysate (1/10 dilution). Lane 2, cell-free extract (supernatant). Lane 3, supernatant after heat treatment. Lane 4, flow through from Ni-NTA column. Lane 5, final wash from Ni-NTA column. Lane 6, pooled fractions of His-tagged Δ19PD after Ni-NTA affinity chromatography. Lane 7, Δ19PD treated with thrombin (1000:1 (w/w)). Lane 8, protein molecular weight markers.

Table 2.2: Purification table of *A. aeolicus* Δ19PD

Step	Volume (mL)	Total Protein (mg)	Total Activity[b] (U)	Specific Activity[b] (U/mg)	Recovery (%)	Purification (fold)
Cell-free extract	85.0	1062	1912	1.8	100	1.0
Heat Treatement	78.0	405	1701	4.2	89	2.3
Ni-NTA:						
Flow through	90.0	206	227	1.1	12	0.6
30 mM imidazole wash	50.0	92	55	0.6	3	0.3
300 mM imidazole wash	15.0	29	557	19.2	29	10.7
Thrombin treatment[c]	15.5	28	588	21.0	31	11.7

[a] Purification was achieved from a 3.0 L culture of *E. coli* BL21(DE3) harboring pΔ19PD

[b] Determined at 55 °C

[c] Values calculated from protease treatment of entire 300 mM imidazole wash

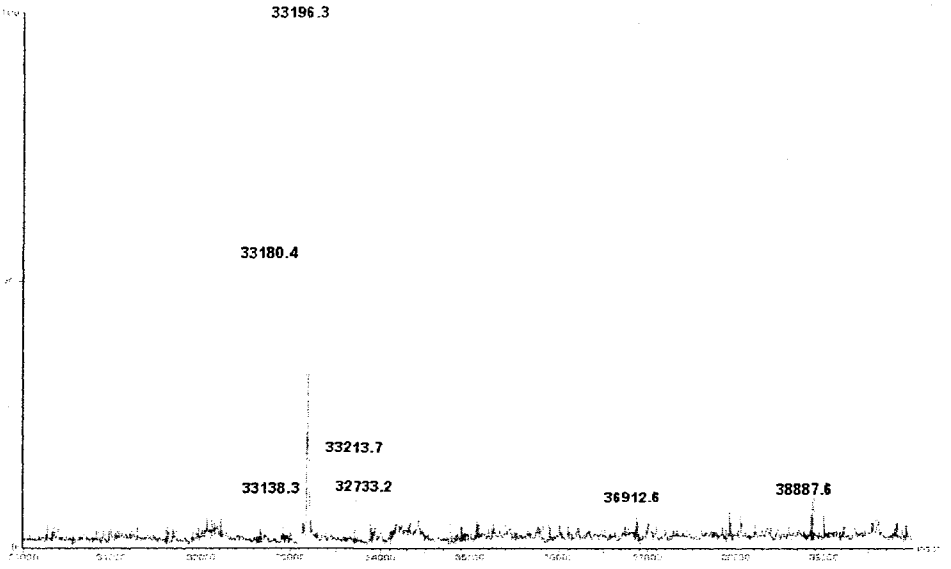

Figure 2.6: Electrospray ionization mass spectra of intact *A. aeolicus* thrombin treated Δ19PD. The enzyme (~5 μM monomer) was resuspended in 0.5-1 mL of a solution of 30% methanol/0.2% FA (v/v) immediately prior to direct injection. ESI-MS method is described in Section 2.1.5.1. Expected $[M+H^+]$ was 33 196.5 Da.

2.2.3 Native Molecular Weight

Analysis of PD and Δ19PD by size exclusion FPLC from 0.1 to 2 mg/mL yielded values of 54 kDa and 52 kDa, respectively (Appendix 2A). These values were less than those predicted for dimeric forms, ~70 kDa and ~66 kDa. However, masses calculated from the primary sequence more closely matched those obtained using sedimentation velocity analytical ultracentrifugation. Average molecular masses of proteins and sedimentation coefficients corrected to 20°C in water are summarized in Table 2.3. Data obtained for PD with both FPLC and AUC are in good agreement with Aponte's previous findings (*106*). Our results were consistent with the thermophilic PDs being dimeric in solution but more compact than the commercially available globular proteins used to calibrate size exclusion columns (*128*). Occasionally our PD and Δ19PD preparations contained a catalytically active oligomer of ~160 kDa (less than 10% of the sample peak on FPLC), which could be detected in the sedimentation velocity analyses (see Appendix 2B). For PD we attributed this oligomer, in part, to disulfide linked subunits (there is one cysteine/monomer). Heterogeneity was removed by size exclusion chromatography prior to spectroscopic analysis.

Table 2.3: Results from sedimentation velocity experiments for PD and Δ19PD.

	PD	Δ19PD
Average molecular weight (kDa)	67.9	62.5
$S_{20,w}$	4.72	4.9

Purified thrombin-cleaved enzymes were exchanged into a buffer containing 50 mM potassium phosphate buffer, 0.3 M NaCl and 0.5 mM TCEP (pH 7.5). PD and Δ19PD (25 μM and 37 μM, respectively) were centrifuged for 10 h at 35,000 rpm and 30°C. Absorbance (280 nm) was collected in continuous mode with a step size of 0.005 cm and five replicate readings at each point. Raw sedimentation data and best-fit *c*(s) distributions are presented in Appendix 2B.

2.2.4 Thermal Stability

The room temperature far-UV CD spectra for PD, Δ19PD, and CM-PD exhibited two local minima at 208 nm and 222 nm (Fig. 2.7) and are typical for proteins that contain a significant content of α-helical structure. Helical contents predicted from the primary sequences of *E. coli* CM-PD and *A. aeolicus* PD (or Δ19PD), using several commercially available programs (PredictProtein (*129*) and Antheprot (*130*)) were ~60% and 50%, respectively. We attempted to obtain values for the apparent melting temperatures (T_m) for the proteins by measuring the ellipticity at 222 nm of the samples when heated from 25° to 95°C. However, under conditions that yielded a very cooperative and irreversible temperature dependent unfolding curve for *E. coli* CM-PD (T_m = 57°C) (Fig. 2.8), the thermostable PDs showed a gradual but steady loss of signal, and post transition baselines could not be established (T_m values >95°C). Aponte reported that most of the CD signal (>95%) from PD could be regained upon cooling (*106*). However, activity measurements at 30° and 55°C that we performed on such a sample showed that K_m values for prephenate were increased twofold and k_{cat} ~20% and implied that refolding to the native structure was not complete.

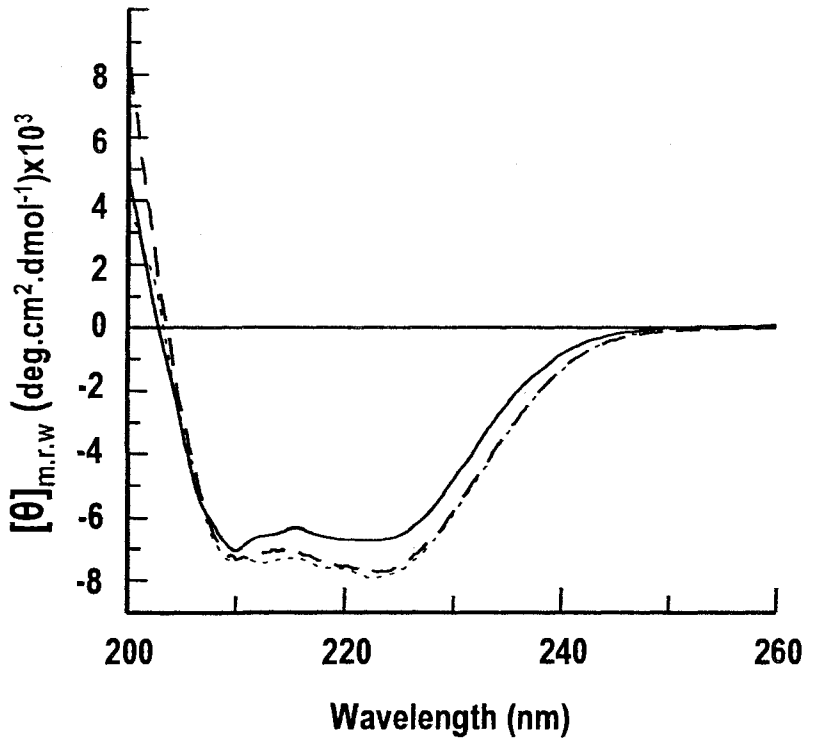

Figure 2.7: Far-UV CD spectra of *E. coli* and *A. aeolicus* enzymes. CM-PD (solid line), PD (dashed) and Δ19PD (dotted), (18 μM (CM-PD) and 21 μM monomer, respectively). [θ] denotes mean residue ellipticity. Spectra were recorded in 0.05 cm path length circular cell connected to a thermostated circulating water bath. Proteins were in 50 mM potassium phosphate, 75 mM NaCl, pH 7.5. For CM-PD, 25% glycerol (v/v) was added to the buffer. Spectra were recorded at 25°C by averaging 10 wavelength scans from 260 to 200 nm (1 nm bandwidth) in 0.2 nm steps at a rate of 50 nm/min, and 0.25 s response.

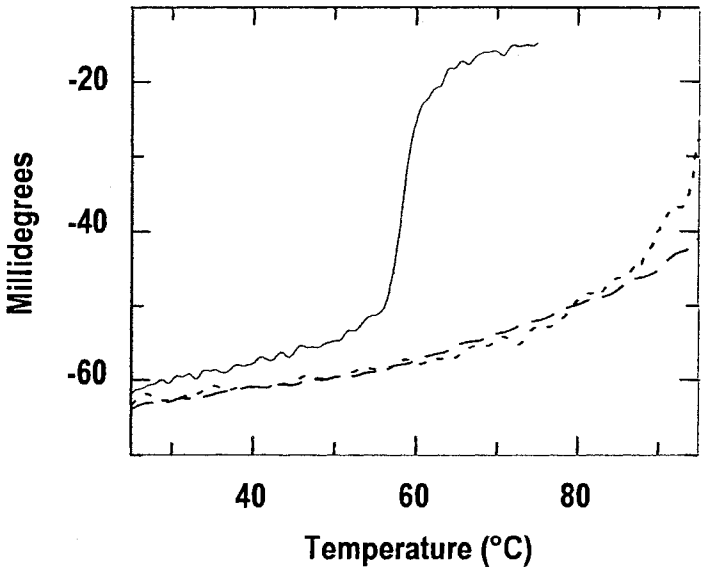

Figure 2.8: Thermal denaturations monitored by CD spectroscopy at 222 nm. Thermal denaturations with 0.75 mg/mL of CM-PD (solid line), PD (dashed) and Δ19PD (dotted) were carried out by following the ellipticity at 222 nm from 25 to 95°C under the same conditions except that for CM-PD, buffer was supplemented with 25% (v/v) glycerol.

2.2.5 Denaturation Studies with Gdn-HCl

The stability of Δ19PD was further addressed by monitoring Gdn-HCl-induced protein unfolding using the CD signal at 222 nm as a probe of α-helical secondary structure and using Trp fluorescence as a probe of tertiary structure. Gdn-HCl was selected as the denaturant after noting that PD did not fully unfold in urea, even at concentrations up to 10 M, as observed by Aponte (*106*).

As shown in Figure 2.9A, the intensity of the CD signal diminished with increasing concentration of Gdn-HCl. When the data was plotted as percent fraction folded as a function of denaturant concentration (Fig. 2.9B), a multistate transition was observed with a distinct plateau between 3 and 4 M Gdn-HCl, and a sharp decrease in fraction folded from 4 to 5 M denaturant. A value for the midpoint in the transition from folded to unfolded conformation ($D_{1/2}$) of 4.8 M was estimated from the plot. Dehydrogenase specific activity increased 220% at 0.5 M Gdn-HCl but was markedly reduced by 3 M denaturant (Fig. 2.10). The presence of 0.5 M Gdn-HCl also had inverse effects on the affinity for prephenate and NAD^+, causing a fourfold increase in K_m for prephenate (to 154 μM) and a twofold reduction for NAD^+ (to 21 μM), relative to the values in the absence of Gdn-HCl (41 μM and 53 μM, respectively). The increase in specific activity in the presence of 0.5 M Gdn-HCl did not overcome the decrease in affinity for prephenate.

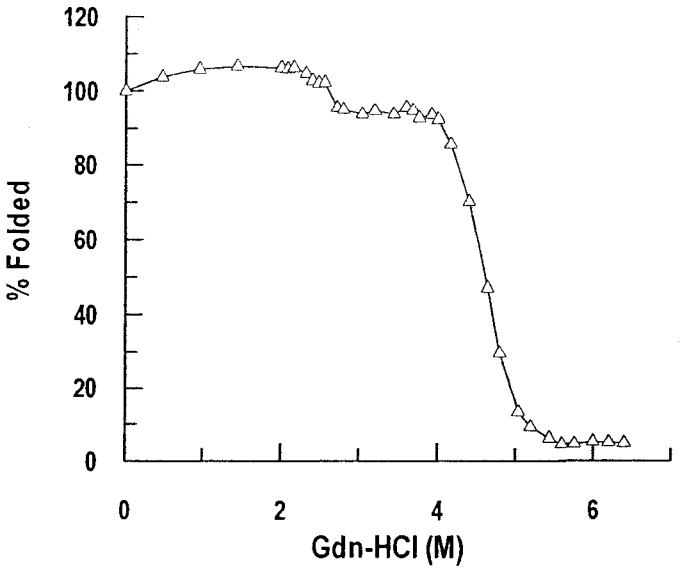

Figure 2.9: The effect of Gdn-HCl on CD signal of *A. aeolicus* Δ19PD. Plot of fraction folded as a function of Gdn-HCl concentration probed by CD at 222 nm (Δ). Fraction unfolded (F_u) was calculated as described by Pace and Scholtz (*124*). Measurements were recorded in 0.05 cm path length circular cell connected to a thermostated circulating water bath. Protein (2.8 μM monomer) was incubated in 50 mM potassium phosphate, 75 mM NaCl and different concentrations of Gdn-HCl at pH 7.5 for 24 h prior to collecting spectra.

Intrinsic Trp fluorescence is very sensitive to the hydrophobic or hydrophilic environments of a folded protein and is a good probe of changes in the accessibility of fluorophores as a function of denaturant. Δ19PD contains two Trp residues per monomer, at positions 190 and 259, which can contribute to the fluorescence spectrum of the protein. Excitation at either 280 or 295 nm (Fig. 2.11) resulted in an unusual emission spectrum, with two maxima at 317 nm and 330 nm. The two maxima were observed in the spectrum even in the presence of three times the protein concentration; therefore the peaks were not an artifact due to a Raman band. These results suggested that the fluorescence emission is dominated by Trp residues residing in hydrophobic environments, one very hydrophobic. The bimodal emission spectra decreased and shifted to a single peak at 350 nm in the presence of 6 M Gdn-HCl as the Trp side chains became solvent-exposed, and resonance energy transfer from one or more of the 10 Tyr molecules per monomer were alleviated in the unfolded protein. A spectrum of 6 μM NATA yielded an emission maximum of 355 nm and indicated that, even at 6 M Gdn-HCl, one or more of the protein Trp residues were not completely solvent-exposed (Fig. 2.12). Although low concentrations of Gdn-HCl had a significant effect on kinetic parameters of the reaction, inspection of the fluorescence emission spectra between 0 and 1 M Gdn-HCl indicated, surprisingly, no shift in the emission maximum at either 317 or 330 nm. When the results from both fluorescence and CD measurements were replotted as percent folded versus Gdn-HCl concentration, the two data sets were similar but not coincident (Fig. 2.13).

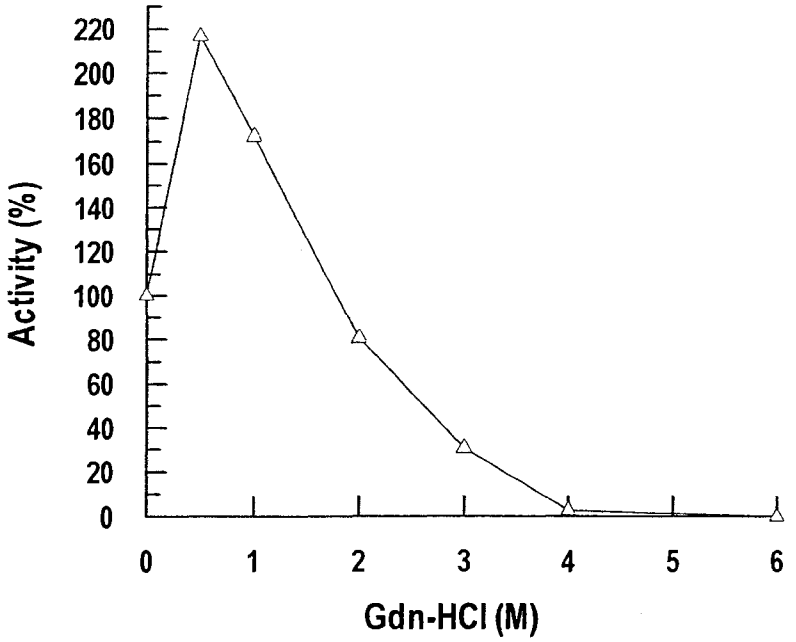

Figure 2.10: The effect of Gdn-HCl on enzyme activity of *A. aeolicus* Δ19PD. Dehydrogenase activity in the presence of increasing concentrations of Gdn-HCl was determined at 30°C using 1 mM prephenate and 2 mM NAD^+ as described section 2.1.4. Specific activity was expressed as a percentage of the value obtained in the absence of denaturant.

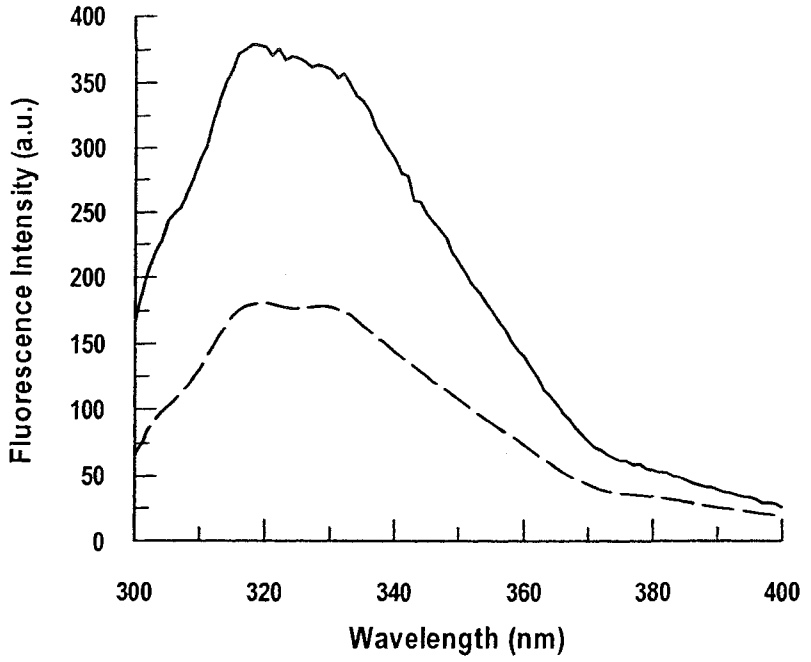

Figure 2.11: Fluorescence emission spectra of Δ19PD. Excitation wavelength was set at 280 nm (solid line) or 295 nm (dashed line). Emission spectra of 2.8 μM monomer Δ19PD in 50 mM potassium phosphate, 75 mM NaCl at pH 7.5 were recorded from 300 to 400 nm in a 3 mL cuvette. Both emission and excitation bandwidths were set at 4 nm. Fluorescence intensity is shown in arbitrary units (a.u.)

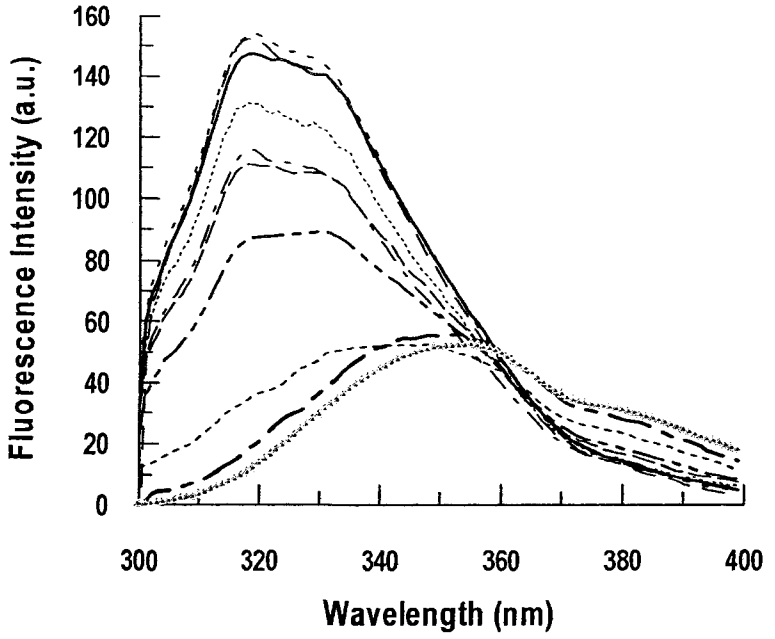

Figure 2.12: Selected fluorescence emission spectra of Δ19PD during Gdn-HCl-induced unfolding. Excitation was at 295 nm. Emission spectra were taken after 20 h incubation of the sample (3 μM monomer Δ19PD) in 50 mM potassium phosphate, 75 mM NaCl at pH 7.5 with increasing concentrations of Gdn-HCl. Denaturant concentrations were 0 M (thick solid line), 1 M (small-dashed line), 2 M (large-dashed line), 2.9 M (dotted line), 3 M (dashed/dotted line), 4 M (large-dashed line), 4.7 M (dashed/dotted/dotted line), 5 M (thick dotted line) and 6 M (thick dotted/dashed line) of Gdn-HCl. The standards (6 μM NATA/ 30 μM NAYA) in 6 M Gdn-HCl are shown as triangles. Fluorescence intensity is shown in arbitrary units (a.u.).

Gdn-HCl-induced unfolding of Δ19PD appeared reversible, as determined spectroscopically and enzymatically (data not shown). Refolded protein yielded fluorescence spectra similar if not identical to those obtained prior to unfolding, after correction for enzyme concentration differences. Moreover, >95% of the enzyme activity was recovered after refolding by dilution.

To determine if dimeric Δ19PD denatured *via* a pathway involving a compact folded monomer and/or a more loosely folded dimer, size exclusion chromatography was performed in the presence of 0-5 M Gdn-HCl at 25°C (Fig. 2.14). A single peak (dimeric enzyme) was observed up to 2 M Gdn-HCl, which then shifted steadily to shorter retention times at higher denaturant concentrations, indicating progressive unfolding of the dimer. By 5 M Gdn-HCl, a second peak with a long retention time (that we interpreted as unfolded monomers) was also resolved. At 3 M Gdn-HCl and above, however, a high molecular weight form of the enzyme (not in the void volume) appeared. Taken together with the spectroscopic results, the data suggest that the quaternary structure of Δ19PD is very stable; dimeric Δ19PD unfolds prior to subunit separation, but this unfolding accompanies the formation of an oligomeric form. All species then denature to unfolded monomers. The complexity of this pathway precludes fitting data to a model, which would yield thermodynamic parameters for the unfolding reaction.

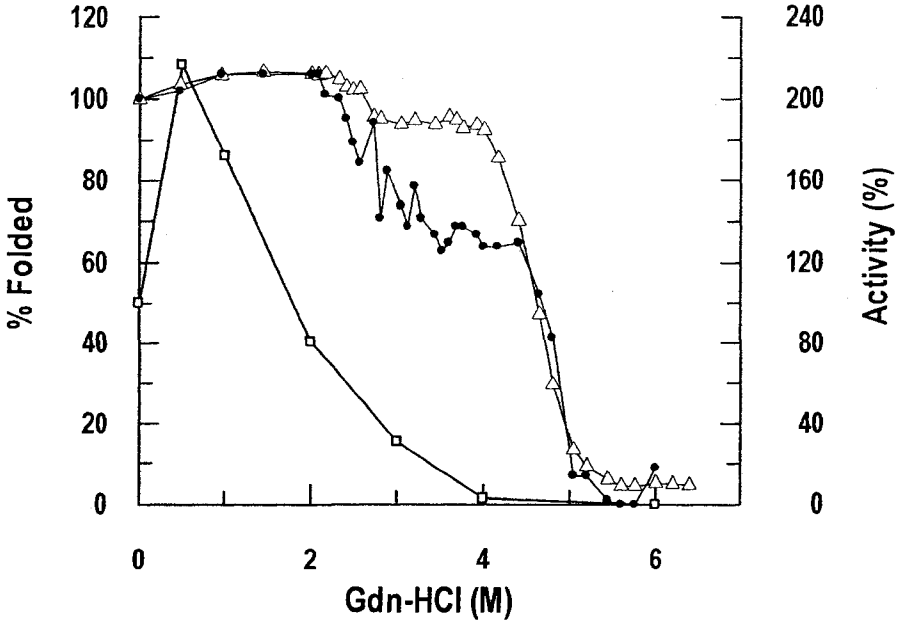

Figure 2.13: Overlay of the effect of Gdn-HCl on intrinsic fluorescence, CD signal, and enzyme activity of *A. aeolicus* Δ19PD. Plot of fraction folded as a function of Gdn-HCl concentration probed by CD at 222 nm (Δ) and by Trp fluorescence emission at 317 nm (•). Fraction unfolded (F_u) was calculated as described by Pace (*124*). Enzymatic activity in the presence of Gdn-HCl was determined at 30°C using 1 mM prephenate and 2 mM NAD^+. The right axis represents the percent residual activity (□).

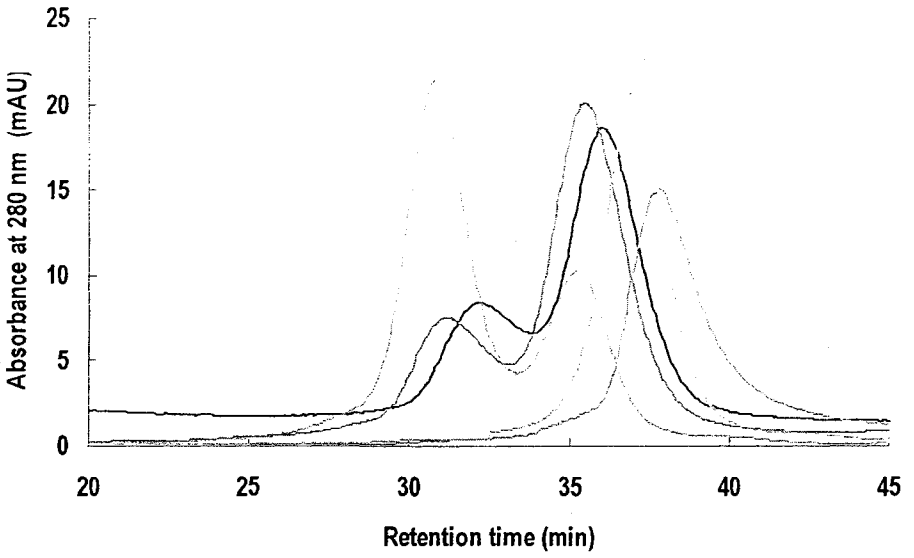

Figure 2.14: Gdn-HCl-induced unfolding of PD monitored by Fast Protein Liquid Chromatography. PD (0.1 mg/mL) was incubated for 20 h at ambient temperature in a buffer containing 50 mM potassium phosphate, 150 mM NaCl at pH 7.5 with increasing concentrations of Gdn-HCl prior to injection. Chromatography was performed with mobile phases containing the buffer with the appropriate concentration of denaturant at a flow rate of 0.4 mL/min and injection volume of 500 µL. Denaturant concentrations were 0 M (blue line), 2 M (grey line), 3 M (black line), 4 M (red line) and 5 M (green line) of Gdn-HCl. Elution was monitored at 256, 280 and 290 nm (here shown is the absorbance at 280 nm).

The binding of 1-anilino-8-napthalene sulfonic acid (ANS) to Δ19PD was performed in the presence of increasing concentrations of Gdn-HCl. Results agreed with our findings above and also showed that none of the partially unfolded subunits resembled a molten globule state, which is characterized by a partial loss of tertiary structure while still retaining significant secondary structure (*131*). ANS is reported to bind well to this form to yield a large increase in fluorescence intensity and a blue shift in emission maximum. A blue shift in emission maximum occurred from 0 to 2 M Gdn-HCl (Fig. 2.15); however, this did not coincide with a large increase in fluorescence intensity. Above 2 M Gdn-HCl fluorescence intensity decreased, and this was accompanied by a gradual red shift in emission maximum (2-8 nm) until large changes were observed by 5 and 6 M denaturant (16 and 30 nm, respectively) with protein unfolding.

2.2.6 Quenching of Fluorescence Emission: Assessment of Trp Accessiblility

The folded state and the degree of accessibility of the two Trp residues in Δ19PD were probed further by acrylamide fluorescence quenching experiments, performed in the presence of different concentrations of Gdn-HCl. Acrylamide is a polar non-ionic agent that can access both surface and buried Trp side chains, except those that are deeply buried within the protein core (*132*). A plot of increasing concentrations of acrylamide versus fluorescence intensity appeared biphasic, indicating that the two Trp residues do not reside in the same environment (Fig. 2.16). Modified Stern-Volmer plots enabled determination of the fraction of fluorescence accessible to quenching (f_a) and the quenching constant K_Q at the different concentrations of Gdn-HCl (see Appendix 2C).

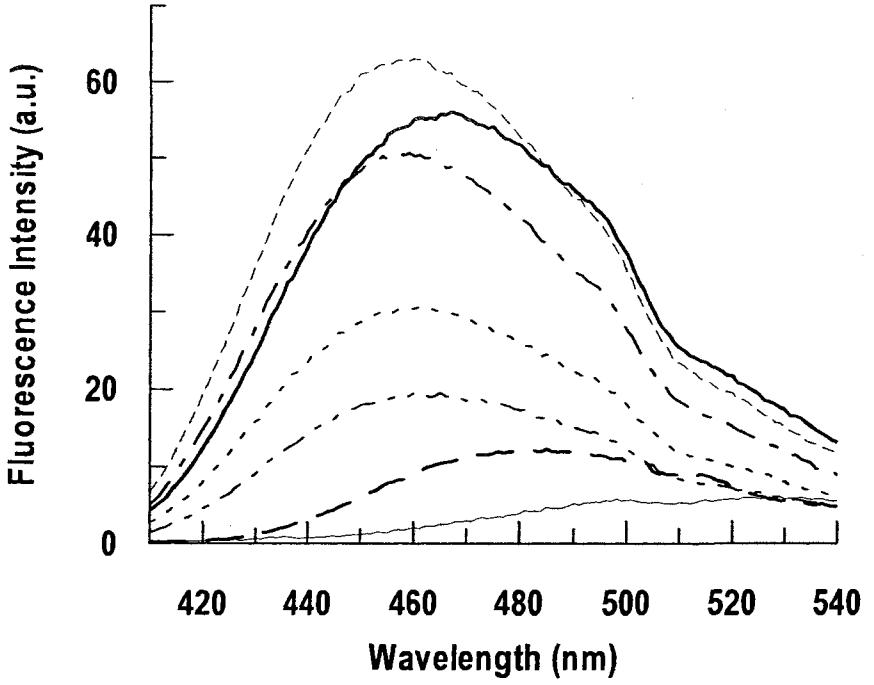

Figure 2.15: Emission spectra of ANS in the presence of Δ19PD at different Gdn-HCl concentrations. Excitation wavelength was set at 370 nm. The fluorescence spectra of the extrinsic fluorophore ANS in complex with Δ19PD were recorded from 400 to 580 nm (410–540 nm shown) as monitored in the presence of Gdn-HCl at 0 (thick solid line), 1 (dashed line), 2 (thick dashed/dotted line), 3 (dotted line), 4 (dashed/dotted line), 5 (thick dashed line), or 6 M (solid line). Fluorescence intensity is shown in arbitrary units (a.u.).

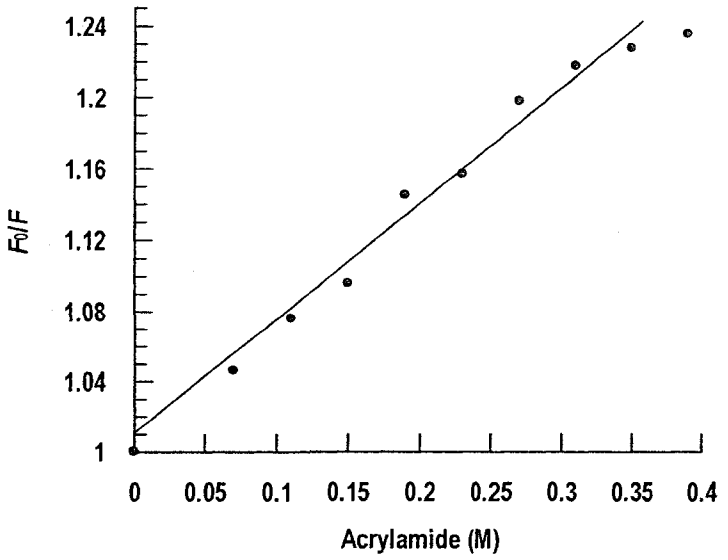

Figure 2.16: Stern-Volmer analysis of *A. aeolicus* Δ19PD fluorescence quenching by acrylamide. Defined amounts of quencher were added to a 2 mL protein solution (3 μM monomer) in PPS buffer (pH 7.5) at 30°C. Excitation wavelength was set at 295 nm and the intrinsic fluorescence emission spectra of protein Trp residues were recorded from 300 to 400 nm after each addition of acrylamide. F_0 and F are the fluorescence intensities in the absence and presence of the quencher, respectively. The equation used to generate the plot is described in section 2.1.7.

Table 2.4: Stern-Volmer quenching constants and percentage of Trp fluorescence quenched by acrylamide and KI in the presence of denaturant or substrates at 30°C.

Gdn-HCl (M)	K_Q (M^{-1})	f_a (%)
0	0.68 (0.125)	0.48 (0.05)
1	0.99	0.4
2	0.94	0.4
3	1.23	0.4
4	1.55	0.5
6	7.34	0.98
Substrate	K_Q (M^{-1})	f_a (%)
0.5 μM NAD^+	0.71	0.45
300 μM Pre	0.135	0.06

Acrylamide and KI concentrations were varied from 0-0.35 M. Values for constants for KI are shown in parentheses. NATA (6 μM) was used as a control and gave a K_Q value of 13.6 M^{-1} and a f_a of 1 with acrylamide. When 5 μM NAD^+ was added to the sample, a f_a of 0 was obtained using acrylamide as a quencher.

The results (Table 2.4 and Appendix 2C) revealed ~50% quenching of Trp fluorescence by acrylamide (f_a = 0.5), consistent with the accessibility of one of the two Trp residues per monomer in Δ19PD. Only in the presence of 6 M Gdn-HCl does the second Trp become accessible. A quenching experiment was then performed in the absence of denaturant but with iodide, a large polar anion that can access surface Trp residues. A value of f_a of 0.05 was obtained and indicated that the Trp that was accessible to acrylamide in the native protein was not accessible to iodide.

Steady-state fluorescence measurements (Figs. 2.17 and 2.18) and acrylamide quenching experiments (Table 2.4 and Appendix 2C) were performed in the presence of NAD^+ or prephenate, in order to determine if one of more Trp residues were in or near the active site and, if so, to obtain a binding constant for the ligand. NAD^+ itself is a strong quenching agent of intrinsic Trp fluorescence of Δ19PD, which is illustrated in Figure 2.17. Thus, titration of the change in fluorescence intensity as a function of NAD^+ concentration (Fig. 2.18) yielded a dissociation constant for NAD^+ from the binary complex (K_d) of 1.42 ± 0.12 μM. Additionally, quenching of Trp fluorescence intensity by acrylamide in the presence of 0.5 μM ($<K_d$) and 5 μM ($>K_d$) NAD^+ yielded values of f_a of 0.45 and ~0, respectively. These data were consistent with bound NAD^+ offering complete protection against acrylamide quenching. Prephenate quenched Trp fluorescence intensity only slightly, although the small change in intensity could be fit to a K_d of 32.6 ± 1.94 μM (Fig. 2.18). Again, binding to the active site was verified by the observation that 300 μM prephenate offered significant protection against quenching of fluorescence intensity by acrylamide (f_a = 0.06). Taken together these results indicate that

the two Trp residues are buried in the protein and one Trp is located in the prephenate binding site.

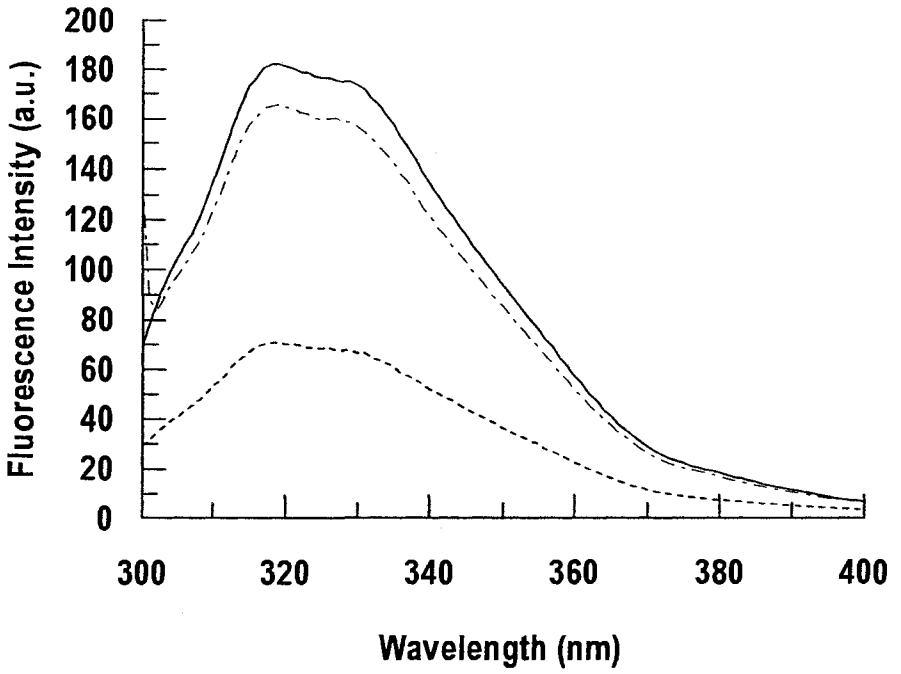

Figure 2.17: Emission fluorescence spectra of Δ19PD in the presence and absence of prephenate and NAD^+. Emission spectra were of Δ19PD (1.6 μM monomer) recorded in PPS buffer (pH 7.5), in the absence (thick line) and the presence of 300 μM prephenate (dashed/dotted line) or 20 μM NAD^+ (dotted line) using an excitation wavelength of 295 nm. All spectra were corrected for inner filter effect and appropriate blanks were subtracted. Fluorescence intensity is shown in arbitrary units (a.u.).

Figure 2.18: Changes in fluorescence intensity of Δ19PD upon binding NAD^+ or prephenate. (A) NAD^+ was varied from 0.2 to 20 μM and Δ19PD fixed at 0.24 μM monomer in PPS buffer (pH 7.5). Only 13 of 25 data points are plotted for clarity. **(B)** Prephenate was varied from 0 to 480 μM and Δ19PD fixed at 1.6 μM monomer. The intrinsic Trp fluorescence was observed by excitation at 295 nm and measuring the emission from 300 to 400 nm. Change of fluorescence intensities (ΔF) at 333 nm was corrected and plotted vs. concentration. The dissociation constants (K_d) for NAD^+ and prephenate were determined by fitting the data to the Michaelis-Menten or the quadratic equations (similar results obtained). Similar results were also obtained with NAD^+ using 1.6 μM or 0.24 μM monomer.

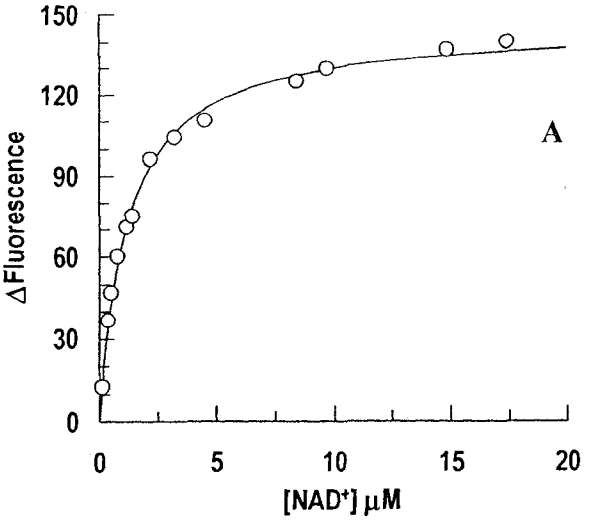
150
120
90
60
30
0
ΔFluorescence
A
0
5
10
15
20
[NAD+] μM

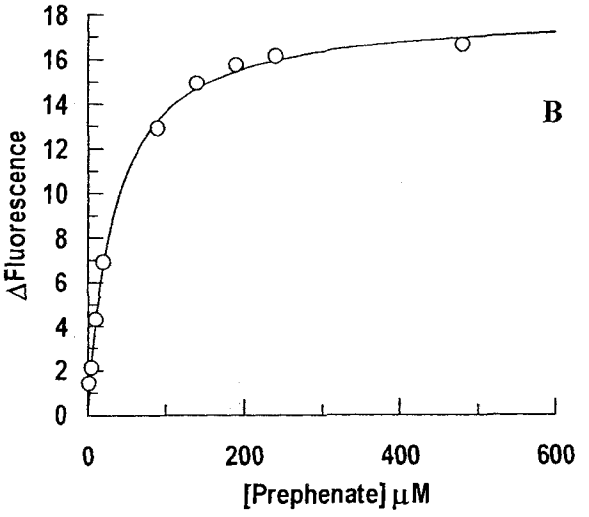
18
16
14
12
10
8
6
4
2
0
ΔFluorescence
B
0
200
400
600
[Prephenate] μM

2.3 DISCUSSION

This chapter reports the biophysical characterization of recombinantly expressed PD and Δ19PD, the N-terminally deleted variant of PD, from the hyperthermophilic bacterium *A. aeolicus*. During the completion of these experiments, the crystal structure of Δ19PD in complex with its cosubstrate NAD^+ was refined to 1.9 Å resolution(*48*), yielding the first reported structure for a TyrA protein from any organism. Our biophysical findings, now published in *Protein Science*(*112*) will be discussed in light of this crystal structure as both bodies of work were prepared as companion papers.

Identification of stable domains of PD

PD from *A. aeolicus* was heterologously expressed in *E. coli* as a fusion protein with a 20-residue N-terminal extension that included a hexa-His tag to facilitate purification by Ni-NTA affinity chromatography and a thrombin recognition site to allow removal of the tag. In agreement with the studies by Aponte (*106*) and later by Sun *et al.* (*48*) SDS-PAGE analysis of dimeric His-tagged PD as monitored during the course of protein purification revealed two distinct species, a doublet comprising a full-length form and shortened form resulting from an N-terminal cleavage. Aponte (*106*) proposed that cleavage may have occurred in the absence of exogenously supplied thrombin by the action of cellular proteases such as protein II or protein Fa at the thrombin recognition sequence (LVPRGS) within the fusion protein's tag (*106*). ESI-MS analysis of the shortened form isolated in the present study however, revealed that the site of proteolysis was instead downstream from the thrombin recognition site between Leu4 and Ser5 in the TyrA sequence (Fig. 2.2). Additionally, it was shown that full-length PD could be

cleaved further, at Lys23 to an even smaller fragment of ~32 kDa when stored for an extended period at 4°C or treated with trypsin —an outcome which also plagued the variant Δ19PD. Thus, our findings are in agreement with those of Sun *et al.* (*48*) who observed the same stable fragment by SDS-PAGE analysis following limited tryptic digestion of PD, although they attributed the shortened form detected during protein purification to this species as well. The insensitivity of the 32 kDa polypeptide to complete tryptic digestion (Figure 2.1, and Sun *et al.* (*48*)) indicated that the residual domain was likely tightly folded and its protease recognition motifs are not easily accessible.

MALDI-ToF MS analyses of *in-solution* and *in-gel tryptic* digests of PD are also consistent with the observation of an N-terminal deletion. The relatively high sequence coverage afforded by our study (73%, Table 2.1) allowed assignment of the protease susceptible region between residues 18 and 26 (numbered from PD's predicted start site). We propose that cleavage by trypsin or by non-specific proteolysis could occur if residues at the N-terminal region of PD are exposed and/or within regions of secondary structure that adopt a mostly random conformation. As supporting evidence, Appendix 2D shows that the first 30 amino acids are confined to a polypeptide region predicted to be rich in loops/unordered structure and, more importantly, precedes a structurally conserved nucleotide binding motif (GXGXXG) commencing at amino acid 37. Alternatively, as the N-terminus of PD expressed in the native organism has not been demonstrated directly, it is possible that the authentic start site that can translate functional protein is actually located further downstream (i.e. Met30) than that annotated in the database. If so, the sensitive proteolytic targets might belong to an unstructured N-

terminal extension of PD. As expected, full-length PD did not yield quality diffraction crystals no doubt because of its unstructured flexible N-terminal region. Nevertheless the engineered Δ19PD, a construct which lacked the first 19 residues, yielded crystals diffracting to a high resolution and was shown to be fully active. The later finding proved serendipitous as purified variants Δ25PD and Δ28PD did not produce well ordered crystals (*48*).

In-solution tryptic treatment of PD did not result in a complete digestion of the protein as shown by SDS-PAGE analysis agreeing with results found by Christendat (*48*). Better sequence coverage was obtained for both our group and Christendat's group when using *in-gel* tryptic digestion (*48*) reported that but we failed to resolve the fragment corresponding to residues 192-242. This fragment (>5 kDa) would likely be resolved using sinapinic acid as a matrix for MALDI-MS analysis.

The architecture of TyrA proteins: the importance of the dimer

Aponte reported earlier that *A. aeolicus* PD is dimeric (*106*). It is not surprising then that an N-terminal deletion construct Δ19PD is also dimeric in its native state. This conclusion, drawn from the results of sedimentation velocity centrifugation and size exclusion chromatography (Table 2.3), agrees with the quaternary structure established by solution studies for other purified monofunctional TyrA proteins, including arogenate dehydrogenase from *Synechocystis* (*36*), cyclohexadienyl dehydrogenases from *P. stutzeri* (*46*), *Z. mobilis* (*39*) and the genetically engineered monofunctional PDs from *E. coli* (*50*) and *E. herbicola* (*51*). This arrangement is in contrast to that of *E. coli* CM-PDT for which it has been established through gel filtration experiments of independently

expressed domains that dimerization is only through adjacent subunits within the mutase portion of this bifunctional enzyme (*70*).

Our solution studies are in keeping with the crystal structure of dimeric Δ19PD complexed with NAD^+ (Chapter 1, Fig. 1.10). Each Δ19PD monomer consists of an N-terminal domain which comprises the α/β dinucleotide-binding domain (represented by a Rossman fold) and a novel α-helical C-terminal domain which is involved in subunit dimerization (Chapter 1, Fig. 1.11). Quaternary structure is a biological necessity if the active site of the enzyme comprises residues contributed by adjacent monomers. Indeed, the crystal structure shows that the active site associated with each monomer is formed at the interdomain cleft of the NAD^+-binding domain and C-terminal domain and contains residues which are shared between monomers (Fig. 2.12). The dimerization domain is held by criss-cross and pair-wise interactions of helical pairs from the C-terminal domain (*48*). This configuration has also been reported for AD from *Synechocystis,* a structure whose protein in complex with $NADP^+$ was published shortly after that of PD. Although the primary sequence of the two enzymes are significantly different (only 27% identity), and their crystal growth conditions unique (AD was crystallized at neutral pH while PD was crystallized at pH 3.2 and represents a catalytically inactive form of the enzyme (data not shown)), their overall global architecture is remarkably similar (See Figure 3, Legrand *et al*.(*43*)) and likely common amongst all TyrA proteins.

The pathway of unfolding

The crystal structure of Δ19PD reveals that the dimerization interface is supported mainly by hydrophobic interactions between monomers (Chapter 1, Fig.1.10). The helical pair

formed by helices α8 and α8' found at the core of the dimer interface is highly buried and provides most of the these hydrophobic contacts (*48*). Accordingly, the results of tryptic digests of PD as analyzed by MALDI-ToF MS could be interpreted in light of this structural feature. Our inability to resolve the fragment corresponding to residues 192-242 is in keeping with the observation that these residues are located on helix α8 of each monomer and at the core of the dimer interface (*48*) rendering them inaccessible to proteases.

The site of dimerization should contribute greatly to the stability of the dimer. Accordingly, Gdn-HCl-induced denaturation commences with the unfolding of the dimer as monitored by the noncoincidence of changes in tertiary and secondary structure (Fig. 2.13) and by size exclusion chromatography (Fig. 2.14) performed in the presence of increasing concentrations of denaturant. This pathway of unfolding is in contrast to that reported for many other dimeric enzymes, for example enolase (*133*), for which dissociation of the dimer precedes denaturation. Interestingly, *E. coli* CM-PD is also predicted to contain an α-helical rich dimerization domain within the C-terminal region of the protein (PredictProtein (*129*)) (Appendix 2D) and has been reported previously to unfold significantly before dissociation into monomers (*53*). Results in the present study suggest that the α-helical structure of Δ19PD is very stable to Gdn-HCl denaturation; $D_{1/2}$ of 4.8 M is about twice that reported for *E. coli* CM-PD under similar conditions (*53*). However, size exclusion chromatography revealed that this increased stabilization stems from, in part, retention of PD's secondary structure as an oligomeric species at the higher concentrations of denaturant (Figure 2.14). No stability studies have been reported for mesophilic monofunctional PDs. For comparison, however, a report contrasting

monofunctional CMs from *E. coli* and from the thermophilic archae *Methanococcus jannaschii* (both of which are highly α-helical) also showed that the dimeric proteins unfolded substantially before dissociation into unfolded monomers in the presence of Gdn-HCl (*134*). Thermophilic CM, with a $D_{1/2}$ of ~4.8 M, was calculated to be more stable than the mesophilic protein by ~5 kcal/mol, by fitting coincident CD and fluorescence data to a 2-state model.

Even low concentrations of chemical denaturant cause marked changes in protein structure. It has been reported that thermophilic enzymes display a very low catalytic rate at ambient temperatures due to insufficient flexibility in their active sites (*135*). Addition of low concentrations of Gdn-HCl to Δ19PD resulted in over a twofold increase in specific activity at ambient temperature (Figure 2.10), and a fourfold increase in K_m for prephenate, perhaps due to increased flexibility at the active site. Similar results have been reported for other thermophilic enzymes upon the addition of low concentrations of urea or Gdn-HCl (*136-141*). Moreover, changes in protein conformation within the hydrophobic NAD^+-binding pocket of PD, induced by low denaturant concentrations, can be illustrated by the coincidence of a *decrease* in K_m for NAD^+ with an increase binding of the amphiphilic dye ANS (Figure 2.15); it has been reported previously that ANS has affinity for such nucleotide-binding sites (*142, 143*).

A. aeolicus PD is thermally stable

When considering *A. aeolicus'* classification as a hyperthermophilic bacterium (*144*), it is not surprising then that the melting temperatures (T_m) of PD and Δ19PD were greater than 100°C as deduced by CD spectropolarimetry. Even the addition of 3 M Gd-

HCl to the enzyme preparation, during variable temperature (VT) CD experiments did not lower the T_m value (data not shown), as the presence of the denaturant likely promoted protein aggregation (Figure 2.14), precluding a cooperative thermal transition at a lower temperature. However, Aponte reported a T_m value of 108°C in the absence of denaturant for PD using variable pressure-capillary differential scanning calorimetry (DSC) (*106*). For comparison, an apparent T_m of 57°C was obtained for *E. coli* CM-PD (*106*). Differences in T_m values of the same magnitude have also been reported using DSC for a hyperthermophilic archaeal acylphosphatase from *Pyrococcus horikoshii* versus its mesophilic counterparts (*135*). Of note, the T_m obtained for CM-PD by DSC was in agreement with values of ~56°C determined by VT-CD measurements reported in this study and ~57°C by VT-Fourier transformed infrared (VT-FTIR) spectroscopy (*106*), even though the experimental conditions were markedly different.

What is the basis for the thermal stability of *A. aeolicus*? Analysis of many thermophilic proteins and their corresponding mesophilic homologues have highlighted such differences as enhanced packing, additional salt bridges and hydrogen bonds or a better arrangement of ionic interactions, abbreviated loops, and restriction of conformational freedom introduced by proline residues (*145, 146*). However, a more recent analysis of structures and sequences of several hyperthermostable proteins indicate that some proteins employ a "structure-based" mechanism for thermostabilization; they are significantly more compact and hydrophobic than their mesophilic homologs, and come from organisms such as hyperthermophilic archaea that originated in an extreme environment. In contrast, other proteins use a "sequence-based" mechanism; instead of showing significant structural differences from mesophile, they show a defined number

of strong interactions, such as ion-pair or H-bonding networks. These protein come from mesophilic organisms that later recolonized hot environment (*109*). Their ultimate strategy depends on evolutionary history of the organism. *A. aeolicus* is unusual in that it is a deeply branched hyperthermophilic bacterium, separated from the rest of bacteria kingdom at early stages of evolution and located closer to archaea.

An extensive analysis of proteins from hyperthermophilic and mesophilic organisms showed that a larger proportion of charged versus polar (uncharged) amino acids is a signature of many hyperthermophilic organisms (*108, 145, 146*). Moreover, the proportion of solvent accessible charged residues at the protein surface markedly increased at the expense of polar residues. *A. aeolicus* PD houses a significantly higher proportion of lysine and glutamate residues (10.6% and 8%, respectively) than found in the PD portion of *E. coli* CM-PD (3.7% and 5.9%, respectively, for example). In fact, the crystal structure of Δ19PD complexed with NAD^+ (*48*) reveals a large ionic network formed by Glu275, Glu278 and Lys285 from one subunit and the same residues from the other subunit, a structural feature which Christendat and coworkers speculate may contribute to the thermostability of the enzyme. Other parameters noted with elevated thermostability and thermal activity of proteins are an increased number of strategically located proline residues, as seen CM from *T. thermophilus* (*87*), or a number of leucine to isoleucine substitutions, noted for *M. jannaschii* CM (*134*). However, sequence analysis of *A. aeolicus* PD does not appear to support these strategies. Interestingly, our sedimentation velocity data from AUC yield a low frictional coefficient of 1.22 for *A. aeolicus* PD suggestive of a compact protein core. Moreover, VT-FTIR results (*106*) support this observation in showing slow H/D exchange at high temperatures, which

would have likely continued well past 95°C degrees except for instrument limitations. It would be interesting to speculate that *A. aeolicus* PD might have adopted elements of "sequenced-based" (ion pairs, H-bonding) and "structure-based" (packing) mechanisms for its thermostabilization of PD (*109*).

Quenching of fluorescence emission corroborates crystallographic data

Results from fluorescence experiments have provided important structural information concerning *A. aeolicus* PD prior to the availability of crystallographic data. Now our findings can be interpreted in terms of the structure of Δ19PD complexed with NAD^+ (*48*), although it should be considered that the conformation of the free protein may be different than in its liganded state. Trp190, on helix-7, is part of a β_7-α_7-β_8 motif which is appended to the central β-sheet of the NAD^+-binding site, and its side chain is buried in the core of the main Rossman fold. Trp259, on helix-11 in the C-terminal domain, is one of several residues lining the wall of the prephenate binding pocket in the shared active site, and is ~16 Å from Trp190. Neither Trp259 nor Trp190 are surface-exposed within the dimer (Fig. 2.19), in keeping with the substantially blue-shifted emission maxima relative to Trp free in solution and their inaccessibility to quenching by KI. Of the two, Trp190 is completely buried and is not accessible to quenching by acrylamide. Furthermore, Gdn-HCl-induced oligomerization may prevent Trp190 from becoming solvent-accessible until substantial protein unfolding at 6 M denaturant (Table 2.4). As expected, catalytically relevant portions of prephenate and NAD^+ are in close proximity. The side chain of Trp259 is within 5 Å of either substrate, and that of Trp190 about ~8 Å and 12 Å from NAD^+ and prephenate, respectively (Fig. 2.20). Accordingly,

changes in fluorescence intensity emission occur with the binding of either NAD^+ or prephenate to the free enzyme. This characteristic has allowed the calculation of dissociation constants of substrates from the enzyme-substrate binary complex, the importance of which will be discussed in Chapter 3. It is likely that the binding of either substrate can prevent quenching of Trp259 emission by acrylamide. Deciphering the contributions of individual Trp residues awaits analysis of site-directed variants.

In the next chapter, we will explore further the effects of temperature on enzyme function and have extended our structure-function studies to the active site of the enzyme. Key targets for site-directed mutagenesis were identified using the crystal structure as a guide, as well as the results from biophysical studies presented above and from sequence alignments of several mono- and bifunctional TyrA proteins. Our studies will show that kinetic and biophysical characterization of these variant proteins help to establish the importance of selected residues in PD's catalytic mechanism (binding or catalysis) or/and in the mode of regulation by L-Tyr.

Figure 2.19: Space filled model of *A. aeolicus* Δ19PD. One subunit is colored blue, the other grey. Trp190 and Trp259 from each subunit are colored red and yellow, respectively. This model was generated using PyMOL.

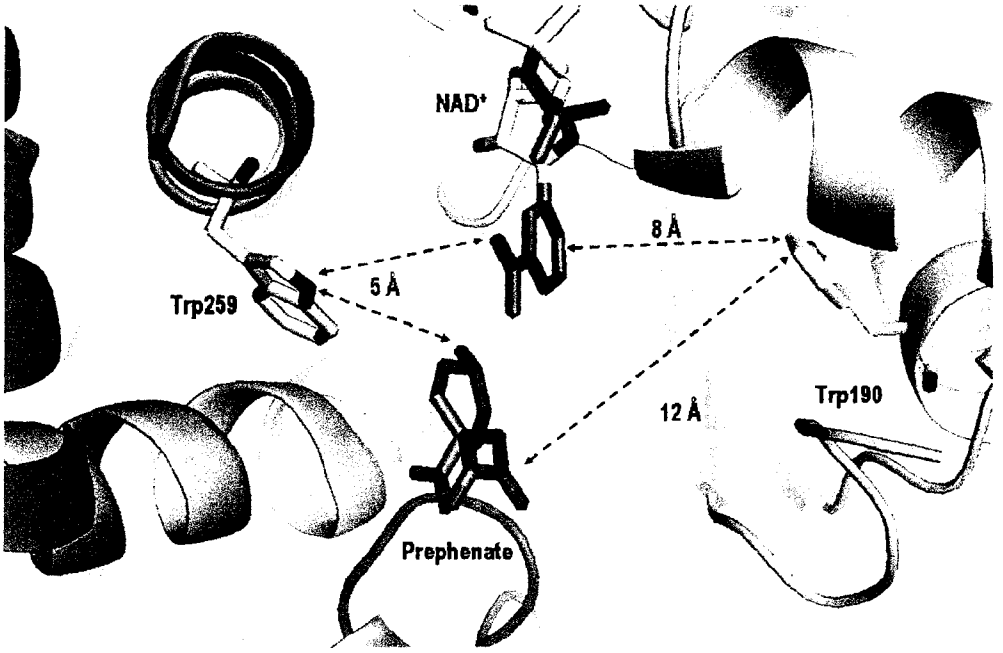

Figure 2.20: ***Aquifex aeolicus*** **Δ19PD active site.** Both Trp190 and Trp259 (yellow sticks) are in close proximity of both substrates (prephenate, gray sticks, is modeled in the active site). The side chain nitrogen of Trp259 is within 5 Å of C4 hydroxyl group of prephenate and the nicotinamide ring of NAD^+. The side chain of Trp190 is within 8 Å and 12 Å of the nicotinamide ring of NAD^+ and the pyruvyl side chain of prephenate, respectively.

Chapter 3

Kinetic Characterization of WT and Variant PDs from *Aquifex aeolicus*

3.0 INTRODUCTION

Only few monofunctional TyrA proteins have been characterized in the purified form. These include dehydrogenases from *Zymomonas mobilis* (*39*), *Pseudomonas* (*46, 147*), *Synechocystis* sp. PCC 6803 (*36*), *Arabidopsis thaliana* (*49*) and *Neisseria gonorrhoeae* (*99*). These studies have centered mainly on delineation of their substrate specificity, as some utilize both L-arogenate and prephenate as a substrate while others use only L-arogenate or only prephenate. However, biochemical analyses of PD from *E. coli* CM-PD have provided the basic framework for understanding the molecular mechanism of the TyrA enzymes (*52, 53*). Initial velocity, product and dead-end inhibition studies and isotope trapping studies have established that the kinetic mechanism of *E. coli* PD conforms to a rapid equilibrium, random kinetic mechanism with catalysis as the rate-limiting step (*63*). Similar kinetic mechanisms have been proposed for ADs from *A. thaliana* (*40*) and *Synechocystis* sp. (*43*), although through the analysis of less rigorous experiments. In contrast, a steady-state random kinetic mechanism, with preferred order (L-arogenate binding first) has also been suggested for AD from *Synechocystis* sp. by Bonner *et al.* (*36*). A model for the catalytic mechanism of the *E. coli* PD activity has been put forward (refer to Fig. 1.8) based on the results of pH profiles and inhibition studies on wild-type and variant proteins (*52, 53*). Briefly, the guanidino group of Arg294 interacts electrostatically with the ring carboxylate of prephenate in the enzyme-NAD^+ binary complex, while His197, the key catalytic group of the reaction, polarizes the 4-hydroxyl group of prephenate by lowering the activation barrier to assist hydride transfer to NAD^+ and concomitant decarboxylation (*53*).

The structures of PD from *Aquifex aeolicus* (*48*) and AD from *Synechocystis* sp. (*43*) have been reported, both proteins in complex with their preferred nucleotide cosubstrate and modeled with the appropriate cyclohexadienyl substrate in the active site. Analyses of these structures have provided positional information on the conserved histidine and arginine residues, although in some cases contradict the findings of the solution studies on the *E. coli* enzyme. The results of structural analysis must be corroborated by solution studies on site-specific variants on PD from *A. aeolicus* and *Synechocystis*. The structure of *A. aeolicus* PD has also led to the identification of other active site residues, that might play important mechanistic roles, most notably Ser126, which Sun *et al.* proposes promotes catalysis by orienting the catalytic histidine and the nicotinamide moiety of NAD^+ in their most catalytically efficient conformations (*48*). Moreover, these authors proposed that access to the active site is regulated by a gated mechanism, which involved an ionic network consisting of Glu153-Arg250-Asp247' of which both Arg and Glu residues are conserved amongst all species. There is a pressing need to obtain structural data with prephenate or prephenate analogues bound in the active site as the full complement of interactions between prephenate and TyrA proteins are still largely unknown,

Preliminarily kinetic studies of PD from *A. aeolicus* have been reported by R. Aponte (*106*). We have extended Aponte's work in this present chapter and report the kinetic parameters of the reaction catalyzed by Δ19PD, the crystallizable form of the enzyme. We have established whether the enzyme from *A. aeolicus* can utilize L-arogenate as a substrate in addition to prephenate and we compare the variation of the kinetic parameters with temperature for both the Δ19 and full-length forms of PD.

Another goal of this study was to investigate the role of active site residues as a step towards further understanding of the PD-catalyzed reaction. Accordingly, our collaborators have carried out cocrystallization studies of *A. aeolicus* Δ19PD-NAD^+ in complex with HPP, with 4-hydroxyphenylpropionate (HPpropionate), a product analogue, and with Tyr (manuscript submitted). Structures were solved at neutral pH and at a resolution of 2.15 Å, 2.25 Å and 2 Å, respectively. These three-dimensional structures of Δ19PD have served as guides to target active site residues, which we consider important for the PD mechanism. We have investigated the role of Ser126, His147, Glu153, His217, Asp247 and Arg250 through the kinetic analysis of site-directed variants correlated with structural analysis of the cocrystal complexes.

3.1 EXPERIMENTAL PROCEDURES

3.1.1 Materials

Prephenate and chorismate were obtained as outlined section 2.1.1 while L-arogenate (barium salt) was a generous gift from Dr. C. Bonner. NAD^+ and $NADP^+$ (free acid) were obtained from Roche. Hydroxyphenylpropionate and 4-hydroxyphenylpyruvic acid were from Sigma. High purity of the substrates was confirmed by either mass spectrometry or NMR. Concentrations of stock substrate solutions were determined using published extinction coefficients (*115*) and/or enzymatic end-point analysis. All other chemical reagents were obtained commercially and were of the highest quality available. Reagents and enzymes for molecular biology were provided by Stratagene, New England Biolabs, and Promega. *E. coli* strains DH5α (Life Technologies Inc.) and BL21(DE3) Gold (Stratagene) were used for plasmid production and for protein expression,

respectively. All relevant portions of constructed plasmids were confirmed by DNA sequencing through the facilities at Bio S & T, (Montreal, Canada). Recombinant *E. coli* CM-PD was generously provided by J. Manioudakis (refer to section 2.1.1).

3.1.2 Preparation of a Stock Solution of 4-Hydroxyphenylpyruvate

Solution of the *keto* form of 4-hydroxyphenylpyruvate was prepared as described by Lindblad *et al.* (*148*) but with slight modifications. Briefly, a solution of 0.1 M of 4-hydroxyphenylpyruvic acid in methanol was purified by shaking with activated charcoal. The solution was filtered through a 0.22 μm syringe filter (Millipore). An equal volume of 1 M potassium hydroxide (KOH) in methanol was added to the solution, and then supplemented with activated charcoal. The solution was kept on ice with gentle stirring for 30 min then filtered again. The filtrate was left to crystallize for 4 h on ice. The resulting crystals were washed four times with 2 mL methanol then dried overnight at 4°C in a dessicator *in vacuo* over P_2O_5. The crystals were resuspended in 50 mM HEPES, 150 mM NaCl at pH 7.5 (reaction buffer). When the crystals were dissolved in the reaction buffer, an ultra-violet spectrum of the *keto* form of 4-hydroxyphenylpyruvate and the concentration of the solution were obtained (ε_{276nm}= 2 mM^{-1}. cm^{-1}) (*149*). A stock solution of HPPropionate was prepared in 50 mM HEPES, 150 mM NaCl at pH 7.5 (reaction buffer) just prior to use and its concentration was determined spectrophotometrically.

3.1.3 Source of Variants Δ19PD of *Aquifex aeolicus*

The expression plasmid (pΔ19PD) encoding residues 20-311 of the *A. aeolicus* VF5 PDH protein (gi:15282445; NP) was provided by Dr. D. Christendat from the University of Toronto, and its construction has been previously described (*117*). This plasmid was used for protein expression and mutagenesis studies. Site-directed mutagenesis was carried out using the QuikChange™ Site-Directed Mutagenesis Kit (Stratagene), whereby complimentary oligonucleotides containing the desired mutations for Δ19PD were used. Table 3.1 summarizes the mutants generated and the respective oligonucleotides used for mutagenesis. Residues Ser126, Glu153, Asp247 were substituted by an alanine and His147 was replaced by an asparagine. These plasmids containing the desired mutation were generously provided by D. Christendat, while mutants encoding Arg250Gln, His217Asn/Ala were produced in our laboratory by W. Hou and J. Bonvin. All mutants were verified by DNA sequencing.

Table 3.1. Forward primers used to generate active site variants

Variants	Forward Primers (5'→3')
Ser126Ala	GGATCAGGGAGCGGTTAAGGGGA
His147Asn	GTTGGAGGGAACCCGATAGCAGGAACGGAG
Glu153Ala	AGCAGGAACGGCGAAATCTGGGG
His217Ala	GTTTCTCACCTTCCCGCCGCGGTTGCGTTTGCACTCG
His217Asn	GTTTCTCACCTTCCCAACGCGGTTGCGTTTGCACT
Asp247Ala	CCCCGGAGGAGGTTTTAAGGCGTTCACGAGGATTGCAAAGAG
Arg250Gln	GTTTTAAGGACTTCACGCAGATTGCAAAGAGCGACC

3.1.4 Expression and Purification of Recombinant and Variant Enzymes

Recombinant *A. aeolicus* PD and Δ19PD (~10 U/mg and 27 U/mg respectively) were expressed and purified as described section 2.1.2. Variant proteins were expressed as for Δ19PD and were purified as described section 2.1.2 with slight modifications. The heat step was omitted to minimize possible thermally induced denaturation of variant proteins. Samples loaded onto a 15 mL Superflow^{TM} Ni-NTA column were washed with at least 400 mL of buffer A containing 30 mM imidazole. The eluate was analysed spectrophotometrically at OD_{280} and by Bio-Rad Protein Assay Kit (Bio-Rad Laboratories) to confirm that all undesired proteins were removed from the column. Bound protein was eluted with buffer A containing 300 mM imidazole and the remaining steps of purification and storage of the enzymes were as described in section 2.1.2. All protein purification steps were carried out at 4°C. Purified proteins were examined by SDS-PAGE to monitor any proteolysis of the protein variants during purification. The exact masses of variant proteins from *A. aeolicus* Δ19PD were confirmed by ESI-MS analysis and samples were prepared and analyzed as described in section 2.1.5.1.1

3.1.5 Determination of Enzyme Activity and Protein Concentration

The oxidative decarboxylation of prephenate or L-arogenate in the presence of NAD^+ was followed at 340 nm as outlined in section 2.1.4, while the conversion of chorismate to prephenate was monitored at 274 nm (*119*). The reactions (total volume 1.0 mL) were monitored continuously by using a Varian Cary 50 spectrophotometer, equipped with a thermostated cuvette holder. When performed at 30°C and 55°C, the standard activity assays were performed as outlined in section 2.1.4. For assays

performed at 80°C and 95°C, the preincubation times for the enzyme and NAD^+ were reduced to 1 min and 15 s, respectively.

Steady-state kinetic parameters k_{cat} and K_m were calculated at 30°C, 55°C and 80°C for the WT enzyme from the initial rates using a minimum of six substrate concentrations ranging from one-half up to at least 7-fold K_m. Concentrations of prephenate (seven times K_m) and NAD^+ (2 mM) were present when used as the fixed substrate. Protein ranged from 1 to 30 μg. Reactions with L-arogenate were initiated with enzyme after preincubation of reaction buffer and substrates at the desired temperature for 2 min. Values of steady-state kinetic parameters k_{cat} and K_m were obtained by fitting initial velocity data to the appropriate rate equations as outlined section 2.1.4.

Turnover numbers were calculated using subunit molecular weights (kDa) of 37.01 (full-length PD), 35.13 (thrombin-cleaved PD), 36.88 (heterodimeric PD), and 33.19 (Δ19PD) and the corresponding molecular weight for each variant proteins, assuming one active site per monomer.

Enzyme half-life was determined by incubating enzyme (1 mg/mL in assay buffer) in capped Eppendorf tubes at 95°C and 70°C (*A. aeolicus* PD and Δ19PD) or at 40°C (*E. coli* CM-PD). For CM-PD, buffer was supplemented with 25% glycerol (v/v). Samples were removed at different time intervals, cooled on ice, centrifuged for 5 min, and residual activity of the supernatant was determined by the standard assay at 55°C (PD) or 30°C (CM-PD). Protein concentration was determined after centrifugation in order to calculate specific activities.

Protein concentration was estimated using the Bio-Rad Protein Assay Kit (Bio-Rad Laboratories) with bovine serum albumin (Sigma) as a standard.

3.1.6 Effect of Temperature on Dehydrogenase Activity of *A. aeolicus* PD, Δ19PD and *E. coli* CM-PD

Assays were performed in the standard reaction mixture using 2.5 to15 μg/mL of *A. aeolicus* PD or Δ19PD, and reaction rates were recorded from 30°C to 95°C with 1 mM prephenate and 2 mM NAD^+. *E. coli* CM-PD was examined between 17°C and 56°C in 3-component buffer (pH 7.5) containing 1 mM DTT, 1 mM prephenate and 2 mM NAD^+. From the data, Arrhenius plots were obtained; activation energy (E_a) values were calculated from the slop and k_{cat} deduced by linear extrapolation using the following equation:

$$k=A * \exp^{(-Ea/RT)} \qquad (3.1)$$

where k is the rate constant, E_a is the activation energy ($kJ.mol^{-1}$), R is the universal gas constant (8.314×10^{-3} $kJ.mol^{-1}.K^{-1}$) and T is the temperature in Kelvin. Activity measurements and spectral scans performed on 50, 500 and 1000 μM samples of prephenate and NAD^+, heat-treated for up to 5 min, verified that there was not significant decomposition of the substrates (~2% at 95°C) during recording of initial rates.

3.1.7 Effects of pH, NaCl and Divalent Metal Ions on the PD Activity

The effect of NaCl on the PD activity was monitored using 10 solutions of 2X reaction buffer containing increasing concentrations of salt (0-2 M). The pH of each buffer was checked and adjusted to pH 7.5 with NaOH as necessary. Reactions were performed at 55°C as described in section 3.1.4, but with both substrates added in the

second step at fixed concentrations of 4 mM NAD^+ and 0.8 mM prephenate. The reaction was initiated with 10 µg of Δ19PD.

The pH optimum for *A. aeolicus* PD and Δ19PD activities was determined at 55°C by measuring specific activity between pH 3.2 and 9.8. Assays were performed in a 3-component buffer system of 0.05 M 2-morpholinoethanesulfonic acid (MES), 0.05 N-ethylmorpholine (NEM), 0.1 M diethanolamine containing 0.15 M NaCl. NAD^+ and prephenate concentrations were kept fixed at 4 mM and 0.8 mM, respectively.

The effect of divalent metal ions on the PD activity for both *A. aeolicus* PD and Δ19PD was measured at 55°C as outlined section 2.1.4 using either EDTA (0-1 mM), $MgCl_2$ and $ZnCl_2$ (0-25 mM) or 2 mM $CoCl_2$. NAD^+ and prephenate concentrations were kept fixed at 4 mM and 0.8 mM, respectively.

3.1.8 Steady-State Velocity Patterns of the *A. aeolicus* PD-Catalyzed Reaction

Variation of initial velocity of *A. aeolicus* PD reaction as a function of the concentration of prephenate and NAD^+ was investigated. Initial rates were recorded at 55°C in a reaction buffer of 50 mM HEPES, 150 mM NaCl, (pH 7.5) as outlined section 2.1.4. Prephenate was varied from 49-493 µM at fixed concentrations of NAD^+ of 35, 70, 140 and 350 µM. Similarly, NAD^+ was varied from 30-495 µM at fixed concentrations of prephenate of: 49, 102, 145 and 495 µM. Experimental conditions for D19PD are described in Appendix 3E. The data were fit to the equation describing a sequential kinetic mechanism, $v = VAB/(K_{ia}K_b + K_aB + K_bA + AB)$, to yield values for V the maximum velocity, K_a and K_b, the Michaelis constants for the substrates A and B, and K_{ia} is the dissociation constant from the enzyme-A complex.

Initial velocities recorded in the presence of HPP and HPpropionate were measured at 55°C in reaction buffer as previously described in section 2.1.4. Prephenate was varied from one-half to 5 x K_m at fixed concentrations of HPP (107, 535 and 1070 μM) or HPpropionate (250, 500 and 1000 μM). NAD^+ was kept constant at 2 mM.

The data were plotted in double reciprocal and were fitted to the equations to obtain values for inhibition constants using the computer program Cleland (*120*). The model of inhibition (competitive or non-competitive) was established by identifying which equation gave the lowest standard error of kinetic constants.

3.1.9 pH-dependence of the Dehydrogenase-Catalyzed Reaction

The activity of Δ19PD was recorded at 55°C over the pH range from 6.08 to 9.79 in a buffer containing 25 mM HEPES, 25 mM 3-(N-morpholino)propanesulfonic acid (MES), 25 mM Tris-HCl with 150 mM NaCl. The concentration of NAD^+ was kept fixed at 4 mM while prephenate was varied from 28 μM to 840 μM. For the data set at pH 6.08, prephenate concentrations were varied from 560 μM to 5.6 mM. The pH of the assay mixture was determined at 55°C before and after the reaction using a Fisher Scientific accumet® 15 pH meter standardized with appropriate reference standard buffers.

The kinetic data were fitted to the appropriate equations using the computer programs of Cleland or Grafit Software version 5.0 (Erathicus Software) as described section 2.1.4. Values for the maximum velocity (*V*), the Michaelis constant (*K*), and the apparent first-order rate constant for the interaction of enzyme and substrate (*V/K*) were deduced from the plots. For the determination of *V/K* values, the concentration of the

fixed substrate was saturating at the pH of the assay. The variation of the values of V and V/K as a function of pH was fitted to the log form of eqs 3.2 and 3.3 as described by Christendat *et al.* (*53*):

$$y = C/(1 + H/K_A) \tag{3.2}$$

$$y = C/(1 + H/K_A + K_B/H) \tag{3.3}$$

Where y represents the value of V or V/K at a particular pH value, C is the pH-independent value of the parameter, H is the hydrogen ion concentration, and K_A and K_B are acid dissociation constants for groups on the enzyme or substrate:

3.1.10 Determination of K_d for Prephenate of Ser126Ala and His147Asn Δ19PD Variants

Values for the dissociation of prephenate from its complex with Ser126Ala and His147Asn Δ19PD were determined at 30°C by monitoring the quenching of protein intrinsic fluorescence as described in section 2.1.7. Titrations were performed by the progressive addition of prephenate (0-700 μM and 0-200 μM for Ser126Ala and His147Asn, respectively) to PPS buffer (2 mL) containing 0.3 μM monomer.

3.2 RESULTS

3.2.1 Determination of the Kinetic Parameters of the Reaction Catalyzed by *A. aeolicus* PD and Δ19PD at 30, 55 and 80°C.

Enzyme assays with purified PD and Δ19PD confirmed expectations that *tyrA* specifies an NAD^+-dependent prephenate dehydrogenase. The enzymes followed Michaelis-Menten kinetics, although substrate inhibition was noted at very high concentrations of prephenate (but not NAD^+). The kinetic parameters for the PD reaction for both enzymes at three different temperatures are shown in Table 3.2. Values obtained at 55°C for k_{cat} and K_m for PD agreed with previous findings (*106*). Values of k_{cat}/K_m increased only ~7- to 10-fold between 30° and 80°C; the dramatic increase in k_{cat} (~30-fold) was offset by a decrease in the apparent binding affinity for substrates. For the most part, PD and Δ19PD were equally effective catalysts, as indicated by comparison of k_{cat}/K_m values. However, N-terminal extensions appeared to cause small but reproducible effects on the values for kinetic parameters; both the k_{cat} and K_m for prephenate for Δ19PD were twice that for PD, notably at 80°C. The purified enzymes did not possess CM activity when assayed at 55°C with 1 mM chorismate, nor were the activities inhibited by the mutase transition state analogue, *endo*-oxabicyclic diacid (120 μM), or by 1 mM chorismate when assayed with 0.1 mM prephenate and 2 mM NAD^+ (data not shown).

Preliminary studies indicated that Δ19PD did not efficiently utilize L-arogenate (NAD^+ as a cosubstrate), primarily due to a poor affinity for this substrate (Table 3.2). Values of k_{cat}/K_m with L-arogenate increased with temperature, but were reduced ~2.5 orders of magnitude compared to those with prephenate. *E. coli* CM-PD (300 μg) did not yield a measurable reaction rate at 30°C in the presence of 44 mM L-arogenate and 4 mM NAD^+. This finding is in contrast to the detectable, albeit poor rates reported for *E. coli* CM-PD with racemic or L-arogenate (*101, 150*). In the present study, negligible rates

(<0.5%) were obtained for either enzyme using $NADP^+$ (1 mM) as a cosubstrate with prephenate (0.5 mM) or L-arogenate (44 mM).

The activities of PD and Δ19PD appeared to decrease exponentially with time (Fig. 3.1) and yielded half-lives at 95°C of 2 h and 55 min, respectively. Both proteins, however, retained full activity even after 20 h at 70°C. By comparison, *E. coli* CM-PD exhibited a half-life of 6 min at 40°C (Appendix 3A). Our values are within the range reported for other proteins isolated from thermophilic organisms (*151-153*), although results are dependent on protein concentration and buffer components.

Table 3.2: Steady-state kinetics parameters for PD and Δ19PD catalyzed reactions at 30°, 55° and 80°C

	Variable Substrate[a,b]	Prephenate (or L-arogenate)			NAD^+		
Enzyme	Temperature (°C)	K_m (μM)	k_{cat} (s^{-1})	k_{cat}/K_m ($M^{-1}.s^{-1}$)	K_m (μM)	k_{cat} (s^{-1})	k_{cat}/K_m ($M^{-1}.s^{-1}$)
PD	30	17 ± 0.3	1.3 ± 0.04	7.5×10^4	25 ± 0.9	1.10 ± 0.03	4.5×10^4
	55	97 ± 0.6	6.8 ± 1.1	7.0×10^4	72 ± 1.02	6.7 ± 0.3	9.3×10^4
	80	136 ± 23	36 ± 1.2	2.6×10^5	109 ± 6	34 ± 1.1	3.1×10^5
Δ19PD	30[c]	41 ± 0.5 (9900 ± 1200)	2.20 ± 0.05 (2.4 ± 0.2)	5.4×10^4 (242)	53 ± 5.8 (63 ± 1.5)	1.50 ± 0.03 (2.6 ± 0.3)	2.8×10^4 (4.1×10^4)
	55[d]	135 ± 12	13 ± 0.3	9.6×10^4 (565)	71 ± 3.2	11.5 ± 0.3	1.6×10^5
	80[d]	249 ± 22	68 ± 1.7	2.7×10^5 (1412)	84 ± 7.5	62 ± 1.3	7.3×10^5

[a] Values were calculated from initial rates using a minimum of six substrate concentrations ranging from one-half K_m up to at least 7-fold K_m. Prephenate (1 mM) and NAD^+ (2 mM) were present in saturating amounts when used as the fixed substrate. Protein concentrations were maintained above 19, 10 and 1 μg/mL for kinetic assays performed at 30°, 55° and 80°C, respectively.

[b] Values in parentheses are the results from assays performed with L-arogenate and NAD^+ in 50 mM HEPES, 0.15 M NaCl (pH 7.5). Protein concentrations were 10 μg/mL.

[c] L-arogenate was varied from 2.2-44 mM in the presence of 4 mM NAD^+, or NAD^+ was varied from 39-1965 μM with L-arogenate fixed at 44 mM.

[d] Values were calculated from the initial slope of a substrate saturation curve using L-arogenate at 5.4, 9, and 13.5 mM with NAD^+ fixed at 4 mM (55°C and 80°C).

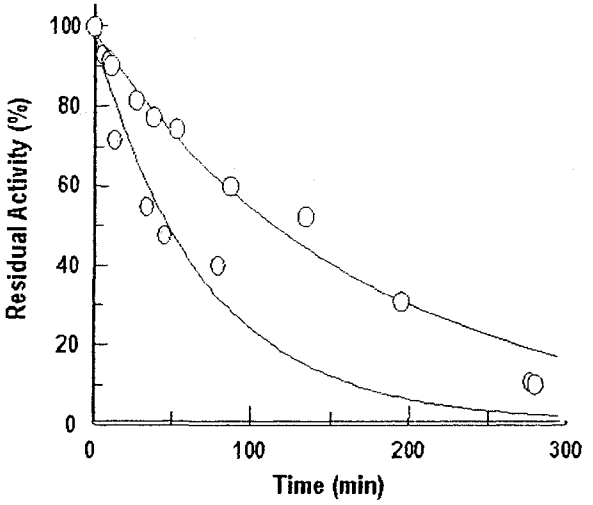

Figure 3.1: Irreversible thermal inactivation of *A. aeolicus* PD and Δ19PD. Enzymes (1 mg/mL in assay buffer) were incubated in capped Eppendorf tubes at 95°C. Samples were removed at different time intervals, cooled on ice, centrifuged for 5 min, and residual activity of the supernatant was determined by the standard assay at 55°C as described section 3.1.5. Data were fitted to a single-exponential decay described by the following equation: $A=A_0\ e^{-kt}$, where A is the specific activity at time t, A_0 is the activity at time zero, k is the rate constant and t the time. Half-life, the time it takes for the enzyme to loose 50% of its activity ($t_{1/2}$) was determined by the following equation: $t_{1/2}=0.693/k$

Both PD and Δ19PD were very sluggish enzymes at temperatures below 45°C and yielded a temperature optimum of ~95°C (PD shown in Fig. 3.2). This is near the physiological optimum growth temperature of the organism (*105*). An Arrhenius plot for PD was linear between 30° and 85°C, indicating a single rate-limiting step with an activation energy (E_a) of 61.8 kcal/mol (Inset in Fig. 3.2). An activation energy (E_a) of 47.4 kJ/mol between 17-56°C was estimated and a k_{cat} of 88.3 s^{-1} at 63°C was obtained. Δ19PD also yielded a linear plot and its parameters are given in Fig. 3.2. Interestingly, when PD activities of either enzyme were determined using low protein concentrations (<10 μg/mL) and at lower assay temperatures (30°C and 55°C), progress curves were punctuated by a significant lag (30 s) before initial velocities were attained. This lag was observed whether enzyme was preincubated with either substrate, or the reaction was initiated with enzyme. This observation could suggest that the enzyme undergoes a conformational change after 30 s in presence of both substrates. The lag was minimized by increasing the protein concentration or conducting assays at high temperatures, and was somewhat reduced by adding 0.2 mg/mL bovine serum albumin. Interestingly, no lag was observed when L-arogenate was the substrate, although product (Tyr) inhibition was apparent.

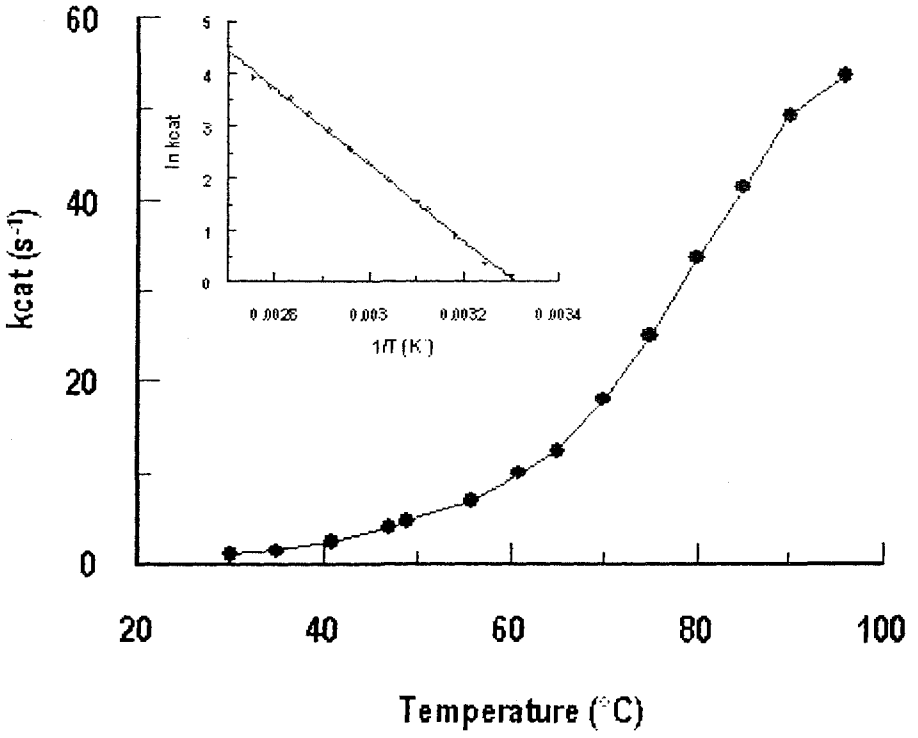

Figure 3.2: Effect of temperature on PD activity of *A. aeolicus*. Assays were performed in the standard reaction mixture using 2.5-15 μg/mL of enzyme, and reaction rates were recorded from 30-95 °C. The inset shows the Arrhenius plot of the same data (30-85°C). From the slope in the Arrhenius plot, an activation energy (E_a) of 61.8 kJ/mol was calculated and k_{cat} estimated as ~88 s^{-1} at 98°C by linear extrapolation. For Δ19PD an activation energy (E_a) of 62 kJ/mol and k_{cat} of ~210 s^{-1} at 98°C were obtained. *E. coli* CM-PD was examined between 17°C and 56°C in 3-component buffer (pH 7.4), containing 1 mM DTT, 1 mM prephenate and 2 mM NAD^+. An activation energy (E_a) of 47.4 kJ/mol between 17-56°C was estimated and a k_{cat} of 88.3 s^{-1} at 63°C was obtained.

3.2.2 Effects of pH, Salt and Divalent Metal Ions on the PD Activity

PD and Δ19PD demonstrated high specific activity within a very narrow pH range. The optimal pH was 7.5 at 55°C (Appendix 3B) when tested between pH 3.2-9.8, using the 3-component buffer system together with 0.8 mM prephenate and 4 mM NAD^+ as outlined in section 3.1.7.

The enzymes were most active when assayed in buffer containing 100-250 mM NaCl; 48% of maximal activity was observed at 2 M NaCl (Appendix 3C). The proteins precipitated slightly when stored in the absence of salt. Hence, a concentration of 75 mM NaCl or above and a pH of 7.5 were adopted for all buffers used in enzyme purification and for all spectroscopic and enzymatic measurements. Reaction rates of purified PD recorded at 55°C were identical whether using 50 mM potassium phosphate, 50 mM HEPES, or the 3-component buffer system (all buffers contained 0.15 M NaCl).

No effect on enzymatic activity was observed upon the addition of EDTA (1 mM), $MgCl_2$ and $ZnCl_2$ (25 mM) to standard reaction mixtures at 55°C. However, the enzymes were weakly inhibited by cobalt, decreasing to a limiting value of 65% of the maximal activity at 0.1 mM $CoCl_2$ (Appendix 3D).

3.2.3 Studies of the Initial Velocity and Product/Product Analogue Inhibition on PD from *A. aeolicus*

Initial velocity patterns constructed for PD at 55°C with either prephenate or NAD^+ as the variable substrate over the concentration range examined, yielded plots that intersected to the left of the *y* axis (Figs. 3.3 A and B). Kinetic parameters obtained from

Figure 3.3: Variation of initial velocity of *A. aeolicus* PD reaction as a function of the concentration of prephenate (A) and NAD^+ (B). In **(A)** prephenate was varied from 49-493 μM at fixed concentrations of NAD^+ of: 35 (♦), 70 (■), 140 (▲) and 350 (●) μM. In **(B)** NAD^+ was varied from 30-495 μM at fixed concentrations of prephenate of: 49 (♦), 102 (■), 145 (▲) and 495 (●) μM. The data were fit to the equation describing a sequential kinetic mechanism, $v = VAB/(K_{ia}K_b + K_aB + K_bA + AB)$, to generate the lines shown in the figure. v is the initial velocity, V is the maximum velocity, A and B are concentrations of reactants, K_a and K_b are Michaelis constants for A and B, and K_{ia} is the dissociation constant from the binary complex. The following kinetic parameters when prephenate was the variable substrate, were calculated as 9.2 s^{-1} (V), 105.3 ± 13.14 (K_a), 66.6 ± 8.95 μM (K_b), 129.8 ± 30.6 μM (K_{ia}). Results for Δ19PD are shown in Appendix 3E.

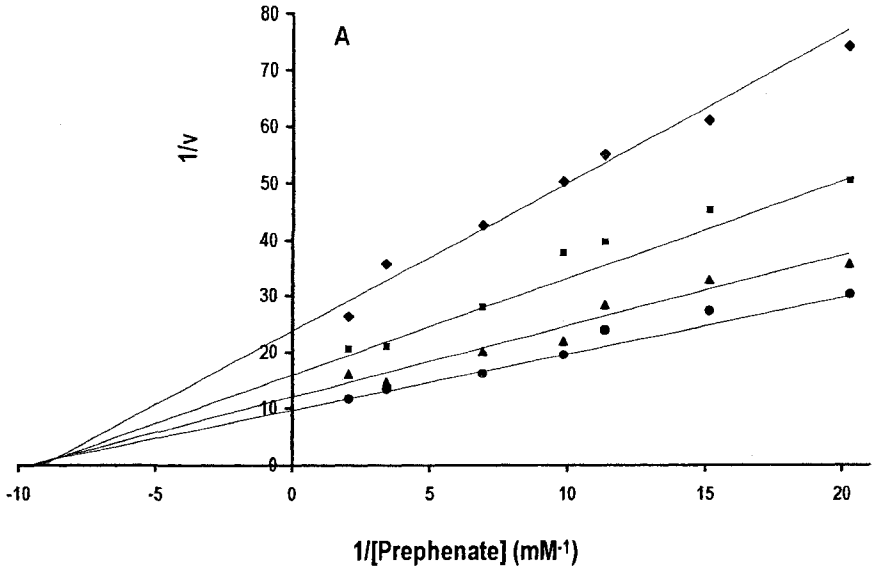
A
1/v
80
70
60
50
40
30
20
10
0
-10
-5
0
5
10
15
20
1/[Prephenate] (mM-1)

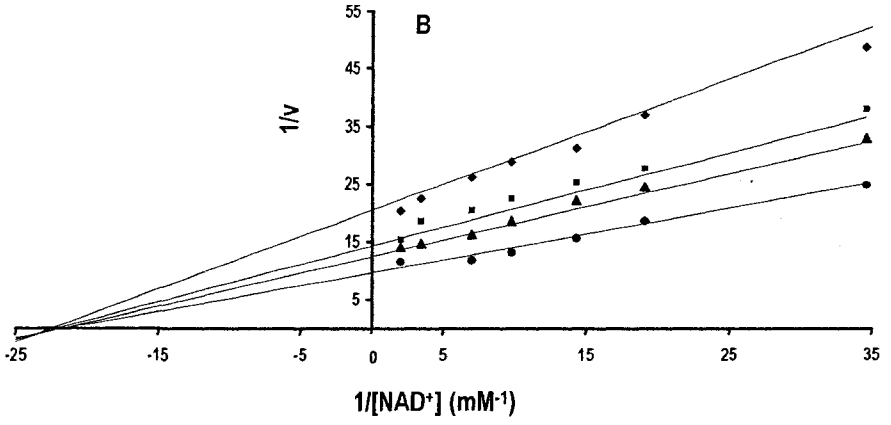
B
1/v
55
45
35
25
15
5
-25
-15
-5
0
5
15
25
35
1/[NAD+] (mM-1)

the fit of these data were in reasonable agreement with those obtained using the Michaelis-Menten equation (see Table 3.2). These results are consistent with a sequential kinetic mechanism resulting from the formation of the ternary complex before product release. Furthermore, over a concentration range of substrates which reportedly yielded concave upward kinetic plots for the PD activity of *E. coli* CM-PD (*119*), the initial velocity patterns for the *A. aeolicus* PD-catalyzed reaction were linear. Similar results were also obtained for Δ19PD and kinetic parameters are provided in the figure legend (see Appendix 3E).

Both HPP and HPPropionate, the immediate product of the reaction and a product analogue, respectively, (see structures in Fig. 3.6) behaved as linear competitive inhibitors with respect to prephenate for the Δ19PD-catalyzed reaction under the experimental conditions described in section 3. The inhibition plots and the values for the inhibition constants (K_{is}) are shown in Appendix 3F. Values for the K_m for prephenate calculated from these data sets are also shown in Table 3.2 and were in agreement with values obtained in Table in Appendix 3F.

3.2.4 pH-dependency of the Δ19PD-Catalyzed Reaction

The pH dependency of V/E_t and $V/K_{prephenate}E_t$ of the Δ19PD-catalyzed reaction was established over a range of pH values from 6.08 to 9.79 at 55°C, by varying the prephenate concentration at a fixed, high concentration of NAD^+ (see section 3.1.9). Analysis of the results indicates that the V/E_t rate profile differs than $V/K_{prephenate}E_t$ profile. The V/KE_t profile is bell-shaped with limiting slopes of -1 on both acid and alkaline sides (Fig. 3.4). Fitting of the data yielded pK values of 6.51± 0.15 and 9.57 ±

0.17 which are comparable than those found for the dehydrogenase reaction of *E. coli* CM-PD (*64*). Results from the VE_t rate profile indicate that a single ionizing group with a p*K* of 6.5 must be deprotonated for catalysis and/or product release.

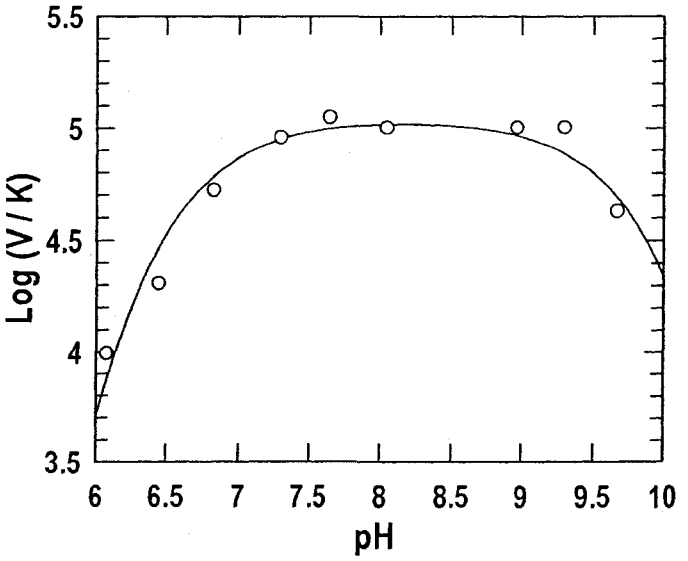

Figure 3.4: Variation with pH of log *V/K* for prephenate dehydrogenase reaction catalyzed. Dehydrogenase activity was recorded at 55°C over the pH range from 6.08 to 9.79 in a buffer containing 25 mM HEPES, 25 mM 3-(N-morpholino)propanesulfonic acid (MES) with 150 mM NaCl. NAD^+ concentration was kept fixed at 4 mM while prephenate was varied from 28 μM-840 μM. For the data set at pH 6.08, prephenate was varied from 560 μM to 5.6 mM. The curve V/KE_1 represents the best fit of the data to equation $y=C/[1+(H/K_A)+(K_BH)]$, using Graphit 5.0. Fit of the log V/KE_1 yielded a pK_a value of 6.5 ± 0.3.

3.2.5 Expression, Purification and Determination of Molecular Weights of Variant Proteins Δ19PD *A. aeolicus*

Ser126Ala, His147Asn, Glu153Ala, His217Asn, Asp247Ala, and Arg250Gln were well expressed as judged by SDS-PAGE analysis (data not shown) and yielded amounts of protein comparable to that obtained for Δ19PD. His217Ala was poorly expressed with a yield of 4 mg/mL and was not stable over time as judged by the appearance of protein precipitate during storage at 4°C for three weeks. ESI-MS was used to confirm that the correct amino acid substitution was made in Δ19PD. Table 3.3 summarizes the expected and calculated masses for selected protein variants. The results are in agreement with the idea that each protein variant analyzed carried the desired amino acid substitution.

Table 3.3: Predicted and observed molecular weights of *A. aeolicus* Δ19PD variants after cleavage of the His-tag by thrombin.

Variants	Predicted $[M+H]^+$	Observed $[M+H]^+$
Ser126Ala	33 180.5	33 180.5
His147Asn	33 173.5	33 172.6
Glu153Ala	33 138.4	33 137.5
His217Ala	33 130.4	33 130.1
His217Asn	33 173.5	33 172.9
Asp247Ala	33 152.5	33 152.3
Arg250Gln	33 168.4	ND

3.2.6 Determination of Kinetic Parameters of the Protein Variants

In the crystal structure of Δ19PD-NAD^+ complex (*48*), both Asp247 and Glu153 are near the prephenate binding site and are shown to be interacting with Arg250. In order to determine the importance of Asp247 and Glu153 in the mechanism, the two aforementioned residues were substituted to alanine residues, eliminating the potential for ionic interactions. Their kinetic parameters (K_m and k_{cat}) are in Table 3.4. Glu153Ala and Asp247Ala substitutions resulted in a 5- and 2-fold decrease in k_{cat}, respectively, but did not markedly affect prephenate binding as judged by their K_m values. The substitution of Arg250 by a glutamine resulted in a 10-fold increase in K_m for prephenate, while the enzyme's affinity for NAD^+ and its turnover rate were almost unchanged. This result is consistent with Arg250 being important for prephenate binding.

To evaluate Ser126's participation in the reaction mechanism, this residue was replaced by an alanine to eliminate the coordinated effect of His147 and NAD^+ observed in the crystal structure(*48*). The kinetic parameters of the Ser126Ala-catalyzed reaction were determined. The turnover number of the reaction catalyzed by Ser126Ala was reduced by ~12-fold. The enzyme also exhibited a 10-fold increase in the K_m value for prephenate (Table 3.4), although the K_m for NAD^+ was only slightly elevated. Substitution of His147 to an asparagine in *A. aeolicus* Δ19PD resulted in a variant that was essentially inactive, however, by adding a large amount of enzyme, a reaction rate could be determined and values for k_{cat} and K_m were calculated. The value for K_m for prephenate was similar to that of wild-type enzyme however, the turnover number was reduced by over three orders of magnitude. This verified the importance of His147 in catalysis. Values for k_{cat} appeared pH independent when activity measurements were

recorded in the presence of 850 μg of enzyme, 2 mM NAD^+ and 600 μM prephenate. At pH 6.2 and pH 7.2 k_{cat} values were identical, at ~3 x 10^{-3} s^{-1}. A thermodynamic measurement for the binding of prephenate to unliganded His147Asn was recorded to corroborate the K_m value for prephenate. Result from titration of the change in fluorescence intensity as a function of prephenate concentration yielded a K_d value of 22 ± 1.4 μM at 30°C which is comparable with the K_m value of Δ19PD (~41 μM) also determined at 30°C. To test the reliability of our fluorescence assay, we determined the dissociation constant of Ser126Ala. A K_d value of 336 ± 11 μM (Fig. 3.5) was obtained for Ser126Ala variant protein which is comparable to its K_m value at 30°C (~300 μM, data not shown).

Table 3.4: Summary of kinetics parameters for WT Δ19PD and variant dehydrogenases at pH 7.4 and 55°C

Variable Substrate[a]	Prephenate			NAD^+		
Protein	K_m (μM)	k_{cat} (s^{-1})	k_{cat}/K_m ($M^{-1}.s^{-1}$)	K_m (μM)	k_{cat} (s^{-1})	k_{cat}/K_m ($M^{-1}.s^{-1}$)
WT Δ19PD	135 ± 12	13.0 ± 0.3	9.6×10^4	71 ± 3.2	11.5 ± 0.30	1.6×10^5
Ser126Ala	1335 ± 39	0.8 ± 0.01	1.4×10^3	99 ± 6	0.8 ± 0.02	8.0×10^3
His147Asn[b]	104 ± 11	3.4×10^{-3}	3.3×10^1	ND	ND	
Glu153Ala	145 ± 14	2.8 ± 0.08	1.6×10^4	14 ± 1.9	2.1 ± 0.05	1.5×10^5
His217Ala	4132 ± 277	0.5 ± 0.02	1.5×10^2	10 ± 0.5	0.6 ± 0.004	6.0×10^4
His217Asn	3213 ± 445	0.8 ± 0.42	8.4×10^3	12 ± 0.2	0.3 ± 0.01	2.5×10^4
Asp247Ala	152 ± 9.4	5.9 ± 0.1	3.8×10^4	36 ± 2.1	5.4 ± 0.08	1.5×10^5
Arg250Gln	1185 ± 118	9.9 ± 0.42	8.4×10^3	89 ± 12	11.6 ± 0.6	1.3×10^5

[a] values were calculated from initial rates using a minimum of five substrate concentrations ranging from one-half K_m up to at least 8-fold K_m for NAD^+, and 8-fold (WT) and 10-fold (variants) for prephenate. When present as the fixed substrate, concentrations of NAD^+ (2 mM) and prephenate (8-fold K_m for WT and 10-fold K_m for variants) were used.

[b] NAD^+ was kept at 2 mM and prephenate was varied from 50 to 600 μM using 630 μg of protein. Parameters for NAD^+ were not determined.

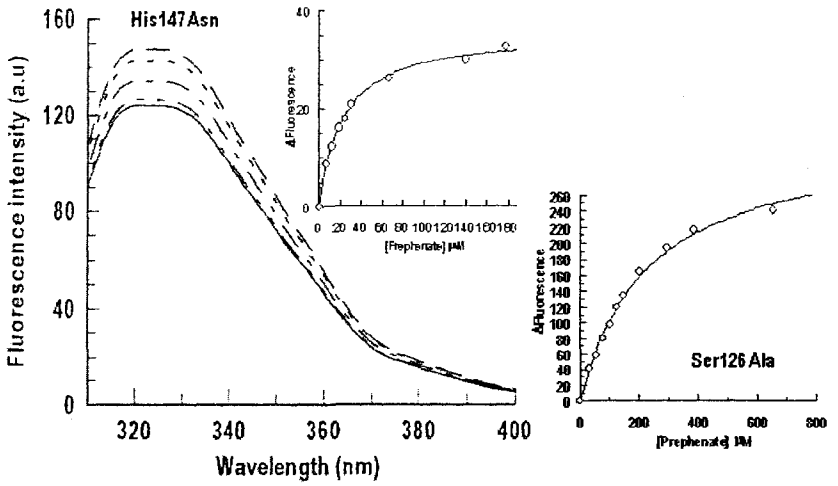

Figure 3.5: Fluorescence emission spectra of His147Asn and Ser126Ala *A. aeolicus* Δ19PD variants in the presence of increasing concentrations of prephenate. Titrations were performed at 30°C by the progressive addition of prephenate (0-200 μM and 0-680 μM for His147Asn and Ser126Ala, respectively) to PPS (2 mL) containing 0.3 μM monomer. Excitation and emission wavelengths were set at 295 nm and 333 nm, respectively. Bandwidths were set at 4 nm. The inset shows the changes in fluorescence upon prephenate binding. A dissociation constant of prephenate from its complex with His147Asn or Ser126Ala were determined to be 22 ± 1.4 μM and 336 ± 11 μM respectively, by fitting the data to the quadratic equation as described in section 2.1.7.

Replacement of the conserved histidine at position 217 by either an alanine or an asparagine led to dramatic change in kinetic parameters. The Michaelis constants for His217Ala and His217Asn were increased by 40- and 30-fold, respectively (see Table 3.4). Thus, these results strongly suggest that this residue is important for prephenate binding. In addition, decrease of the k_{cat} values by 10 to 20-fold indicate that His217 was also important for catalysis.

3.3 DISCUSSION

The heterologously expressed TyrA protein from the hyperthermophilic bacterium *A. aeolicus* functions *in vitro* as an NAD^+-dependent cyclohexadienyl dehydrogenase, but very poorly. Hence, its annotation as a PD in this report is to reflect the much preferred substrate, prephenate. Those TyrA proteins that effectively utilize both L-arogenate and prephenate, such as from *Ps. stutzeri* (*46*), *Z. mobilis* (*39*) and *Ps. aeruginosa* (*147*), do so with values of k_{cat}/K_m for L-arogenate and prephenate that are within an order of magnitude of one another.

In addition to being more resistant to heat denaturation than their mesophilic counterparts, thermophilic enzymes generally exhibit low activity at ambient temperatures and higher activity at elevated temperatures (*154*). *A. aeolicus* PD fulfills these criteria as its maximal activity is achieved at 95°C or higher, with a 33-fold increase in k_{cat} relative to that at 30°C, a half-life at 95°C of ~2 h and an estimated T_m value of about 108°C (*106*). PD, to our knowledge, is the most thermal stable enzyme from *A. aeolicus* reported to date. In contrast, significantly lower temperature optima (*155*) and only moderate half-lives at 40°C have been found for *E. coli* CM-PD (Appendix 3A) and

for other TyrA proteins (*36, 46, 147*). The half-life of Δ19PD is about half that of PD, at 95°C indicating that Δ19PD is globally more unstable or "looser". This is surprising, as the results from the protein purification, gel filtration, and secondary structure prediction (Chapter 2 in the present study) and those of tryptic proteolysis of PD yielding a crystallizable domain (Chapter 2 in this study and Sun *et al.* (*48*)), together, are consistent with PD adopting a compact structure with a floppy N-terminal region. In further support, the kinetic parameters of PD and Δ19PD-catalyzed reactions are similar but not identical, particularly at the high temperatures (Table 3.2). The N-terminal region appears to provide some structural benefits, although its role is not apparent from the crystal structure; the N-terminal residues Δ19PD (denoted 20-29 in PD) are unordered (they display weak electron densities in the crystal structure) and far removed from the central core of the active site (*48*). They immediately precede the structurally important GXGXXG motif of the NAD^+ binding domain however (Appendix 2D), so perhaps small structural perturbations transmitted to the active site are magnified at the higher temperatures. Increased flexibility has been proposed to account for the changes in kinetic parameters of the enzyme in the presence of low concentrations of Gdn-HCl (Chapter 2); this same mechanism likely accounts for the small but reproducible differences in kinetic parameters between PD and Δ19PD.

It is well known that metal ions play an important role in maintaining stable and active enzymes. It has already been reported that some thermophilic and hyperthermophilic enzymes contain metal ions that are absent in their mesophilic homologs (*156, 157*). In general extremozymes possess unusual properties at solvent-exposed surface areas which increase stability; they often require higher salt

concentrations than mesophilic enzymes to be fully active. In agreement, maximum catalytic activity was achieved with concentrations of NaCl or KCl concentrations between 100-250 mM suggesting that *A. aeolicus* PD activity is sensitive to the ionic strength of the medium. Presence of salt might increase the enzyme flexibility rendering it more active. The crystal structure did not reveal the presence of bound metal (*48*), nor is PD predicted to require metals for catalysis or structure. Accordingly, addition of the chelating agent EDTA or divalent metal ions Mg^{2+} and Zn^{2+} did not alter the dehydrogenase activity. Interestingly, slight inhibition was observed in the presence of Co^{2+}.

The intersecting initial velocity patterns obtained at 55°C for *A. aeolicus* PD (Fig. 3.3), and changes in tryptophan fluorescence noted at 30°C from the combination of NAD^+ or prephenate with Δ19PD (section 2.2.5, Figs. 2.18 A and B), indicate that the reaction follows a sequential kinetic mechanism with substrates adding to the enzyme in either order. However, the possibility exists that substrate binding may not be in rapid equilibrium. In such a mechanism, the Michaelis constants for substrates (K_m) are true dissociation constants of substrates (K_d) and should yield the same value. Our finding that the K_d for NAD^+ (~1.4 μM) determined thermodynamically is over an order of magnitude lower than the kinetically derived K_m value (~25 μM), suggests that a step other than catalysis may be rate-limiting, at least at temperatures lower than optimum for the enzyme. The results would also be consistent with NAD^+ binding in an altered conformation to the enzyme under our experimental conditions. In support of either case, a significant lag in attaining linear initial velocity conditions was noted at the lower temperatures, and is consistent with a slow conformational change upon the binding of

substrates. Surprisingly, the Arrhenius plot showed no break at temperatures between 30° and 85°C, which would typically indicate a change in the rate-limiting step (*158*). Although a rapid equilibrium random kinetic mechanism has been reported for CM-PD from *E. coli* (*63*) and *A. aerogenes* (*95*), and AD from *A. thaliana* (*40*), a steady-state random mechanism, but with a preferred order for L-arogenate binding first, has been proposed for the monofunctional AD from *Synechocystis* (*36*).

Hypotheses concerning the kinetic mechanism have also been formulated based on recently available structural data. Δ19PD has been cocrystallized at pH 7.5 with NAD^+ and with NAD^+ plus prephenate, HPProprionate or with L-Tyr. (The presence of HPP in the structure indicates that prephenate was enzymatically converted to HPP during the co-crystallization studies). Christendat and colleagues noted that although two molecules of NAD^+ were associated with the enzyme (one on each monomer), only one molecule of the product or product analogue was identified per dimer. This could result if substrate binding and product release were ordered with NAD^+ binding first and NADH released last, or if the binding of prephenate to one monomer inhibited its binding to the second monomer. Our solution studies do not support an ordered kinetic mechanism hypothesized from the crystallographic data for several reasons. First, an ordered mechanism as described above is contrary to our thermodynamic binding studies on Δ19PD which indicate that prephenate can bind to the free enzyme (Chapter 2). Both the prephenate and NAD^+ binding pockets appear independently accessible as judged by the structures of liganded protein(Chapter 1, Figure 1.10) although the possibility does exist that prephenate may block access to the NAD^+ binding pocket in the unliganded enzyme. Regrettably, there is no structurally data available for the apoenzyme; NAD^+ binding

appears to promote protein crystallization. Second, the initial velocity patterns obtained at 55°C were linear indicating that the binding of prephenate (or NAD^+) to each monomer of the dimer is independent of one other (Chapter 2). A full understanding of this kinetic mechanism awaits the results from comprehensive product and dead-end inhibition studies at different temperatures including one close to the optimum for the enzyme. Additionally, experiments will be conducted using microcalorimetry or equilibrium dialysis methods which are designed to address the stoichiometry of binding of either substrate to the free enzyme and to HPP with the enzyme-NAD^+ complex.

In this chapter we have also endeavored to clarify the roles of selected active site residues of *A. aeolicus* through kinetic and biophysical analysis of protein variants. Additionally, we have compared our findings with previous mutagenesis results and have correlated these with the current structures of the enzyme—mainly that of Δ19PD-NAD^+ alone and in complex with the immediate product HPP. There are some notable differences between the structures of prephenate and HPP; HPP is aromatic rather than a cyclohexadiene and lacks the ring carboxyl group associated with prephenate. However, HPP acts as a linear competitive inhibitor with respect to prephenate and binds to the enzyme NAD^+ complex with the same apparent affinity as does prephenate (Appendix 3F) so interactions between HPP and active site residues in PD should closely reflect those with prephenate. Of the six residues chosen for mutagenesis studies, Ser126, His147 and Arg250 are conserved in the sequences all TyrA proteins identified to date while Glu153, His217 and Asp247 show moderate to high conservation (Fig. 1.9).

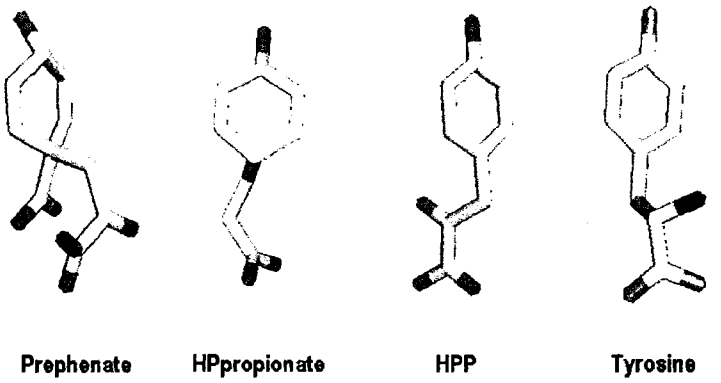

Figure 3.6: Structures of the substrate and product and product analogues of the PD-catalyzed reaction. All these structures possess a C4-hydroxyl group. The primary difference between the ligands resides the C1-sidechain; HPP has a keto group in addition to the conserved carboxyl, Tyr has an amino group and HPpropionate is lacking a group at the corresponding position. Prephenate is the only non aromatic compound.

As shown in Figure 3.7 the imidazole ring of His147 interacts with the C-4 hydroxyl of HPP and participates in a hydrogen bonding network between Ser126, Ser213 and a bound water molecule (WAT 1). Additionally, C4 of the ligand resides within 2.5 Å from the N1 portion of the nicotinamide ring of NAD^+. These interactions support the kinetic data from *E. coli* CM-PD (*52*) which identifies the invariant His197 (corresponding to the *A. aeolicus* His147) as a key catalytic group.

The results for the pH dependence of $VEt/K_{prephenate}$ and VEt reaction catalyzed by *Δ19PD* indicated that a single ionizing group with a p*K*a value of about 6.5 was deprotonated for catalysis while a second group with a p*K*a of about 9.5 was protonated and likely involved in binding prephenate to the enzyme-NAD^+ complex. As our results are consistent with the pH activity profiles observed for *E. coli* CM-PD (*52*), we assigned this deprotonated group to His147. Kinetic analysis was also performed on the *A. aeolicus* PD variant His147Asn to confirm its role solely in catalysis. His147Asn is essentially inactive, but binds prephenate with an apparent affinity similar to that of the wild-type enzyme, as determined by its kinetic parameters (Table 3.4), and as determined by thermodynamic measurements which monitor the quenching of tryptophan fluorescence emission by prephenate yielding a true dissociation constant (Fig. 2.18). Additionally, we showed that the activity of the variant was pH independent thus permitting assignment of this titrating group to His147. Together, our findings further support the catalytic function of His147 in directly polarizing the C4-hydroxyl group of prephenate or perhaps helping the bound water molecule to carry out this function to facilitate hydride transfer from prephenate to NAD^+. In the crystal structure of AD from

Synechocystis the residue equivalent to His147 (His112) is also shown to hydrogen bond with the C-4 hydroxyl group of L-arogenate (*43*).

Ser126 participates in a H-bonding network with His147, the N1 atom of NAD^+ and C4-hydroxyl group of HPP (Fig. 3.7). To test the importance of these H-bonding interactions in the catalytic mechanism, Ser126 was substituted with Ala to eliminate the H-bonding capabilities of the side chain. This substitution reduced the turnover number by 16-fold and increased the Michaelis constant for prephenate by 10-fold, while the K_m for NAD^+ remained unchanged (Table 3.4). As both K_m and k_{cat} are affected, our findings suggest that Ser126 likely coordinates the relevant functional groups on His147, NAD^+ and prephenate (or HPP) in a catalytically competent conformation. Additionally, Ser126 may help to bind prephenate or HPP in the active site.

Arg250 in *A. aeolicus* PD which was also under investigation; the corresponding residue Arg294 in *E. coli* CM-PD was identified as a key binding residue for the PD reaction(*53*) as deduced through kinetic analysis of Arg294Gln. Kinetic analysis of *A. aeolicus* Arg250Gln revealed that the Michaelis constant for prephenate was increased 10-fold relative to the value for wild-type enzyme without a significant change in the enzyme's apparent affinity for NAD^+ or its turnover number (Table 3.4). This indicates that this residue is important in prephenate binding and is in accordance with the crystal structures of Δ19PD-NAD^+ bound with HPP or any of the product analogues that the carboxylate of the pyruvyl side chain of the ligand(s) interact with the guanidinium group of Arg250 (HPP bound structure shown in Figure 3.8). The magnitude of the

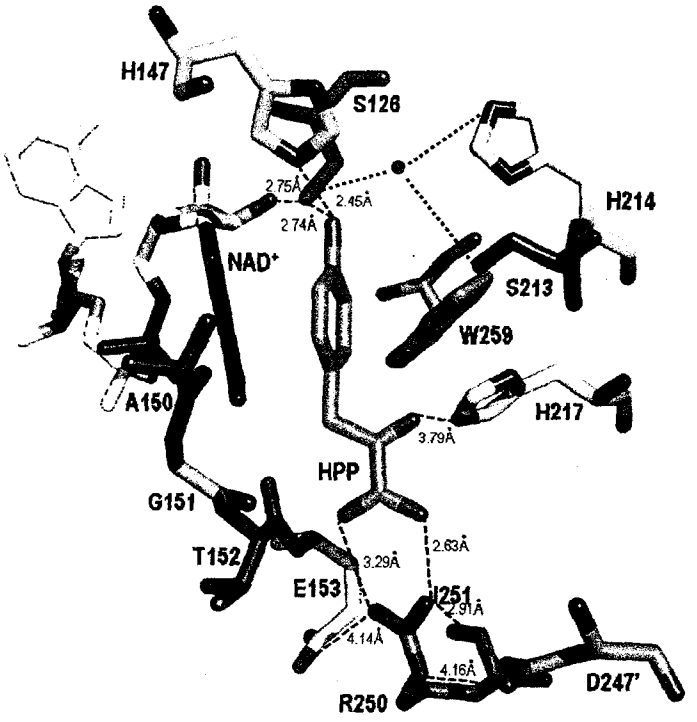

Figure 3.7: Active site representation of Δ19PD in complex with HPP and NAD^+.

apparent binding affinity (~1.4 kcal/mol or a H-bond) however, is lower than expected for the loss of an ionic interaction in this relatively buried active site. It may be that for this variant, a water molecule or perhaps another cationic residue such as Lys246 which occupies a position close to the side chain pyruvyl group, can fulfill this role (see Figure 5 in Sun *et al.* (*48*)). By comparison with previous findings on the *E. coli* Arg294Gln enzyme, the K_m for prephenate was an order of magnitude higher than we observed for Arg250Gln from *A. aeolicus* suggesting a variation in the active site architecture between the two proteins. (Note that the *E. coli* enzyme lacks the equivalent residue of Lys246 in this binding motif (see Figure 1.9 in Chapter 1, motif R/KxxxR as described by Bonner *et al.* (*45*)). Additionally, studies examining the binding of product and product analogues to wild-type and Arg294Gln CM-PD suggested that prephenate interacts with the ring carboxylate (*53*), a finding which is not supported by these current crystal structures.

Coordinated with its role in prephenate binding, the crystal structure of the enzyme-NAD^+ complex shows that Arg250 is involved in an ionic network with Glu153 from one subunit and with Asp247' from the adjacent monomer. These residues are located on the loop region between β6 and α6, and on the α10 and α10′ helices that collectively cap the active site and shift in conformation upon the binding of HPP. Sun *et al.* describes this triad as a "gate" that modulates substrate access to the active site (48). The most notable shift occurs in the loop located between β6 and α6 (residues 149 - 156), a region which defines the hydrophobic region, a wall, of the active site. Gly151 shifts 2.46 - 3.36 Å away from this pocket upon ligand binding to avoid a steric clash between it and the side chain of HPP or product analogues, bringing Glu153 along with it. Additionally, the side chain of Arg250 is shifted 1.25 Å closer to the active site pocket.

Thus Arg250 and Glu153 adopt different positions in the unliganded and bound structures while Asp247 maintains interactions with Arg250 in both states (Chapter 3, Fig. 3.8).

To probe these ionic interactions on substrate binding, Glu153 and Asp247 were individually changed to alanine residues. These substitutions effectively eliminate the ionic interactions between these residues and we predicted that these should have an effect on the kinetic parameters of the reaction, notably prephenate binding. The Glu153Ala and Asp247Ala substitutions reduced the turnover rate by 5-fold and 2-fold, respectively, although they did not have a marked affect on the Michaelis constants for prephenate (Table 3.4). These effects on k_{cat} are not large, and might reflect small differences in the electronic environment associated with these residues, or small perturbations in the position of catalytically important residues. In both of these variants the Michaelis constant for NAD^+ is significantly lowered; such an effect has also been observed for wild-type enzyme in the presence of low concentrations of guanidine-HCl (*112*), and highlights the sensitivity of the active site to its environment.

If the Michaelis constant was considered as a true dissociation constant then its value would depend on the "on" and "off" rate constants of prephenate from the enzyme As k_{cat} is reduced in the variants but not K_m, it may be that the release of product from the enzyme (reflected in the k_{cat} term) and substrate association are reduced equally by the amino acid substitutions. As such, these diffusion processes would be subject to the effects of a viscogens and could be tested. These types of experiments have been performed for the chorismate mutase reaction from *B. subtilis* (*159*). Additionally, a series of double mutants and a triple mutants could be generated and the variants

expressed and characterized in order to test the additivity of the changes in the kinetic parameters.

The structure of the Δ19PD-NAD^+-HPP complex shows that the imidazole group of His217 along with the main chain carbonyl of Gly243 makes important interactions with the keto group on the pyruvyl side chain of the ligand (Fig. 3.7). Thus it was predicted that substitutions of His217 to either alanine or asparagine would produce significant changes in the kinetic parameters for the Δ19PD-catalyzed reaction. The Michaelis constant for prephenate was increased by 40-fold and 30-fold for His217Ala and His217Asn respectively thus indicating the importance of His217 in prephenate binding. However these substitutions also coincided with a 10 to 20-fold decrease in k_{cat} thus indicating that this interaction with the keto group of the substrate may assist in positioning prephenate in a catalytically competent conformation. Alternatively, the His217Ala and His217Asn substitutions might have perturbed the structure of the active site, presumably due to the disruption of the hydrophobic stacking of His217 with the neighbouring Trp259 and Ile251. Evidence for this latter statement comes from stability studies with Gdn-HCl (W. Hou, unpublished) which indicate that the variant His217Ala is less stable than WT enzyme. Additionally, the K_m for NAD^+ was lowered by 7-fold for both variants (Table 3.4), a characteristic that is noted with a few other variants and with the addition of Gdn-HCl. As mentioned previously, these results are in keeping with structural perturbations of the active site which might allow for altered or non-productive binding of NAD^+.

Christendat and coworkers have further illustrated the importance of His217 in maintaining ligand conformation. Superimposition of the crystal structures of the

enzyme-NAD^+ complex bound with HPP or HPpropionate clearly shows that the propanoyl side chains are not superimposable; the HPpropionate side chain is shifted more, by 2 Å, towards His217 (Fig. 3.8). HPpropionate, lacks the side chain keto group and as such cannot participate in the hydrogen bonding interaction with His217 and the carbonyl of Gly243. One would predict then that binding energy contributed by the interaction of the keto group with its H-bonding partners would be significant. The differences in K_i values (Table in Appendix 3F), which describe the binding of HPP and HPpropionate to Δ19PD-NAD^+ complex, is relatively small, however, about 4-fold or a ΔG of ~0.8 kcal/mol; a comparable ΔG value (~1.5 kcal/mol) was calculated for the same interaction in *E. coli* CM-PD (*53*).

Christendat and coworkers (unpublished) have compared structures of $NADP^+$ bound AD from *Synechocystis* and NAD^+ bound PD from *A. aeolicus* and have modeled in HPP in AD's active site. They noted that the active site of AD is more open and accessible, relative to that of PD; α10 and the β6-α6 loop region, which comprise the base and wall of the pocket, respectively, are shifted ~3.1-6.5 Å away from the active site. Nevertheless, from the modeling studies they show that L-arogenate can interact with Ser92, His112 and Arg217, which correspond to Ser126, His147 and Arg250 in Δ19PD. This proposed interaction with Arg217 contradicts Legrand *et al.* (*160*) who have suggested that this arginine is too far from the active site pocket to play a role in substrate binding. The most notably difference in the active site of AD is the presence of a large

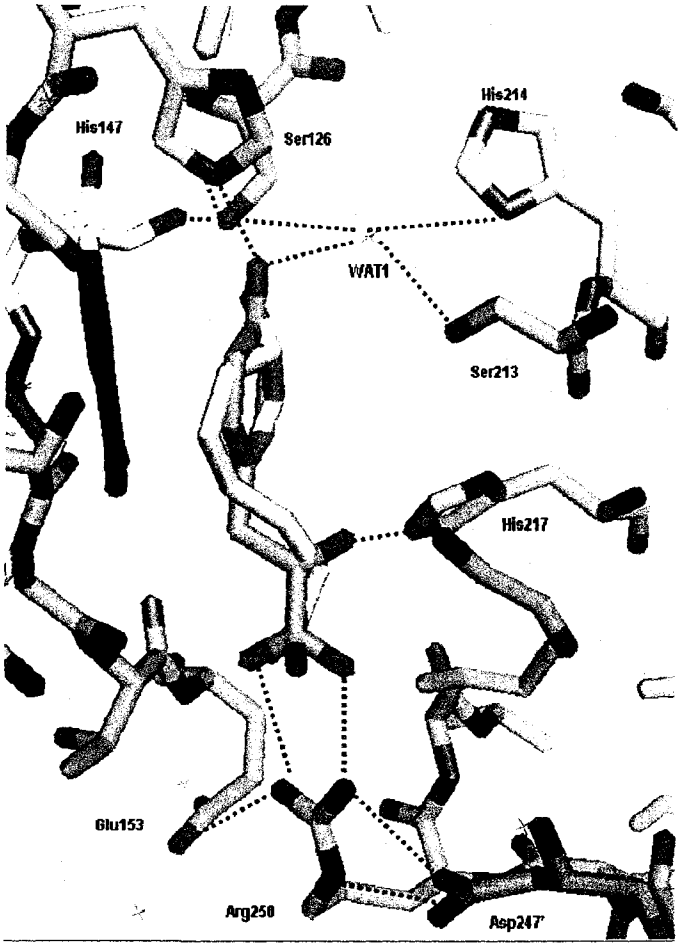

Figure 3.8: Illustration of substrate superimposition in the active site. Superimposition of HPP (green) and HPpropionate (yellow) indicates the twist in HPpropionate. The keto group of HPP mediates an interaction with His217.

pocket results from the absence of bulky Trp and His residues (Trp259 and His217 in PD). These missing residues likely help bind prephenate. Additionally, Legrand *et al.* (*43*) has identified a series of hydrophobic side chains near the ring carboxylate of L-arogenate modeled into the AD active site that Cleland and others (*94*) have speculated may promote its decarboxylation. This structural feature would be in keeping with solution studies on *E. coli* CM-PD using heavy atom isotope effects which show decarboxylation and hydride transfer are concomitant reactions (*94*). As this structural feature has not been readily identified in the model of prephenate modeled with *A. aeolicus* PD (*48*) it may be that the thermophilic enzyme follows a different catalytic mechanism in this regard. Further mechanistic studies will include site-directed mutagenesis on AD from *Synechocystis* in our laboratory.

Chapter 4

Investigation of the Mechanism of Feedback Inhibition by L-Tyrosine

4.0 INTRODUCTION

Within the metabolic pathways dictated by TyrA proteins, L-Tyr can function as a direct product product of a reaction (as with dehydrogenases which use L-arogenate as a substrate) or can act as an end product of a pathway. In many cases, L-Tyr is reported to compete directly with the substrate at the active site, be it prephenate or L-arogenate. These inhibition studies include those performed on the bifunctional PD from *E. coli* (*65, 100*), *E. herbicola* (*51*) and on the monofunctional *B. subtilis* PD (*161*). Additionally, Bonner *et al.* suggested that L-Tyr act as a competitive inhibitor with respect to L-arogenate in AD from *Synechocystis* (*36*) while Legrand *et al.* reported that the same enzyme was insensitive to feedback inhibition by Tyr (*43*). Interestingly, some TyrA proteins such as *Z. mobilis*, *N. europaea*, *N. gonorrhoeae* or *Acidovorax facilis* are not sensitive at all to Tyr inhibition (*39, 45*).

The *E. coli* bifunctional enzyme has received considerable attention since Tyr modulates both the mutase and the dehydrogenase activities (*56*). This enzyme also exhibits kinetics suggestive of positive cooperativity in the binding of prephenate in the PD-catalyzed reaction and that this cooperativity is enhanced in the presence of L-Tyr. Several models have been proposed for the mechanism of allosteric inhibition by L-Tyr. One model has been proposed derived from sedimentation velocity and equilibrium experiments that indicate the enzyme can undergo an allosteric transformation from dimer to tetramer; L-Tyr binding preferentially to the inactive tetramer but at the same site that prephenate can bind. In contrast, Christopherson (*100*) and Turnbull *et al.* (*101*) have proposed through fitting of kinetic models for inhibition, the effects of L-Tyr are manifested through tertiary structural changes transmitted through the dimer without any

changes in quaternary structure. Thus the binding of L-Tyr to one subunit positively influences the binding of L-Tyr to the second subunit. Turnbull suggested that L-Tyr must illicit its effects however, by binding to a separate allosteric site since L-arogenate is a very poor substrate in the *E. coli* PD-catalyzed reaction.

The residues involved in the interaction between TyrA proteins and L-Tyr are largely unknown. Using a directed evolution approach Lüktke-Eversloh and Stephanopoulos (*102*) introduced random mutations in the *E. coli tyrA* gene by error-prone PCR (nucleotide analogue mutagenesis) then selected for growth on media containing a Tyr analogue m-fluoro-DL-Tyr. They identified, for the first time, Tyr-insensitive variants. Sequencing of the *tyrA* gene of the feedback-inhibition-resistant variants revealed that the residues Tyr263, Ala354 and Phe357 of *E. coli* CM-PD were likely involved in the mechanism of Tyr inhibition. The structural significance of these results are unclear.

In this chapter, we have extended Aponte's work, investigating the effect of L-Tyr on *A. aeolicus* PD and Δ19PD activities over a broad range of temperatures. Protein variants from *A. aeolicus* Δ19PD characterized in the previous chapter and one variant from *E. coli* CM-PD were assayed for Tyr inhibition to determine which of the residues might be involved in the inhbition. To monitor the binding of L-Tyr by thermodynamic methods, two rapid assays were developed. Analytical size exclusion chromatography and analytical ultracentrifugation were performed to determine whether or not the binding of Tyr is accompanied by quaternary structural changes as reported for the WT *E. coli* enzyme.

To gain more insight into the catalytic and regulatory mechanism of the *E. coli* enzyme, our results will be interpreted in the context of of the crystal structure of Δ19PD in complex with NAD^+ and L-Tyr reported by our collaborators, and additionally of a genetically engineered monofunctional PD from *H. influenzae* CM-PD also in complex with NAD^+ plus L-Tyr (unpublished structure by JCSG, www.jcsg.org). As a primilary study, the monomeric structure of the PD domain of *E. coli* CM-PD was modeled using as a template the liganded form of the dimeric PD domain of *H. influenza.* These two dehydrogenase-containing domains share a sequence identity of only 55% but residues shown to be important for the activity of the *E. coli* enzyme are all conserved. Important groups involved in Tyr inhibition were identified.

4.1 EXPERIMENTAL PROCEDURES

4.1.1 Materials

Prephenate (sodium salt) was obtained as previously described by Dudzinski and Morrison (*113*). L-tyrosine was obtained from ICN while NAD^+ (Grade I) was from Roche. 1-anilino-naphatlene sulfonic acid (ANS) was purchased from Sigma. High purity of the substrates was confirmed by either mass spectrometry or NMR. Concentrations of stock substrate solutions were determined using published extinction coefficients (*115*) and/or enzymatic end-point analysis. All other chemical reagents were obtained commercially and were of the highest quality available.

4.1.2 Source of Enzymes

Purified thrombin-treated *A. aeolicus* PD, Δ19PD and Ser126Ala, Glu153Ala, His217Ala Asp247Ala and Arg250Gln variants were expressed and purified as described in sections 2.1.3 and 3.1.3, respectively, and stored at -20°C at a concentration >3 mg/mL in storage buffer. Plasmid DNA of pVIV1 (*tyrA* in pSE380) carrying the mutation encoding His257Ala was prepared by D. Christendat(*52*). *E. coli* CM-PD (~30 U/mg) and His257Ala CM-PD variant were expressed and purified by J. Manioudakis as previously described (*53*). CM-PD enzymes were stored at –86°C at a concentration > 2 mg/mL in 0.1 M N-ethylmorpholine (pH 7.5), 1 mM EDTA, 20% (v/v) glycerol, 5 mM DTT.

4.1.3 Effect of L-Tyr on PD Activity of WT and variants of *E. coli* and *A. aeolicus* enzymes

Standard activity assays for *A. aeolicus* PD and Δ19PD were measured at 30, 55 and 80°C as described previously (section 2.1.4). Standard assays for the mutase and dehydrogenase activities *E. coli* CM-PD were performed at 30°C as previously described (*53*). CM activity is usually monitored by following the disappearance of chorismate at 273 nm. The effect of L-Tyr on mutase activity however, was measured in the presence of NAD^+ (required to help Tyr bind) and at 290 nm (due to the high absorbance of Tyr at 280 nm) and by taking into the account the contribution of NADH and HPP at 340 nm. The initial rates were calculated as described by Heyde and Morrison (*95*).

Inhibition by Tyr (0-1 mM) on the dehydrogenase activity of PD and Δ19PD was recorded at 30, 55 and 80°C using concentrations of 2 mM NAD^+ and ~4 x K_m for

prephenate. Tyr inhibition on *A. aeolicus* PD and Δ19PD activity were also monitored with prephenate as the variable substrate keeping NAD^+ fixed, and with increasing concentrations of L-Tyr (see figure legends for details). When appropriate, the Hill coefficient was obtained from the slope of a plot of $\log[v/(V_{max} - v)]$ versus log [substrate], using values of v (initial velocity) between 10% and 90% V_{max} (maximum velocity).

The different variants of *A. aeolicus* Δ19PD were screened for inhibition by Tyr (0-1 mM) at 55°C, using concentrations of 2 mM NAD^+ and ~4 x K_m for prephenate for each enzyme, except for His217Ala and Arg250Gln, where prephenate concentrations were kept at ~2 x K_m for prephenate and the variants were assayed up to 8 mM L-Tyr. For the mesophilic *E. coli* WT and His257Ala CM-PDs, assays in the presence of Tyr (0-0.8 mM) were performed at 30°C using concentrations of 2 mM NAD^+ and ~4 x K_m for prephenate or chorismate for each enzyme.

4.1.4 Monitoring L-[3,5-^{3}H]Tyrosine Binding in the Presence and the Absence of Ligands

The ability of WT and variant proteins from *E. coli* CM-PD and *A. aeolicus* Δ19PD to bind L-Tyr was assessed by radiolabeling experiments. MicroSpin™ G-50 Columns (Amersham Biosciences) were equilibrated in 25 mM Tris (pH 7.4), 75 mM NaCl, (25 mM NaCl for CM-PD and His257Ala), 1 mM DTT and 2 mM NAD^+. Proteins were buffer exchanged using a NAP™ 5 column (Amersham Biosciences) in the same buffer and concentrated using Ultrafree® -0.5 Centrifugal Filter Device (Millipore). Each protein (~2 μM monomer) was incubated with the same molar ratio of L-[3,5-

^{3}H]Tyrosine (53.0 mCi/mmol, Amersham Biosciences). The entire reaction volume (36 µL) was then gently transferred to the center of a MicroSpin^{TM} G-50 Column. Proteins were eluted by spinning the columns at 2000*g* for 1 min at room temperature. Then, the resin was gently washed 4 times with 36 µL of cold buffer by the same means, careful to deliver the sample and washes to the center of the column. Elution fraction and washes were collected and 10 µL aliquots were added to 4 mL of scintillation fluid (ICN). Radioactivity was monitored using a 1414 WinSpectral^{TM} liquid scintillator counter (Wallac). Protein concentration of each fraction was estimated using the Bio-Rad Protein Assay Kit (Bio-Rad laboratories) using Bovine Serum Albumin (Sigma) as a standard. Control experiments were done as described above using BSA (ICN).

4.1.5 Monitoring ANS Fluorescence Emission in the Presence and the Absence of Ligands

The binding of ligand (L-Tyr and/or NAD^+) was followed by fluorescence at 30°C using an Aminco Series 2 Luminescence Spectrometer equipped with a thermostated holder connected to a circulating water bath. WT CM-PD, Δ19PD and their respective variants His257Ala and His214Ala (2 µM monomer each) prepared with the different ligands and were incubated with 50 µM 1-anilino-8-naphtalene sulfonic acid (ANS) in the dark at 30°C in either 50 mM potassium phosphate, 75 mM NaCl (pH 7.5) for the *A. aeolicus* enzymes or 50 mM potassium phosphate and 1 mM DTT (pH 7.5) for the *E. coli* enzymes. The ANS/protein mixture contained either no ligand, 0.5 mM NAD^+, 1 mM Tyr or 0.5 mM NAD^+/1 mM Tyr, all in their respective buffers. Measurements were performed using a 1 cm path-length cuvette (reaction volume 2 mL). Excitation

wavelength was set at 370 nm and emission spectra were recorded from 400 to 600 nm with bandwidths of 4 nm each. Fluorescence spectra were obtained by subtracting the appropriate blank and were corrected for inner filter effect(*125*).

4.1.6 Determination of Molecular Weight in the Presence and the Absence of Ligands

4.1.6.1 Analytical Size Exclusion Chromatography

The native molecular weights of *A. aeolicus* Δ19PD and *E. coli* CM-PD and selected mutants were determined in the absence and presence of 0.5 mM NAD^+ and 1 mM L-Tyr at ambient temperature by a Pharmacia Akta FPLC system fitted with a Superdex G-200 column (HR 10/30, Pharmacia). Chromatography was performed with mobile phases containing PPS (pH 7.5) for *A. aeolicus* Δ19PD and 50 mM potassium phosphate, 25 mM NaCl (pH 7.5) and 1 mM DTT for the *E. coli* enzymes, with and without ligands. Flow rate was set at 0.75 mL/min and injection volume was 500 μL. Elution was monitored at 290, 300 and 310 nm, and fractions (1 mL) were assayed for enzyme activity and inhibition by L-Tyr. Bio-Rad gel filtration protein standards included vitamin B_{12} (1.35 kDa), equine myoglobin (17 kDa), chicken ovalbumin (44 kDa), bovine γ-globulin (158 kDa), thyroglobulin (670 kDa). Void volume and total bed volume were evaluated with Blue Dextran and DTT, respectively.

4.1.6.2 Analytical Ultracentrifugation

Native molecular weight of Δ19PD in the absence and the presence of 1 mM L-Tyr/NAD^+ was investigated by sedimentation velocity experiments. Samples were

prepared as outlined in section 2.1.5.2 and the sedimentation data were acquired with the interference optical scanning system of the Beckman XL-I analytical ultracentrifuge. Values for the sedimentation coefficient (s) and an average molar mass were calculated as previously described (see section 2.1.5.2).

4.1.7 Modeling of the PD domain of *E. coli* CM-PD

Modeller 9v3 was used to model the monomeric PD domain of CM-PD against the known structure of *H. influenzae* CM-PD (PDB access code 2pv7). A structure-based alignment of *E. coli* CM-PD with the *H. influenzae* protein was obtained using the FFAS03 server (http://ffas.ljcrf.edu/ffas-cgi-cgi/ffas.pl). The FFAS03-generated alignment was used as input for Modeller 9v3, which generated a 3 D model of *E. coli* PD on this input.

4.2 RESULTS

4.2.1 Effects of Tyr on PD Activity at Different Temperatures

Inhibition studies were performed on both *A. aeolicus* PD and Δ19PD at 30, 55 and 80°C using varying amounts of L-Tyr (0-1.0 mM) at fixed concentrations of prephenate and NAD^+. PD was inhibited up to 60% by 1 mM L-Tyr (Figure 4.1), when assayed at 30°C or 55°C in the presence of 2 mM NAD^+ and at a prephenate concentration 4 x K_m at each temperature. This value increased to 90% inhibition at 80°C, which is similar to the pattern for *E. coli* CM-PD at 30°C obtained using similar ratios of substrate concentration to K_m (*56*). These trends were also noted for Δ19PD, although the degree of inhibition was lower. When the data were plotted as specific activity as a

function of Tyr concentration, however, activity decreased to a limiting value of ~4 U/mg (PD) or ~26 U/mg (Δ19PD) at 55°C and 80°C, respectively (Fig. 4.1). This indicates that the apparent increase in inhibition at the higher temperature is only relative. Hudson *et al.* (*65*) reported that the binding of Tyr to *E. coli* CM-PD is enhanced by NAD^+ and vice-versa. Nevertheless, doubling the concentration of NAD^+ to 4 mM did not result in any further inhibition of activity by L-Tyr at any of the three temperatures tested (data not shown). Inhibition of the PD reaction by L-Tyr was also examined with prephenate as the variable substrate at fixed concentrations of NAD^+ of 1 mM and 2 mM (Fig. 4.2). Double reciprocal plots were concave upward in the presence of L-Tyr. Deviations from linearity were more pronounced at the higher concentrations of NAD^+ and lowest concentrations of prephenate. Similar results have also been reported for PD of *E. coli* CM-PD by Turnbull *et al.* (*101*), Hudson *et al.* (*65*) and Christopherson (*100*), and are consistent with Tyr promoting cooperative interactions between the subunits. This is evidenced by a fit of the velocity data in Figure 4.2 (2 mM NAD^+) to the Hill equation to yield Hill coefficients of 1.0, 1.2 and 1.8 with 0, 0.1 and 0.5 mM Tyr, respectively. A value of 2 is consistent with two molecules of L-Tyr binding per dimer. One set of lines in the double reciprocal plot did not appear to intersect on the y axis indicating that at this assay temperature, L-Tyr might be binding to an allosteric site. Phe (1 mM) did not inhibit PD activity at any of the three temperatures.

Inhibition of the Δ19PD reaction by L-Tyr was monitored under conditions which allowed us to examine closely the y-intercept of a double reciprocal plot. The data fit well to the equation describing linear competitive inhibition, yielding a value for K_i of 15.9 ± 1.3 μM. The Michaelis constant derived from this plot (122 ± 15 μM) agreed well with

the value given in Table 3.2. It is noteworthy that the double reciprocal plots generated for Δ19PD also displayed some non-linear behaviour at the highest concentration of L-Tyr (0.2 mM) and the lowest concentration of prephenate.

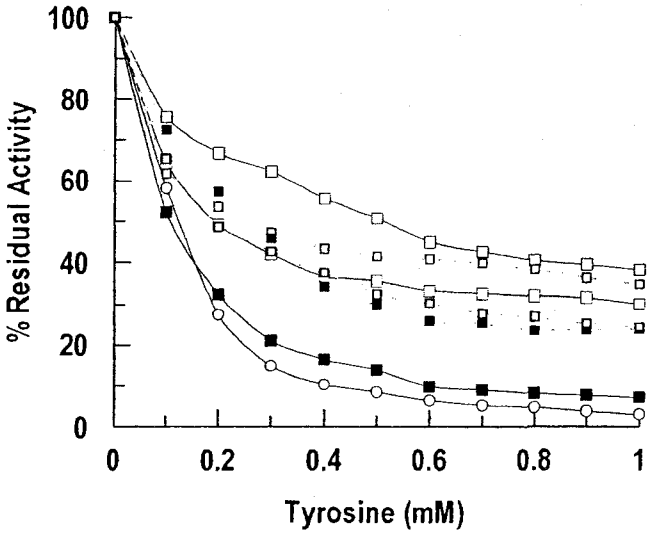

Figure 4.1: Effects of Tyr on PD activity. Inhibition of dehydrogenase activity of *A. aeolicus* PD (squares), Δ19PD (small squares, broken lines) and *E. coli* CM-PD (circles) by Tyr. Reactions with PD and Δ19PD were performed at 30 (□), 55 (□) and 80°C (■) using ~4 x K_m for prephenate for each temperature and NAD^+ was fixed at 2 mM. The pH of the buffer was adjusted to the desired values at 55°C and 80°C. Data for CM-PD were obtained at 30°C in the presence of 160 μM prephenate. Assays were performed as described in section 4.1.3

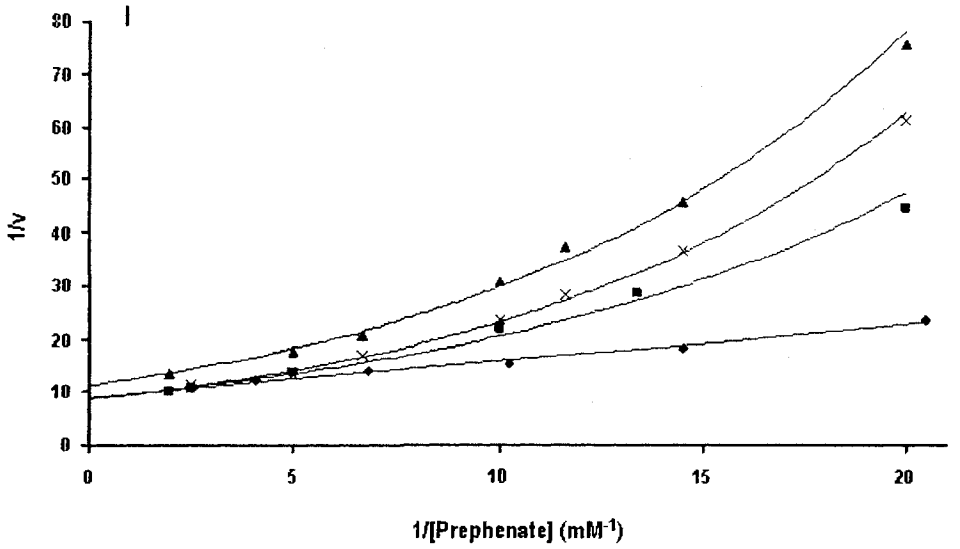

Figure 4.2: Double reciprocal plots of the inhibition of PD by Tyr at 55°C. PD activity was assayed at Tyr concentrations of 0 (♦), 0.1 (■) and 0.5 mM (▲) with NAD^+ kept at 2 mM, and at 0.5 mM Tyr with 1 mM NAD^+ (x). 1/v is expressed as µmol NADH formed/min/mg.

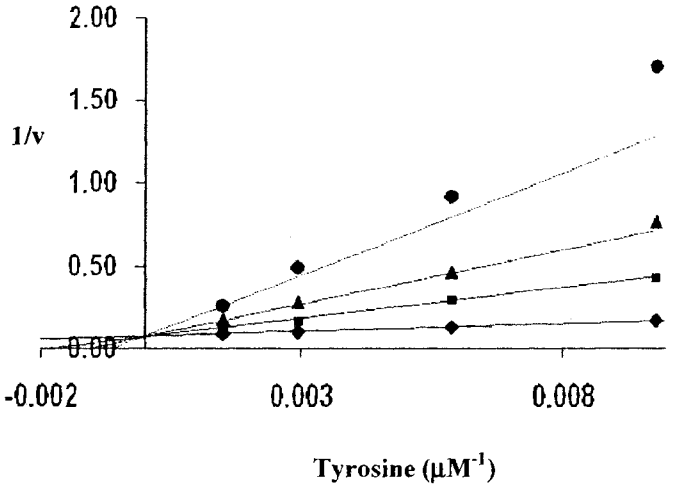

Figure 4.3: Double reciprocal plot of the inhibition of *A. aeolicus* Δ19PD by L-Tyr at 55°C. PD activity was recorded by varying prephenate concentrations from 102-680 μM, keeping NAD^+ fixed at 2 mM and in the presence of L-Tyr from 0 (●), 50 (■), 100 (▲) and 200 (●) μM. The data were fit to the equation describing linear competitive inhibition to generate the family of lines shown in the figure.

4.2.2 Effects of L-Tyr on the PD Activity of WT Enzymes and Variants from *A. aeolicus* Δ19PD and *E. coli* CM-PD

Aquifex aeolicus enzymes

The PD activity of WT and variant *E. coli* and *A. aeolicus* enzymes were examined in the presence of increasing concentration of L-Tyr and the results are shown in Figures 4.3, 4.5 and 4.6. As previously shown, the activity of Δ19PD appears only partially inhibited, up to about 70% by 1 mM Tyr at 55°C. Under the same experimental conditions, the activity of the variants Ser126Ala, Asp247Ala and Glu153Ala were also inhibited by L-Tyr, however with the ranking of WT = Ser126Ala < Glu153Ala << Asp246Ala (at the higher Tyr concentrations). The most striking result is that His217Ala activity is not inhibited at all by L-Tyr. Extending the Tyr concentration up to 8 mM produced the same results (see Figure 4.4). The effect of L-Tyr on Arg250Gln activity was also tested, revealing that this variant is clearly less sensitive to feedback inhibition by Tyr than the WT protein. His217Ala or Arg250Gln displayed K_m values for NAD^+ that were comparable to WT enzyme (see Chapter 3 Table 3.4), hence the feedback resistance was not due to poor binding of the cofactor.

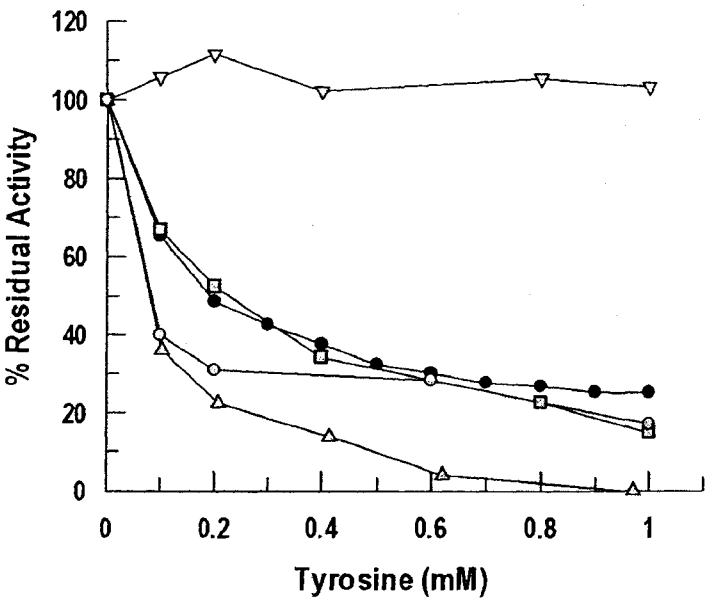

Figure 4.4: Effects of L-Tyr on PD activity of WT and Variants.

A. aeolicus Δ19PD (●) and Ser126Ala (▣), Glu153Ala (◆), His217Ala (▼) and Asp247Ala (▲) variant proteins were assayed in the presence of Tyr (0-1.0 mM). Reactions were carried out in reaction buffer using ~4 x K_m for prephenate and NAD^+ concentration was fixed at 2 mM at 55°C. Due to the high K_m value of His217Ala for prephenate, ~2 x K_m was used instead, keeping NAD^+ concentration at 2 mM.

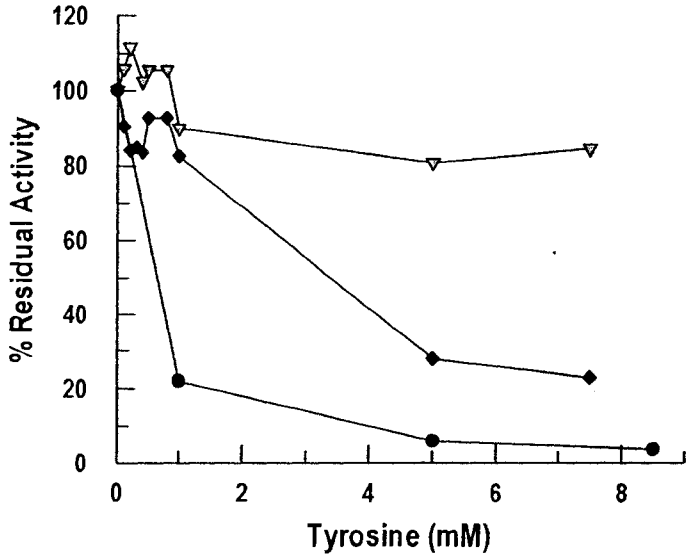

Figure 4.5: Effect of high concentrations of L-Tyr on PD activity of WT and Selected Variants of Δ19PD.

A. aeolicus Δ19PD (●), His217Ala (▽) and Arg250Gln (♦) variant proteins were assayed in the presence of Tyr (0-8.5 mM). Reactions were carried out in reaction buffer using ~4 x K_m for prephenate and NAD^+ concentration was fixed at 2 mM at 55°C. Due to the high K_m values of His217Ala and Arg250Gln for prephenate, ~2 x K_m was used instead, keeping NAD^+ concentration at 2 mM.

E. coli enzymes

The effect of L-Tyr on the CM and PD activities of *E. coli* CM-PD and His257Ala was also investigated. Under the experimental conditions given in the text, both mutase and dehydrogenase activities were inhibited by L-Tyr to the same extent, and hence contrasts previous reports that PD was more sensitive to inhibition than CM (*101*). His257Ala exhibited kinetic parameters for the PD reaction in the absence of L-Tyr that were comparable to the values obtained for WT enzyme, although k_{cat}/K_m value for the mutase reaction was reduced by over an order of magnitude by the mutation (see Table 4.1). Under conditions that yielded almost complete inhibition of WT CM-PD activities, the variant was insensitive to the effects of L-Tyr. These results are in agreement with previous work done in our lab by T. Lee.

Table 4.1: Steady-state kinetics parameters for WT and His257Ala *E. coli* CM-PD at 30°C

Protein	Mutase Activity			Dehydrogenase Activity					
	Chorismate			Prephenate			NAD^+		
	K_m (μM)	k_{cat} (s^{-1})	k_{cat} / K_m ($M^{-1}s^{-1}$)	K_m (μM)	k_{cat} (s^{-1})	k_{cat} / K_m ($M^{-1}s^{-1}$)	K_m (μM)	k_{cat} (s^{-1})	k_{cat} / K_m ($M^{-1}s^{-1}$)
WT CM-PD	40 ± 3	54.7 ± 0.8	1.4×10^6	35 ± 1	37.6 ± 0.3	1.1×10^6	142 ± 13	40.7 ± 0.9	2.9×10^5
His257Ala	102 ± 8	9.8 ± 0.2	8.8×10^4	64 ± 3	33.9 ± 0.6	5.3×10^5	269 ± 64	32.7 ± 0.4	1.2×10^5

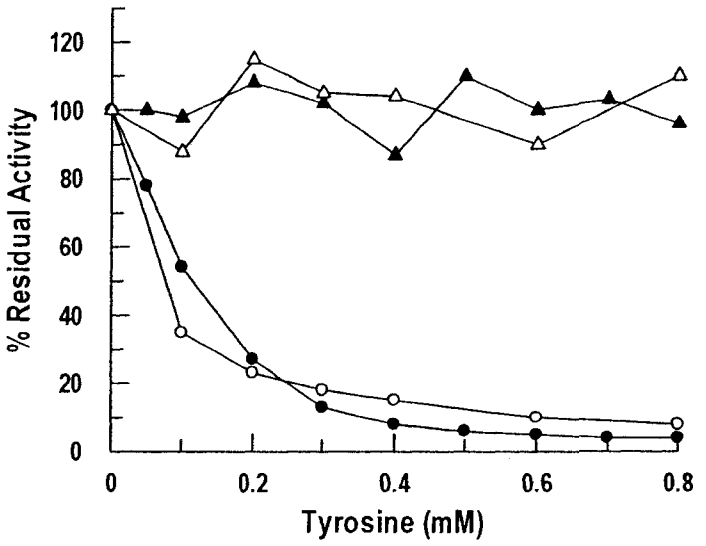

Figure 4.6: The effect of L-Tyr on the mutase and dehydrogenase activities of WT and His257Ala *E. coli* CM-PD. All activity assays were performed at 30°C. Prephenate concentration was fixed at 0.2 mM to follow the dehydrogenase activity of WT (•) and His217Ala (▲), while chorismate as held at 0.3 mM to measure mutase activity of WT (○) and His257Ala (Δ). NAD^+ was held constant at 4 mM in all assays.

4.2.3 Binding of L-Tyr to the WT and Variant Enzymes Assessed by Radiolabeling Experiments

We have established a qualitative method to rapidly monitor L-Tyr binding. This method follows the elution pattern of a radiolabelled small molecule as it passes through a size exclusion column. Briefly, if the radiolabeled Tyr (small molecule) binds to a protein (large molecule) then it will travel faster through size exclusion media, whereas unbound Tyr is more easily trapped within the beads of the column media and the elution of the radiolabel is retarded. The eluate is assayed during different time periods for radioactivity (scintillation counting) and protein content (Bio-Rad protein assay) as the column is washed in order to detect the presence of a protein-ligand complex. In the experiments presented here, the binding of L-[3,5-^{3}H]Tyrosine to *A. aeolicus* Δ19PD or *E. coli* CM-PD (1:1 molar ratio) was monitored as these species traveled through MicroSpin^{TM} G-50 size exclusion columns. NAD^{+} (2 mM) was present in all solutions since NAD^{+} has been reported previously to promote Tyr binding(*65*). The results are presented in Table 4.2. WT protein (either *E. coli* CM-PD or *A. aeolicus* Δ19PD) co-eluted with radiolabel in the first fraction signifying that these proteins could bind L-Tyr. In contrast, results for the variant proteins (either His257Ala CM-PD or His217Ala Δ19PD) showed that the highest amount of radioactivity was associated with the protein-free fraction, indicating that these variants did not bind Tyr or possessed a much weaker affinity for the ligand compared to their wild-type counterparts. A control experiment was performed with BSA (a protein that does not bind Tyr) which clearly shows

radioactivity in the latter fractions. A similar result was obtained when the experiment was performed in the absence of protein (data not shown).

Table 4.2: Radiolabelling experiments[a].

	BSA		WT CM-PD		His257Ala	
Fractions	cpm[b]	OD_{595nm}[c]	cpm	OD_{595nm}	cpm	OD_{595nm}
Elution	301	0.395	9512	0.295	195	0.306
Wash I	1014	0.0092	942	0.0053	2701	0.0087
Wash II	2729	0.0027	3143	0.0028	2528	0.0017

	WT Δ19PD		His217Ala	
Fractions	cpm	OD_{595nm}	cpm	OD_{595nm}
Elution	1693	0.185	90	0.197
Wash I	889	0.007	718	0.0051
Wash II	1127	-	1059	-

[a]Radiolabelling experiments were carried out as described in section 4.1.4. BSA was used as a control in both experiments.
[b] represents counts per minute
[c] represents the absorbance obtained at 595 nm from the mixture of an aliquot (10 µL) of collected fraction with 1 mL of Bradford reagent allowing protein content determination.

4.2.4 ANS Binding Experiments

A fluorimetric assay was developed to monitor Tyr binding and/or conformational changes which may occur upon the interaction of L-Tyr with WT and His257Ala *E. coli* CM-PD and the corresponding Δ19PD enzymes of *A. aeolicus*. The fluorescent dye 1-anilinonaphtalene-8-sulphonic acid (ANS) has been widely used to study protein conformational changes. The assay is based on the intrinsic increase in ANS fluorescence quantum yield upon noncovalent binding to hydrophobic region of proteins(*162*). ANS is also reported to bind to pockets of charged residues within proteins to illicit similar

effects. Upon addition of NAD^+ to all the proteins the fluorescence intensities decreased (Fig. 4.7), consistent with a conformational change that reduces either the hydrophobic surface area or alters the surface charge distribution of the proteins, or with the displacement of ANS by NAD^+ since the dye has been reported to bind at nucleotide-binding sites(*142, 143*). Upon the addition of Tyr in the presence of NAD^+, the fluorescence intensity for WT CM-PD *E. coli* and *A. aeolicus* Δ19PD decreased further which signifie s Tyr binding. Interestingly, His257Ala of *E. coli* CM-PD and His217Ala Δ19PD of *A. aeolicus*, whose activities were not inhibited by Tyr, exhibited only very small changes in ANS fluorescence intensity in the presence of Tyr and/or NAD^+ (Figures 4.7).

4.2.5 Molecular Weight of WT and Variant Proteins in the Presence and Absence of Ligands

To determine if inhibition by L-Tyr is accompanied by tetramer formation as previously noted for CM-PD(*65*), size exclusion FPLC was performed at ambient temperature with a mobile phase containing 0.5 mM NAD^+ and 1 mM L-Tyr, and the results were compared with those in the absence of ligands. This assay was performed on WT and variant *E. coli* CM-PDs and *A. aeolicus* PDs (50-60 μM monomer). The mobilities of the standards were essentially identical in the presence and absence of ligands (data not shown). In the presence of 1 mM L-Tyr and 0.5 mM NAD^+, WT CM-PD underwent a shift in retention time corresponding to a

Figure 4.7: Emission spectra of ANS complexed with WT and His257Ala *E. coli* CM-PD in the absence and the presence of ligands.

For each spectrum, 2 μM monomer and 50 μM ANS were mixed together with (—) no ligand, (—) 1 mM Tyr, ( ) 0.5 mM NAD^+, (—) 1 mM Tyr/0.5 mM NAD^+ in 50 mM potassium phosphate, 75 mM NaCl (pH 7.5) buffer. (—) is the spectrum of 50 μM ANS/1 mM Tyr/0.5 mM NAD^+ without enzyme in the same buffer. Excitation was set at 370 nm and fluorescence spectra were recorded from 400 to 600 nm. Emission spectra were corrected from for background and for inner filter effects when appropriate (*125*).

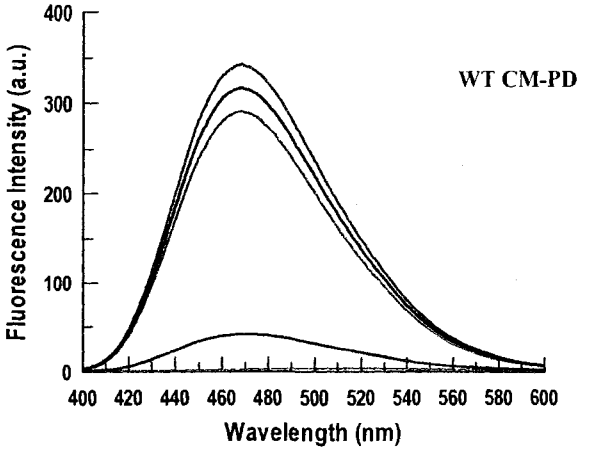
WT CM-PD
Fluorescence Intensity (a.u.)
400
300
200
100
0
400 420 440 460 480 500 520 540 560 580 600
Wavelength (nm)

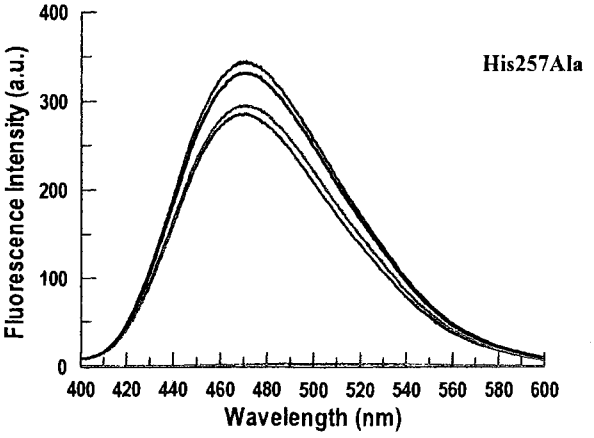
His257Ala
Fluorescence Intensity (a.u.)
400
300
200
100
0
400 420 440 460 480 500 520 540 560 580 600
Wavelength (nm)

molecular weight increase from 89 kDa (no ligands) to 174 kDa (with ligands), indicating tetramer formation. This result coincides with previously reported data (*65*). Interestingly, in the presence of both Tyr and NAD^+, His257Ala CM-PD eluted mainly as a dimer; the estimated molecular weight increased from 74 kDa to only 99 kDa. Some tetrameric species (in rapid equilibrium with the dimer) may be present, promoted by the binding of NAD^+ as previously reported for the *E. coli* enzyme (*65*). Neither PD (54 kDa) nor Δ19PD (52 kDa) showed altered retention times when ligands were present (Table 4.3), confirming the previous report by Aponte(*106*). Further analysis of *A. aeolicus* PD using interference sedimentation velocity experiments yielded sedimentation coefficient values for the enzyme that were similar in the absence and presence of L-Tyr plus NAD^+ thus indicating that PD remained dimeric (data not shown).

Table 4.3 Retention times and estimated molecular weights from analytical size exclusion chromatography

	No ligand		0.5 mM NAD^+/1 mM Tyr	
Proteins	Retention time (min)	Estimated MW (kDa)	Retention time (min)	Estimated MW (kDa)
WT CM-PD	19.08	84	17.65	174
His257Ala	19.19	74	18.73	99
WT PD	20.12	54	20.08	55
Δ19PD	20.14	52	20.13	54

The native molecular weights of *E. coli* CM-PD, His257Ala and *A. aeolicus* WT PD and Δ19PD were determined in the absence or presence of NAD^+ and Tyr by a Pharmacia Akta FPLC system fitted with a Superdex G-200 column (HR 10/30, Pharmacia) at ambient temperature. Samples of 0.4 mg of protein were introduced in a 500 µl sample loop. Chromatography was performed with mobile phase containing 50 mM potassium phosphate, 150 mM NaCl and 1 mM DTT (pH 7.5) for the *A. aeolicus* enzyme and 50 mM potassium phosphate, 25 mM NaCl and 1 mM DTT (pH 7.5) for the *E. coli* enzymes at a flow rate of 0.75 mL/min and injection volume of 500 µL with and without 0.5 mM NAD^+ and 1 mM Tyr. Protein elution was monitored at 290, 300 and 310 nm. Bio-Rad gel filtration protein standards (range of 1.35-670 kDa) were resolved in both mobile phases in order to follow changes in retention time associated with the presence of NAD^+ and Tyr in the mobile phase. A standard curve was generated using these proteins to correlate retention time with native molecular weight.

4.3 DISCUSSION

End-product inhibition of PD provides a major regulatory control in the pathway of Tyr biosynthesis (*56, 161*). In this report, we explored the effects of L-Tyr on the activity and quaternary structure of PD from *A. aeolicus*. Most importantly, from the analysis of variant proteins of *A. aeolicus* Δ19PD and *E. coli* CM-PD, we identified a key residue involved in Tyr inhibition. These findings, in combination with recent crystallographic data of the enzyme-NAD^+ complex bound with HPP, HPPropionate or L-Tyr (manuscript submitted), were used to develop a possible model describing how the enzyme can accommodate a ligand in the active site that carries a keto versus an amino group on its propanyl side chain. To aid in our studies, two binding assays have been developed to monitor the association of L-Tyr to PD in the absence of prephenate.

We have shown that *A. aeolicus* PD is inhibited by L-Tyr over a broad temperature range, although the full-length protein appears more sensitive to L-Tyr's effects than the Δ19PD variant. This observation documents a further example whereby the N-terminal region of PD appears to provide an important structural element. The kinetics in the presence of Tyr are suggestive of positive cooperativity between subunits at 55°C. However, inhibition does not appear to accompany a shift in equilibrium from active dimer to inactive tetramer promoted by NAD^+ and/or Tyr, as noted for *E. coli* CM-PD (*65*). The latter can be concluded from the results of gel filtration experiments (Table 4.3) and sedimentation velocity experiments in the presence and absence of NAD^+ plus L-Tyr; while *E. coli* CM-PD formed a tetramer under these conditions, PD from *A. aeolicus* did not.

If the mechanisms of inhibition by *A. aeolicus* PD and of *E. coli* CM-PD are identical then our results are consistent with suggestions that any cooperativity is manifested through tertiary structural changes transmitted between subunits (*100, 101*), and that tetramerization of the *E. coli* enzyme is an "artifact" observed at high protein concentrations. It is worth noting that TyrA from *Ps. stutzeri* forms tetramers at high protein concentrations but in the absence of ligands (*46*). While other studies report inhibition of the activity of TyrA proteins by Tyr (*46, 49, 69, 161*), this is the first examination of any ligand-induced structural changes for a monofunctional TyrA protein under conditions that should promote tetramer formation (relatively high concentrations of protein, Tyr and NAD^+). Studies on CM-PDT by Ganem and colleagues also showed that this bifunctional enzyme undergoes oligomerization upon Phe binding (*70, 163*). Moreover, fusion of the N-terminal CM domain directly to the C-terminal Phe binding domain, resulted in activation of the enzyme by the end product, but no oligomerization. They proposed that residues involved in the oligomerization are found within the PDT domain. Interestingly, Sun *et al.* reported that Δ19PD complexed with NAD^+ crystallized as a tetramer as would be expected for an enzyme that undergoes an allosteric transition. However, only three pairs of interdomain interactions were observed (*48*). Hence, it remains to be determined if this tetrameric species is biologically relevant. The possibility arises that *A. aeolicus* PD does form tetramers but only at temperatures nearer to the activity optimum. Size exclusion chromatography was performed at an ambient temperature. At 55°C, we did not observe cooperativity in the binding of prephenate to the enzyme (Chapter 3), although it is enhanced upon Tyr addition. It may be that at a

temperature considerably below the optimum, the protein is less flexible and thus less sensitive to changes that promote interactions between subunits.

Through studies presented in this chapter, we have identified a residue that is critical for the regulation of PD activity in two TyrA proteins: His217 in *A. aeolicus* PD and the homologous residue in *E. coli* CM-PD, His257. This was achieved by examining the inhibition of PD activity by L-Tyr on WT *A. aeolicus* Δ19PD and the series of variant proteins characterized in Chapter 3 (Ser126Ala, Glu153Ala, His217Ala/Asn, Asp247Ala and Arg250Gln) to determine which, if any, of these residues played a role in Tyr inhibition. Of the variants tested, His217Ala/Asn was markedly resistant to feedback inhibition followed by Arg250Gln (Figs. 4.4, 4.5 and 4.6). Not surprisingly, insensitivity to inhibition by L-Tyr was also noted for the equivalent variant in *E. coli* CM-PD, His257Ala (Fig. 4.6), and this resistance affected both mutase and dehydrogenase activities equally. Our finding was even more striking when considering that the Michaelis constants for prephenate and chorismate, determined in this study (Table 4.1) or in the work by Christendat *et al.* (*52*), were only modestly increased, about 2 to 3-fold relative to the WT enzyme, in keeping with the loss of a weak H-bond between the His257 and the keto group on pyruvyl side chain of prephenate. Thus, for *E. coli* CM-PD, we report the identification of a residue in the dehydrogenase domain that is essential for Tyr inhibition rather than supplying considerable binding energy towards the enzyme's combination with prephenate or chorismate.

Moreover, analysis of the crystal structure of Δ19PD from *A. aeolicus* suggests that this residue is likely in the active site of the *E. coli* enzyme (see Fig. 4.9). Lükte-Eversloh and Stephanopoulos (*102*) reported the identification of feedback resistant

variants of *E. coli* CM-PD, obtained by error prone PCR and selecting for growth on media containing a Tyr analogue. Interestingly, two residues (Ala354 and Phe357) are confined to the C terminal region of the enzyme while one lay in the middle of the primary sequence of the PD domain (Tyr263). In agreement with our results with His257Ala, both activities of the variants were L-Tyr insensitive. Additionally, our findings can also be compared to those by Ganem and coworkers on *E. coli* CM-PDT (*163*) who pinpointed four residues within the dehydratase portion of this bifunctional enzyme that were important for Phe inhibition/binding. These residues were not conserved between the two bifunctional enzymes in *E. coli*, however.

Our kinetic results were confirmed by binding studies although those obtained by using our radiolabeled Tyr assay (Table 4.2) must be interpreted respecting experimental limitations: the low specific activity for the ^{3}H-Tyr meant that a high concentration of L-Tyr could not be tested. A second, fluorescence based assay we developed was rapid, inexpensive, and could be performed at relatively low protein and higher L-Tyr concentrations. It exploited the affinity that the external fluorophore ANS has for many proteins as well as its increase in quantum yield that occurs with binding. This was particularly useful in our case as our ligand (L-Tyr) was an intrinsic fluorophore. ANS fluorescence emission was quenched upon the addition of NAD^{+} plus Tyr to either WT *E. coli* CM-PD or WT *A. aeolicus* Δ19PD (Fig. 4.7), although less so, for the *A. aeolicus* enzyme which is reported to be less inhibited by Tyr than the *E. coli* enzyme. The results were also in keeping with the observation by Hudson *et al.* (*65*) that the presence of Tyr helps NAD^{+} bind and *vice versa*. For the variant proteins fluorescence quenching was relieved indicating that the Tyr did not bind or did not bind well. It is likely for both

proteins that ANS was binding to the sites where either NAD^+ and/or Tyr combine as it has been reported that ANS binds to nucleotide binding sites (*22, 23*). The quenching of ANS fluorescence emission upon the addition of NAD^+ plus L-Tyr to WT *E. coli* CM-PD (Fig. 4.7) could be interpreted in part, due to the oligomerization of the enzyme as surface hydrophobic sites became inaccessible for the binding of ANS. It is well documented that ANS can bind to such patches and additionally, it has been noted empirically that *E. coli* CM-PD likely possesses a very hydrophobic surface. Although not performed in this study, we could have readily determined K_d values for Tyr's and NAD^+'s interaction with WT enzyme and and for variants whose affinity for the ligands were not too poor.

The crystal structure of Δ19PD from *A. aeolicus* co-crystallized with NAD^+ and L-Tyr shows without ambiguity that L-Tyr binds in the active site (Fig. 4.8). This is not surprising given that *A. aeolicus* PD can utilize L-arogenate as a substrate yielding L-Tyr as the product of the oxidative decarboxylation. Tyr's side chain carboxylate interacts with the guanidinium group of Arg, an interaction which should be significantly weakened with this Gln substitution. Our solutions studies (Fig. 4.4) are in agreement with the crystal structure which show that the activity of this variant is less inhibited by L-Tyr than the activity of WT enzyme. By contrast the Ser126's hydroxyl group appears not to be involved in inhibition by Tyr even though it has been implicated in the binding of HPP through the same interactions as that of Tyr. Two residues at the "entry way" to the active site (Glu153 and Asp247') were also tested and found to be more sensitive to the effects of L-Tyr than WT enzyme; possible reasons for these results require more analysis.

Under the assay conditions described, our kinetic data are also consistent with a model whereby L-Tyr binds at the active site of Δ19PD. A value for the dissociation of Tyr from the enzyme-NAD complex, at about 16 μM. This value is within the range (10-100 μM) reported by fitting kinetic data to models whereby L-Tyr competes at the active site, or at an allosteric site (*56, 65, 100*). The K_i value is about 8-fold lower than the Michaelis constant for prephenate suggesting that the end product inhibitor combines more tightly to the enzyme than does prephenate. The kinetic data also reveal concave upward kinetics for the binding of L-Tyr (Fig. 4.2). A model consistent with this feature in addition to competitive inhibition would have L-Tyr and prephenate simply competing with each other for binding to the active site, with L-Tyr binding with positive cooperativity. Fitting initial velocity data for the inhibition of PD of CM-PD, Christopherson (*100*) proposed a similar model but which included positive cooperative effects for the binding of prephenate as well. It is worth noting that the crystal structure of Δ19PD shows only one Tyr binding per monomer. Thus, the solution studies and the crystal structure are not in total agreement. Additionally, steady-state kinetic mechanisms can also yield concave upward double reciprocal plots (*164*). Thus, a more thorough analysis of these types of complex initial velocity patterns, along with the analysis of initial velocity patterns in the presence of HPP and L-Tyr must be undertaken.

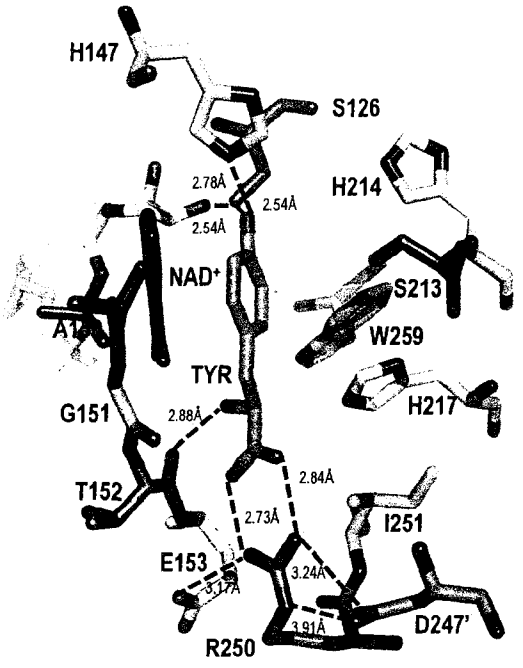

Figure 4.8: Active site representation of the combination of L-Tyr with *A. aeolicus* Δ19PD-NAD$^+$.

A number of residues interacting with Tyr were identified in the prephenate binding pocket: both His147 and Ser126 interact with the C4-hydroxyl group of L-Tyr. Arg250's guanidinium group is within H-bonding distance of the carboxylate moiety of L-Tyr.

The crystal structure of the enzyme bound with L-Tyr or HPP reveals that the amino group of L-Tyr interacts with the main chain carbonyl of Thr152 but the side chain keto group of HPP interacts with the imidazole of His217 (Fig. 4.8 and Chapter 3, Fig. 3.7). For this structural change, which would appear to confer ligand specificity, Christendat and coworkers speculated that the side chain of His217 must be in the protonated state. While the interaction of a keto group with a protonated imidazole is favoured, an amino group on the same position of the ligand would produce a repulsive effect and therefore direct the interaction of Tyr's amino group away from His217 towards the main chain carbonyl group of Thr152. Replacing His217 with Ala/Asn eliminates this repulsive effect and Tyr is no longer directed towards the carbonyl of Thr152. We attempted to conduct pH rate profiles of His217Ala to determine if the protonated group (p*K* 9.5) whose ionization is observed in the pH profile for WT Δ19PD is that of His217. Regrettably, His217Ala was prone to precipitation at high pH values however, and its activity could not be confidently monitored.

Are the interactions that hold prephenate and/or L-Tyr in the active site the same as for *E. coli* CM-PD or other PDs? The crystal structure of an engineered monofunctional PD from *H. influenza* bound with NAD^+ and L-Tyr (unpublished) again places L-Tyr in the active site of the enzyme (Fig. 4.9). This enzyme is dimeric and binds two molecules of NAD^+ and two of L-Tyr per dimer. Additionally, many of the residues located within Δ19PD's active site are also found in that of *H. influenza* PD (see Fig 4.9 and description in figure legend). Of interest, Tyr at position 306 replaces Trp259 in *A. aeolicus* PD; this residue is shown to interact directly with the amino group of L-Tyr. We

are currently modeling the PD domain of *E. coli* CM-PD using as a template the structure of PD from *H. influenza*. Regrettably, a loop region (amino acids 111-119) in the modeled *E. coli* PD monomer adopts a conformation that is distinct from that of the same loop found in the *H. influenza* PD dimer (residues 141-149). Thus, a dimeric *E. coli* PD cannot be readily reconstructedn(Appendix 4A). Interestingly residues that Lükte-Eversloh and Stephanopoulos (*102*) propose are the important for generating feedback resistance in *E. coli* CM-PD are at the C-terminal end of the protein, which appears distant from the active site. It may be that the C-terminal end of the protein adopts a different orientation in the bifucntional CM-PD of *E. coli* and *H. influenza*. We have commenced peptide mapping and site-directed mutagenesis studies on the *E. coli* enzyme based on the new available structures.

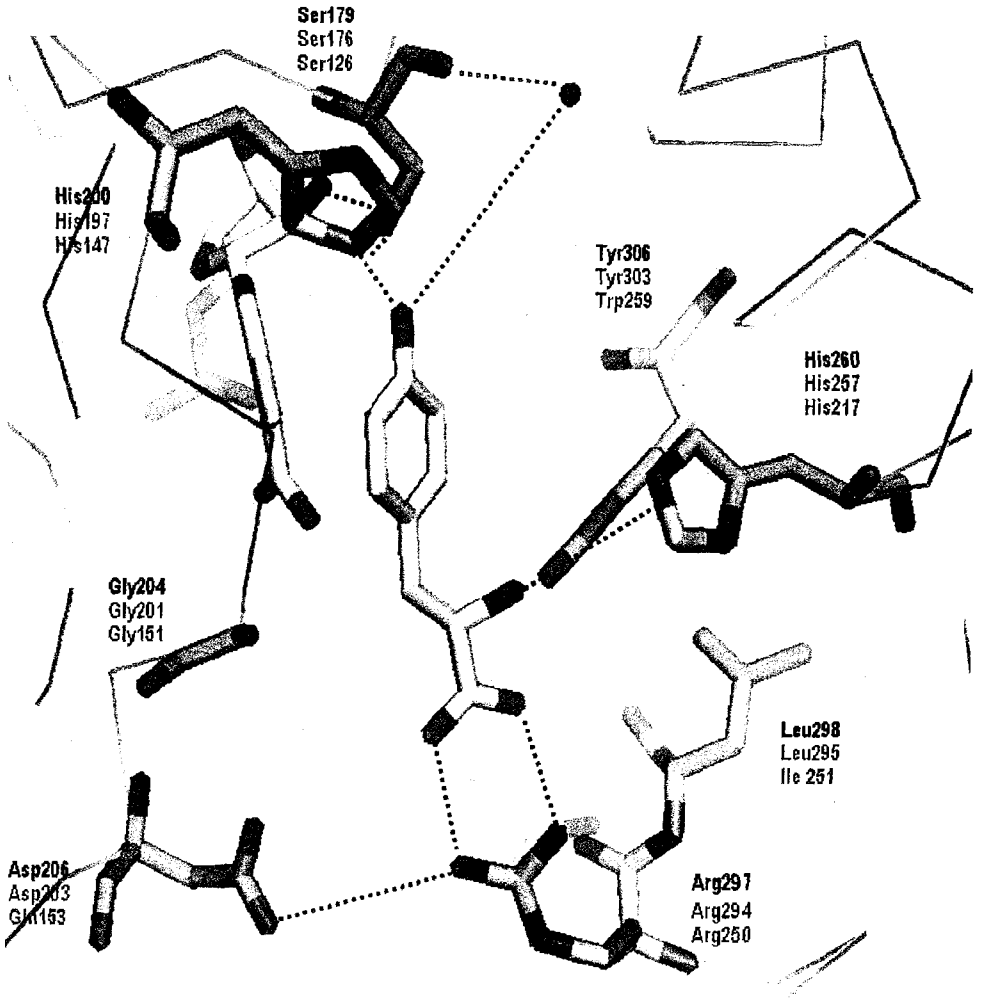

Figure 4.9: Active site representation of *H. influenzae* CM-PD in complex with NAD^+ and L-Tyr.

References

1. Kaneko, M., Hwang, E. I., Ohnishi, Y., and Horinouchi, S. (2003) *J Ind Microbiol Biotechnol 30*, 456-461.
2. Rescigno, A., Rinaldi, A. C., and Sanjust, E. (1998) *Biochem Pharmacol 56*, 1089-1096.
3. Meganathan, R. (2001) *FEMS Microbiol Lett 203*, 131-139.
4. Moller, B. L., and Conn, E. E. (1979) *J Biol Chem 254*, 8575-8583.
5. Memelink, J. (2004) *Nat Biotechnol 22*, 1526-1527.
6. Frick, S., and Kutchan, T. M. (1999) *Plant J 17*, 329-339.
7. Davis, B. D. (1955) *Adv Enzymol Relat Subj Biochem 16*, 247-312.
8. Sprinson, B. D. (1961) *Adv Carbohydrate Chem 15*, 235-270.
9. Brown, K. D., and Doy, C. H. (1966) *Biochim Biophys Acta 118*, 157-172.
10. Smith, L. C., Ravel, J. M., Lax, S. R., and Shive, W. (1962) *J Biol Chem 1962*, 3566-3570.
11. Dayan, J., and Sprinson, D. B. (1971) *Biochem J 108*, 1174-1180.
12. Ahmad, S., and Jensen, R. A. (1988) *FEMS Microbiol Lett 52*, 109-116.
13. Coggins, J. R., Abell, C., Evans, L. B., Frederickson, M., Robinson, D. A., Roszak, A. W., and Lapthorn, A. P. (2003) *Biochem Soc Trans 31*, 548-552.
14. Haslam, E. (1974) *The Shikimate Pathway*, Whiley, New York.
15. Steinrucken, H. C., and Amrhein, N. (1980) *Biochem Biophys Res Commmun 94*, 1207-1212.
16. Herrmann, K. M. (1995) *Plant Physiol 107*, 7-12.
17. Berry, A., Dodge, T. C., Pepsin, M., and Weyler, W. (2002) *J Ind Microbiol Biotechnol 28*, 127-133.
18. Schmid, J. W., Mauch, K., Reuss, M., Gilles, E. D., and Kremling, A. (2004) *Metab Eng 6*, 364-377.
19. Kramer, M., Bongaerts, J., Bovenberg, R., Kremer, S., Muller, U., Orf, S., Wubbolts, M., and Raeven, L. (2003) *Metab Eng 5*, 277-283.
20. Grinter, N. J. (1998) *ChemTech 28*, 33-37.

21. Cabrera-Valladares, N., Martínez, A., Piñero, S., Lagunas-Muñoz, V. H., Tinoco, R., de Anda, R., Vázquez-Duhalt, R., Bolívar, F., and Gosset, G. (2006) *Enzyme and Microbial Technology 38*, 772-779.
22. Seetharam, G., and Saville, B. (2002) *Enzyme and Microbial Technology 31*, 747-753.
23. Ikram, U.-H., and Ali, S. (2002) *Curr Microbiol 45*, 88-93.
24. Bourke, S. L., and Kohn, J. (2003) *Adv Drug Deliv Rev 55*, 447-466.
25. Patnaik, R., Zolandz, R. R., Green, D. A., and Kraynie, D. F. (2008) *Biotechnol Bioeng 99*, 741-752.
26. Rippert, P., Scimemi, C., Dubald, M., and Matringe, M. (2004) *Plant Physiol 134*, 92-100.
27. Yanofsky, C. (1988) *J Biol Chem 263*, 609-612.
28. Herrmann, K. M., and Weaver, L. M. (1999) *Annu Rev Plant Physio Plant Mol Biol 50*, 473-503.
29. Chávez-Béjar, M. I., Lara, A. R., López, H., Hernández-Chávez, G., Martinez, A., Ramírez, O. T., Bolívar, F., and Gosset, G. (2008) *Appl Environ Microbiol 74*, 3284-3290.
30. Stenmark, S. L., Pierson, D. L., Glover, G. I., and Jensen, R. A. (1974) *Nature 247*, 290-292.
31. Zamir, L. O., Jensen, R. A., Arison, B., Douglas, A., Albers-Schonberg, G., and Bowen, J. R. (1980) *J Am Chem Soc 102*, 4499-4504.
32. Mayer, E., Waldner-Sander, S., Keller, B., Keller, E., and Lingens, F. (1985) *FEBS Lett 179*, 208-212.
33. Keller, B., Keller, E., and Lingens, F. (1985) *Biol Chem Hoppe Seyler 366*.
34. Hall, G. C., Flick, M. B., Gherna, R. L., and Jensen, R. A. (1982) *J Bacteriol 149*, 65-78.
35. Fazel, A. M., and Jensen, R. A. (1979) *J Bacteriol 138*, 805-815.
36. Bonner, C. A., Jensen, R. A., Gander, J. E., and Keyhani, N. O. (2004) *Biochem J 382*, 279-291.
37. Fazel, A. M., Bowen, J. R., and Jensen, R. A. (1980) *Proc Natl Acad Sci U S A 77*, 1270-1273.

38. Patel, N., Pierson, D. L., and Jensen, R. A. (1977) *J Biol Chem 252*, 5839-5846.
39. Zhao, G., Xia, T., Ingram, L. O., and Jensen, R. A. (1993) *Eur J Biochem 212*, 157-165.
40. Rippert, P., and Matringe, M. (2002) *Eur J Biochem 269*, 4753-4761.
41. Rippert, P., and Matringe, M. (2002) *Plant Mol Biol 48*, 361-8.
42. Siehl, D. L., and Conn, E. E. (1998) *Arch Biochem Biophys 260*, 822-829.
43. Legrand, P., Dumas, R., Seux, M., Rippert, P., Ravelli, R., Ferrer, J.-L., and Matringe, M. (2006) *Structure 14*, 767-776.
44. Song, J., Bonner, C. A., Wolinsky, M., and Jensen, R. A. (2005) *BMC Biol 3*, 1-30.
45. Bonner, C. A., Disz, T., Hwang, K., Song, J., Vonstein, V., Overbeek, R., and Jensen, R. A. (2008) *Microbiol Mol Biol Rev 72*, 13-53.
46. Xie, G., Bonner, C. A., and Jensen, R. A. (2000) *Comp Biochem Physiol C Toxicol Pharmacol 125*, 65-83.
47. Song, J., Bonner, C. A., Wolinsky, M., and Jensen, R. A. (2005) *BMC Biol 3*, 13.
48. Sun, W., Singh, S., Zhang, R., Turnbull, J. L., and Christendat, D. (2006) *J Biol Chem 281*, 12919-12928.
49. Rippert, P., and Matringe, M. (2002) *Plant Mol Biol 48*, 361-368.
50. Chen, S., Vincent, S., Wilson, D. B., and Ganem, B. (2003) *Eur J Biochem 270*, 757-763.
51. Xia, T., Zhao, G., Fischer, R. S., and Jensen, R. A. (1992) *J Gen Microbiol 138*, 1309-1316.
52. Christendat, D., Saridakis, V. C., and Turnbull, J. L. (1998) *Biochemistry 37*, 15703-15712.
53. Christendat, D., and Turnbull, J. L. (1999) *Biochemistry 38*, 4782-4793.
54. Koch, G. L., Shaw, D. C., and Gibson, F. (1971) *Biochim Biophys Acta 229*, 795-804.
55. Cotton, R. G., and Gibson, F. (1965) *Biochim Biophys Acta 100*, 76-88.
56. Turnbull, J., and Morrison, J. F. (1990) *Biochemistry 29*, 10255-10261.
57. Sampathkumar, P., and Morrison, J. F. (1982) *Biochim Biophys Acta 702*, 204-211.

58. Hudson, G. S., and Davidson, B. E. (1984) *J Mol Biol 180*, 1023-1051.
59. Heyde, E. (1979) *Biochemistry 18*, 2766-2775.
60. Koch, G. L., Shaw, D. C., and Gibson, F. (1972) *Biochim Biophys Acta 258*, 719-730.
61. Hudson, G. S., Wong, V., and Davidson, B. E. (1984) *Biochemistry 23*, 6240-6249.
62. Christopherson, R. I., Heyde, E., and Morrison, J. F. (1983) *Biochemistry 22*, 1650-1656.
63. Sampathkumar, P., and Morrison, J. (1982) *Biochim Biophys Acta 702*, 212-219.
64. Turnbull, J., Cleland, W. W., and Morrison, J. F. (1991) *Biochemistry 30*, 7777-7782.
65. Hudson, G. S., Howlett, G. J., and Davidson, B. E. (1983) *J Biol Chem 258*, 3114-3120.
66. Vincent, S., Chen, S., Wilson, D. B., and Ganem, B. (2002) *Bioorg Med Chem Lett 12*, 929-931.
67. Christendat, D., and Turnbull, J. (1996) *Biochemistry 35*, 4468-4479.
68. Duggleby, R. G., Sneddon, M. K., and Morrison, J. F. (1978) *Biochemistry 17*, 1548-1554.
69. Xia, T., Zhao, G., and Jensen, R. A. (1992) *Appl Environ Microbiol 58*, 2792-2798.
70. Zhang, S., Pohnert, G., Kongsaeree, P., Wilson, D. B., Clardy, J., and Ganem, B. (1998) *J Biol Chem 273*, 6248-6253.
71. Stewart, J., Wilson, D. B., and Ganem, B. (1990) *J Am Chem Soc 112*, 4582-4584.
72. Lee, A. Y., Stewart, J. D., Clardy, J., and Ganem, B. (1995) *Chem Biol 2*, 195-203.
73. Chipman, D. M., and Shaanan, B. (2001) *Curr Opin Struct Biol 11*, 694-700.
74. Pohnert, G., Zhang, S., Husain, A., Wilson, D. B., and Ganem, B. (1999) *Biochemistry 38*, 12212-12217.
75. Zhang, S., Wilson, D. B., and Ganem, B. (2003) *Bioorg Med Chem 11*, 3109-3114.

76. Strater, N., Schnappauf, G., Braus, G., and Lipscomb, W. N. (1997) *Structure 5*, 1437-1452.

77. Andrews, P. R., Smith, G. D., and Young, I. G. (1973) *Biochemistry 12*, 3492-3498.

78. Görisch, H., and Lingens, F. (1974) *Biochemistry 13*, 3790-3794.

79. Copley, S. D., and Knowles, J. R. (1987) *J Am Chem Soc 109*, 5008-5013.

80. Guilford, W. J., Copley, S. D., and Knowles, J. R. (1987) *J Am Chem Soc 109*, 5013-5019.

81. Andrews, P. R., and Heyde, E. (1979) *J Theor Biol 78*, 393-403.

82. Sogo, S. G., Widlanski, T. S., Hoare, J. H., Grimshaw, C. E., Bertchold, G. A., and Knowles, J. R. (1984) *J Am Chem Soc 106*, 2701-2703.

83. Ma, J., Zheng, X., Schnappauf, G., Braus, G., Karplus, M., and Lipscomb, W. N. (1998) *Proc Natl Acad Sci U S A 25*, 14640-14645.

84. Andrews, P. R., Cain, E. N., Rizzardo, E., and Smith, G. D. (1977) *Biochemistry 16*, 4848-4852.

85. Bartlett, P. A., Nakagawa, Y., Johnson, C. R., Reich, S. H., and Luis, A. (1988) *J Org Chem 53*, 3195-3210.

86. Xue, Y., Lipscomb, W. N., Graf, R., Schnappauf, G., and Braus, G. (1994) *Proc Natl Acad Sci U S A 91*, 10814-10818.

87. Helmstaedt, K., Heinrich, G., Merkl, R., and Braus, G. H. (2004) *Arch Microbiol 181*, 195-203.

88. Xu, H., Yang, C., Chen, L., Kataeva, I. A., Tempel, W., Lee, D., Habel, J. E., Nguyen, D., Pflugrath, J. W., Ferrara, J. D., Arendall, W. B. r., Richardson, J. S., Richardson, D. C., Liu, Z. J., Newton, M. G., Rose, J. B., and Wang, B. C. (2005) *Acta Crystallogr D Biol Crystallogr. 61*, 960-966.

89. Okvist, M., Dey, R., Sasso, S., Grahan, E., Kast, P., and Krengel, U. (2006) *J Mol Biol 357*, 1483-1499.

90. Chook, Y. M., Ke, H., and Lipscomb, W. N. (1993) *Proc Natl Acad Sci U S A 90*, 8600-8603.

91. Zhang, S., Kongsaeree, P., Clardy, J., Wilson, D. B., and Ganem, B. (1996) *Bioorg Med Chem 4*, 1015-1020.

92. Liu, D. R., Cload, S. T., Pastor, R. M., and Schultz, P. G. (1996) *J Am Chem Soc 118*, 1789-1790.

93. Vamvaca, K., Butz, M., Walter, K. U., Taylor, S. V., and Hilvert, D. (2005) *Protein Sci 14*, 2103-2114.

94. Hermes, J. D., Tipton, P. A., Fisher, M. A., O'Leary, M. H., Morrison, J. F., and Cleland, W. W. (1984) *Biochemistry 23*, 6263-6275.

95. Heyde, E., and Morrison, J. F. (1978) *Biochemistry 17*, 1573-1580.

96. Bonner, C. A., and Jensen, R. A. (1987) *Methods Enzymol 142*, 488-494.

97. Byng, G. S., Whitaker, R. J., Shapiro, C. L., and Jensen, R. A. (1981) *Mol Cell Biol 1*, 426-38.

98. Hund, H. K., Bär, G., and Lingens, F. (1989) *Z Naturforsch [C] 44*, 797-801.

99. Subramaniam, P., Bhatnagar, R., Hooper, A., and Jensen, R. A. (1994) *Microbiol 140*, 4582-4584.

100. Christopherson, R. I., and Morrison, J. F. (1985) *Biochemistry 24*, 1116-1121.

101. Turnbull, J., Morrison, J. F., and Cleland, W. W. (1991) *Biochemistry 30*, 7783-7788.

102. Lütke-Eversloh, T., and Stephanopoulos, G. (2005) *Appl Environ Microbiol 71*, 7224-7228.

103. Monod, J., Wyman, J., and Changeux, J. P. (1965) *J Mol Biol 12*, 88-118.

104. Koshland, D. E. J., Némethy, G., and Filmer, D. (1966) *Biochemistry 5*, 365-385.

105. Deckert, G., Warren, P. V., Gaasterland, T., Young, W. G., Lenox, A. L., Graham, D. E., Overbeek, R., Snead, M. A., Keller, M., Aujay, M., Huber, R., Feldman, R. A., J.M., S., Olsen, G. J., and Swanson, R. V. (1998) *Nature 392*, 353-358.

106. Aponte, R. A. (2003), Overexpression, Purification and Preliminary Characterization of Prephenate Dehydrogenase from the Hyperthermophilic Bacterium *Aquifex aeolicus*, Concordia University, Montreal, QC, Canada, M. Sc.

107. Fukuchi, S., and Nishikawa, K. (2001) *J Mol Biol 309*, 835-843.

108. Cambillau, C., and Claverie, J. (2000) *J Biol Chem 275*, 32383-32386.

109. Berezovsky, I. N., and Shakhnovich, E. I. (2005) *Proc Natl Acad Sci 102*, 12742-12747.

110. Querol, E., Pérez-Pons, J., and Mozo-Villariá, A. (1996) *Prot Eng 9*, 265-271.

111. DeLano, W. L. (2002) *The PyMOL Molecular Graphics System*, San Carlos, CA.

112. Bonvin, J., Aponte, R. A., Marcantonio, M., Singh, S., Christendat, D., and Turnbull, J. L. (2006) *Protein Sci 15*, 1417-1432.

113. Dudzinski, P. K., and Morrison, J. F. (1976) *Preparative Biochemistry and Biotechnology 6*, 113-121.

114. Rieger, C. E., and Turnbull, J. (1996) *Prep Biochem Biotechnol 26*, 67-76.

115. Dawson, C. M. R., Elliott, C. D., Elliott, H. W., and Jones, M. K. (1986) *Data for Biochemical Research*, 3rd ed., Oxford Science Publications, Clarendon Press.

116. Edelhoch, H. (1967) *Biochemistry 6*, 1948-1954.

117. Christendat, D., Saridakis, V. C., Dharamsi, A., Bochkarev, A., Pai, E. F., Arrowsmith, C. H., and Edwards, A. M. (2000) *J Biol Chem 75*, 24608-24612.

118. Laemmli, U. K. (1970) *Nature 227*, 680-685.

119. Turnbull, J., Cleland, W. W., and Morrison, J. F. (1990) *Biochemistry 29*, 10245-10254.

120. Cleland, W. W. (1979) *Methods Enzymol 87*, 103-138.

121. Weinglass, A. B., Whitelegge, J. P., Verner, G. E., Faull, K. F., and Kaback, H. R. (2003) *EMBO J 22*, 1497-1477.

122. Lamm, O. (1929) *Ark Mat Astr Fys 21B*, 1-4.

123. Laue, T. M., Senear, D. F., Eaton, S. F., and Ross, J. B. A. (1992) (Chemistry, R. S. o., Ed.) pp pp.90-125, Cambridge.

124. Pace, C. N., and Scholtz, J. M. (1998) in *Protein Structure: A Pratical Approach* (Creighton, T. E., Ed.) pp 299-321, Oxford University Press, New York.

125. Lakowicz, J. R. (1999) *Principles of Fluorescence Spectroscopy*, Kluwer Academic/Plenum, New York.

126. Engel, P. C. (1996) *Enzymology*, Bio Scientific Publishers, Oxford, UK.

127. Lehrer, S. S. (1971) *Biochemistry 10*, 3254-3263.

128. Jaenicke, R. (2000) *Proc Natl Acad Sci U S A 97*, 2962-4.

129. Rost, B., Yachdav, G., and Liu, J. (2004) *Nucleic Acids Res 32 Web Server issue*, W321-W-326.

130. Deleage, G., Combet, C., Blanchet, C., and Geourjon, C. (2001) *Comput Biol Med 31*, 259-267.

131. Ptitsyn, O. B. (1995) *Adv Protein Chem 47*, 83-229.

132. Eftink, M. R., and Ghiron, C. A. (1981) *Anal Biochem 114*, 706-709.

133. Kornblatt, M. J., and Hui Bon Hoa, G. (1987) *Arch Biochem Biophys 252*, 277-283.

134. MacBeath, G., Kast, P., and Hilvert, D. (1998) *Biochemistry 37*, 10062-10073.

135. Cheung, Y. Y., Lam, S. Y., Chu, W. K., Allen, M. D., Bycroft, M., and Wong, K. B. (2005) *Biochemistry 44*, 4601-4611.

136. Inui, T., Ohkubo, T., Urade, Y., and Hayaishi, O. (1999) *Biochem Biophys Res Commmun 266*, 641-646.

137. Kujo, C., and Oshima, T. (1998) *Appl Environ Microbiol 64*, 2152-2157.

138. Natrayanasami, R., Nishimura, J. S., McMilllan, K., Roman, L. J., Shea, T. M., Robida, A. M., Horowitz, P. M., and Masters, B. B. M. (1997) *Nitric Oxide 1*, 39-49.

139. Zhang, H. J., Sheng, X. R., Pan, X. M., and Zhou, J. M. (1997) *Biochem Biophys Res Commmun 238*, 382-386.

140. Thomas, T. M., and Scopes, R. K. (1998) *Biochem J 330*, 1087-1095.

141. Zoldác, G., Sut'ák, R., Antalik, M., Sprinzl, M., and Sedlák, E. (2003) *Eur J Biochem 270*, 4887-4897.

142. McLaughlin, A. C. (1974) *J Biol Chem 249*, 1445-1452.

143. Cox, M. J., Davis, C. A., Chan, C., Jourden, M. J., Jorjorian, A. D., Brym, M. J., Snider, M. J., Borders, C. L., and Edmiston, P. L. (2003) *Biochemistry 42*, 1863-1871.

144. Huber, R., Wilharm, T., Huber, D., Trincone, A., Burggraf, S., König, H., Rachel, R., Rockinger, I., Fricke, H., and Stetter, K. O. (1992) *System Appl Microbiol 15*, 340-351.

145. Vogt, G., Woell, S., and Argos, P. (1997) *J Mol Biol 269*, 631-643.

146. Szilagyi, A., and Zavodszky, P. (2000) *Struct Fold Des 8*, 483-504.

147. Xia, T. H., and Jensen, R. A. (1990) *J Biol Chem 265*, 20033-20036.

148. Lindblad, B., Lindstedt, G., Lindstedt, S., and Rundgren, M. (1977) *J Biol Chem 252*, 5073-5084.

149. Knox, W. E., and Pitt, B. M. (1957) *J Biol Chem 225*, 675-688.

150. Ahmad, S., and Jensen, R. A. (1987) *FEBS Lett 216*, 133-9.

151. Duewel, H. S., Sheflyan, G. Y., and Woodard, R. W. (1999) *Biochem Biophys Res Commun 263*, 346-51.

152. Hansen, T., Urbanke, C., Leppanen, V. M., Goldman, A., Brandenburg, K., and Schafer, G. (1999) *Arch Biochem Biophys 363*, 135-147.

153. Park, T. H., Choi, K. W., Park, C. S., Lee, S. B., Hang, H. Y., Shon, K. J., Park, J. S., and Cha, J. (2005) *Appl Microbiol Biotechnol 5*, 1-12.

154. Zuber, H., and Friedman, S. M. (1978) *Biochemistry of Thermophily*, Academic Press, New York.

155. Turnbull, J. (1988), Australian National University, Canberra.

156. Fujii, T., Hata, Y., Oozeki, M., Moriyama, H., Wakagi, T., Tanaka, N., and Oshima, T. (1997) *Biochemistry 36*, 1505-1513.

157. Teplyakov, A. V., Kuranova, I. P., Harutyunyan, E. H., Vainshtein, C., Frommel, W. E., Hohne, W. E., and Wilson, K. S. (1990) *J Mol Biol 214*, 261-279.

158. Buchanan, C. L., Connaris, H., Danson, M. J., Reeve, C. D., and Hough, D. W. (1999) *Biochem J 343*, 563-570.

159. Mattei, P., Kast, P., and Hilvert, D. (1999) *Eur J Biochem 261*, 25-32.

160. Legrand, P., Dumas, R., Seux, M., Rippert, P., Ravelli, R., Ferrer, J. L., and Matringe, M. (2006) *Structure 14*, 767-76.

161. Champney, W. S., and Jensen, R. A. (1970) *J Bacteriol 104*, 351-359.

162. Stryer, L. (1965) *J Mol Biol 13*, 482-495.

163. Zhang, S., Wilson, D. B., and Ganem, B. (2000) *Biochemistry 39*, 4722-4728.

164. Segel, I. H. (1993) *Enzyme Kinetics: Behavior and Analysis of Rapid Equilibrium and Steady-State Enzyme Systems*.

Appendix 2A

Determination of the native molecular weights of *A. aeolicus* PD and Δ19PD by analytical size exclusion chromatography. (**A**) FPLC tracings of 150 μg of Δ19PD (solid line) or PD (dotted line) chromatographed on a Pharmacia Akta FPLC system fitted with a Superdex G-200 column (HR 10/30, Pharmacia). Chromatography was performed with mobile phase containing 50 mM potassium phosphate, 150 mM NaCl (pH 7.5) at a flow rate of 0.75 mL/min and injection volume of 500 μL. Elution was monitored at 254, 280 and 290 nm, and fractions (1 mL) were assayed for enzyme activity (here is shown A_{280}). The arrows show the elution time corresponding to each protein of the Bio-Rad gel filtration protein standards including vitamin B_{12} (1.35 kDa), equine myoglobin (17 kDa), chicken ovalbumin (44 kDa), bovine γ-globulin (158 kDa) and thyroglobulin (670 kDa). (**B**) Logarithm of protein standard molecular weights and their respective retention times were used to generate a calibration curve to estimate *A. aeolicus* PD (red dot) and Δ19PD (green dot) molecular weights.

Appendix 2A

A

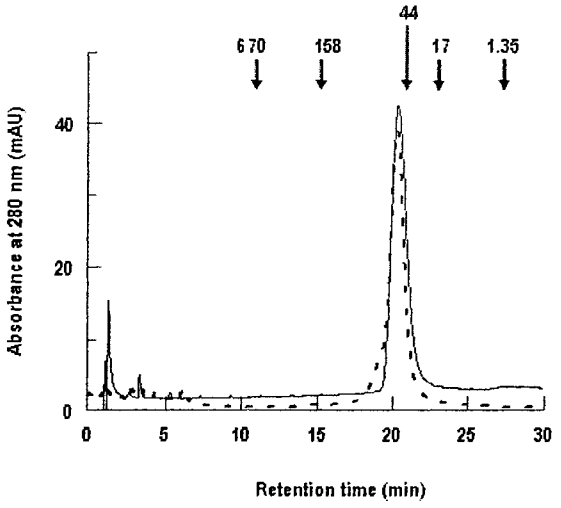

B

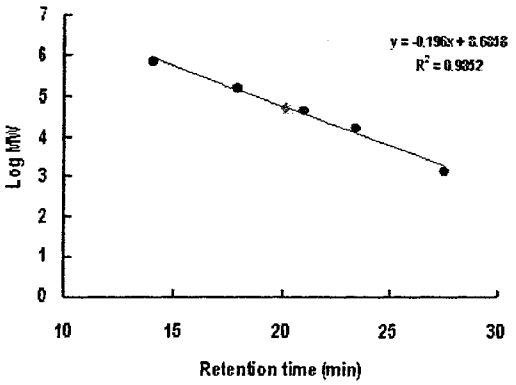

Appendix 2B

Sedimentation velocity analysis of *A. aeolicus* PD and Δ19PD. The protein concentrations were 25 μM and 37 μM, respectively; the buffer was 50 mM potassium phosphate, 0.3 M NaCl and 0.5 mM TCEP (pH 7.5). Sedimentation velocity was carried out at 35,000 rpm at 30°C for 10 h. Top panel: Raw sedimentation data (circles, every second scan shown) and fit with the *c*(*s*) model (solid lines). The middle panel shows the residuals of the fit. The best-fit *c*(*s*) distribution is shown in the bottom panel.

Appendix 2B (continued)

PD

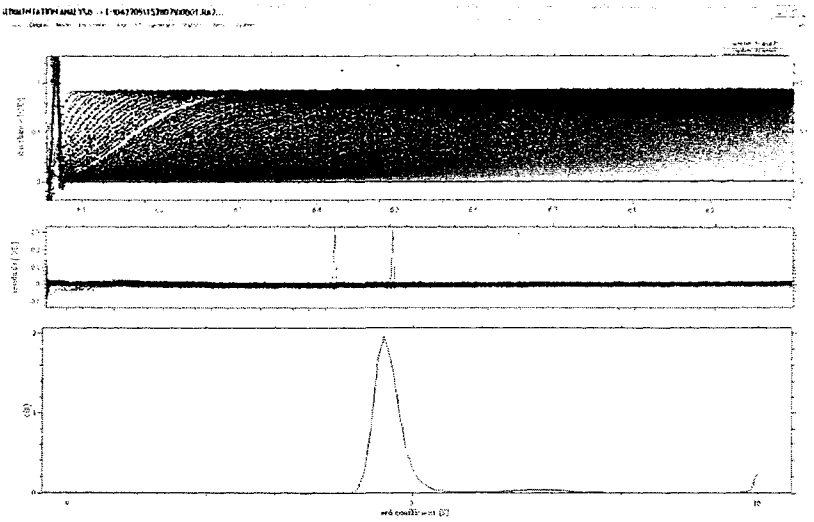

Δ19PD

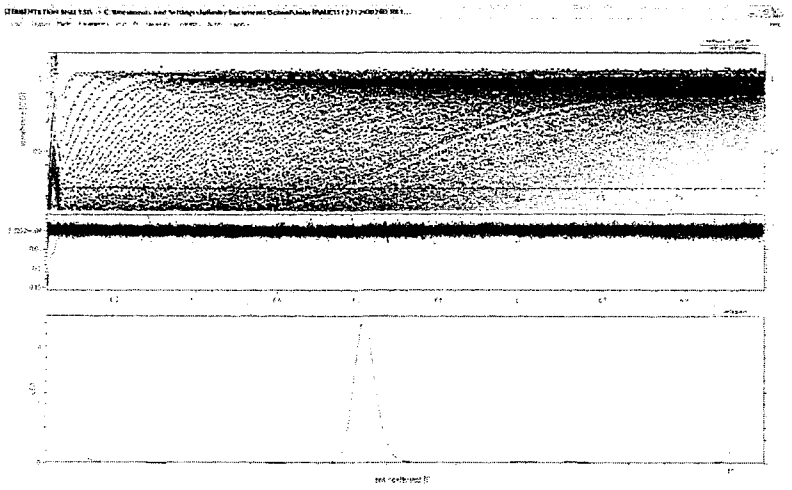

Appendix 2C

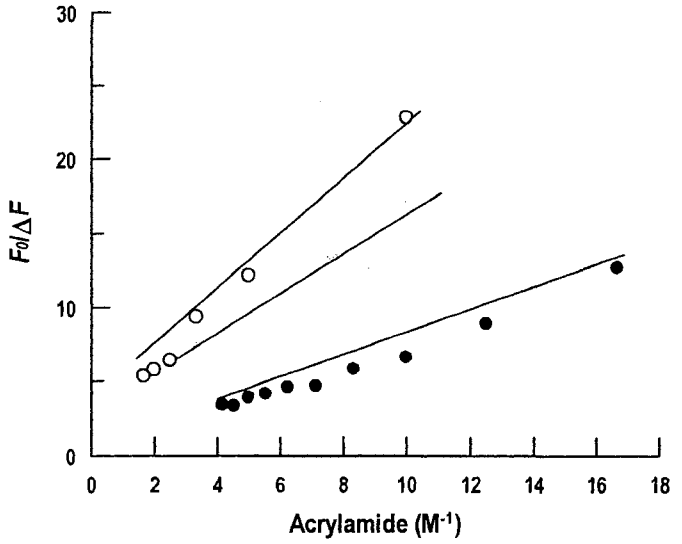

Modified Stern-Volmer plots of acrylamide quenching of Δ19PD in the absence and presence of NAD^+ or Gdn-HCl. The titration of Δ19PD (3 μM monomer) by acrylamide was performed in PPS buffer at 30°C. Acrylamide quenching was monitored in the absence (○) and the presence of 0.5 μM NAD^+ ( ) or 6 M Gdn-HCl (●). The modified Stern-Volmer plot was constructed by plotting $F_o/(F_o-F)$ *versus* 1/[acrylamide]. Extrapolations to the ordinate of the points at the lowest quencher concentrations allow the determination of the quenching parameters.

Appendix 2D

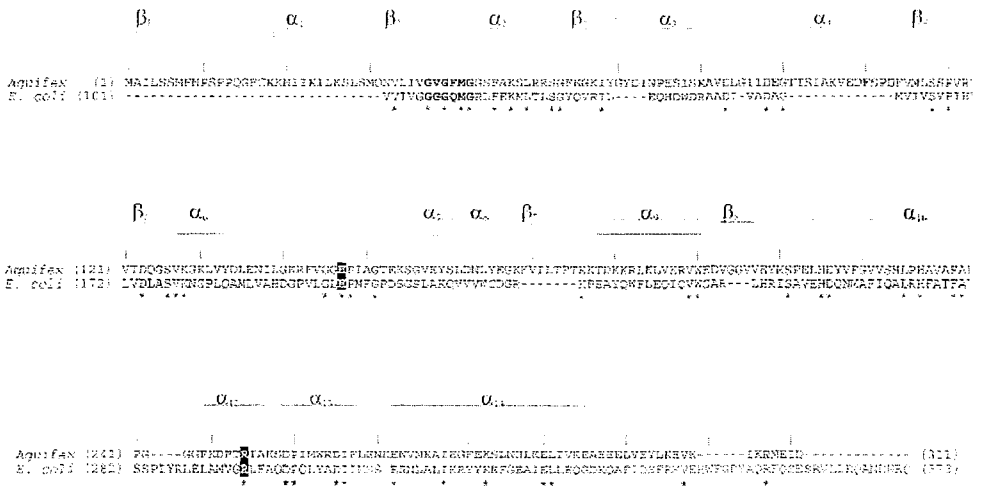

Appendix 3A

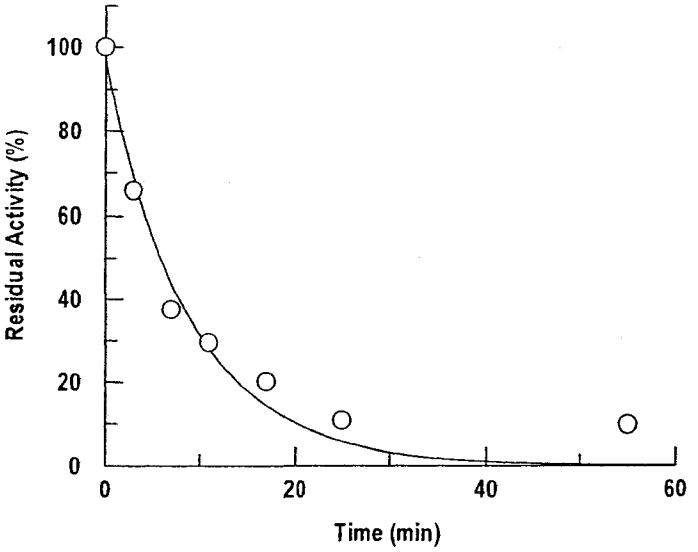

Irreversible thermal inactivation of *E. coli* CM-PD. Enzyme (1 mg/mL in assay buffer) was incubated in capped Eppendorf tubes at 40°C. Samples were removed at different time intervals, cooled on ice, centrifuged for 5 min, and residual activity of the supernatant was determined by the standard assay at 30°C as described section 3.1.5. Data were fitted to a single-exponential decay described by the following equation: $A=A_0 e^{-kt}$, where A is the specific activity at time t, A_0 is the activity at time zero, k is the rate constant and t the time. Half-life, the time it takes for the enzyme to loose 50% of its activity ($t_{1/2}$) was determined by the following equation: $t_{1/2}=0.693/k$. A half-life of 6 min at 40°C was estimated.

Appendix 3B

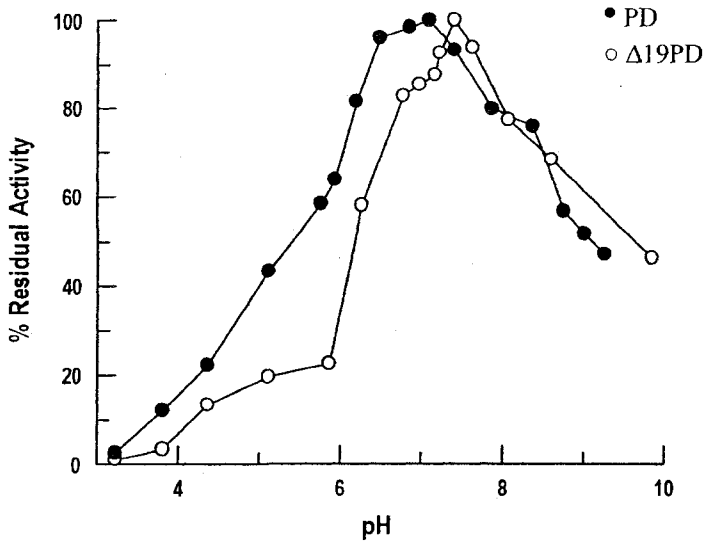

The optimum pH for the PD activity. The pH dependence of the dehydrogenase activity of *A. aeolicus* PD and Δ19PD was monitored between pH 3.2 and 9.8. Assays were performed at 55°C in a 3-component buffer system of 0.05 M 2-morpholinoethanesulfonic acid (MES), 0.05 N-ethylmorpholine, and 0.1 M diethanolamine, (containing 0.15 M NaCl), plus 0.8 mM prephenate and 4 mM NAD^+.

Appendix 3C

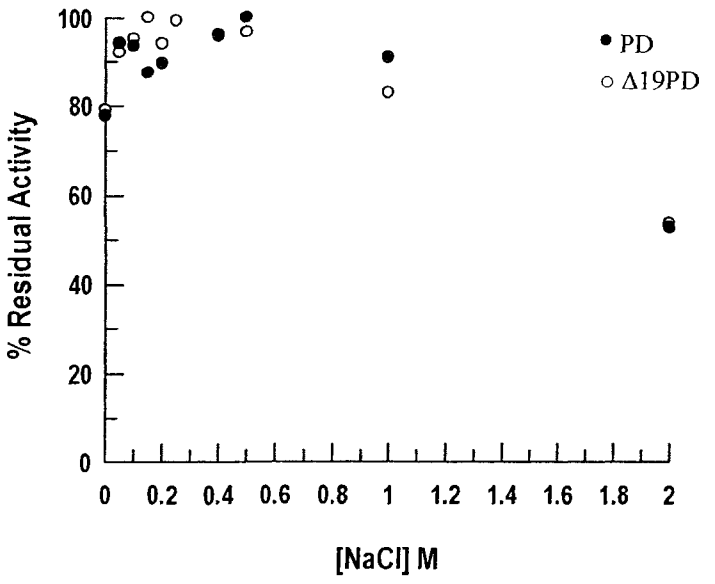

Effect of NaCl on PD and Δ19PD activities. Assays were performed at 55°C in 50 mM HEPES and 0 to 2 M NaCl at pH 7.5. NAD^+ and prephenate concentration were fixed at 4 mM and 0.8 mM, respectively.

Appendix 3D

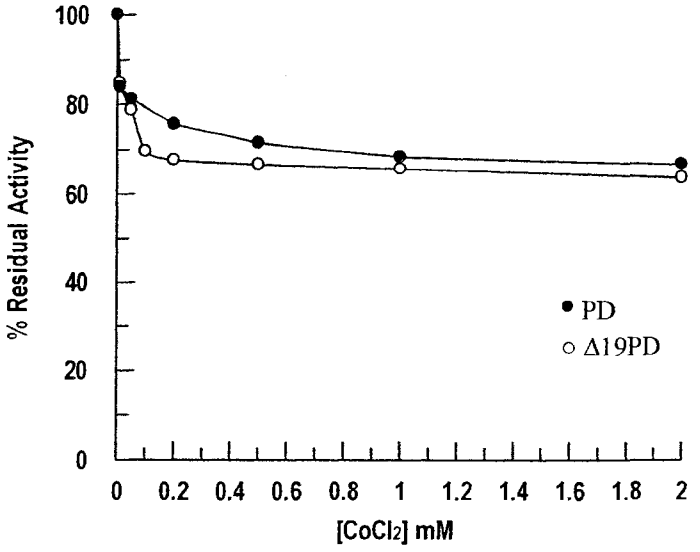

Effect of $CoCl_2$ on PD and Δ19PD activities. Assays were performed at 55°C in 50 mM HEPES and 150 mM NaCl at pH 7.5. NAD^+ and prephenate concentrations were fixed at 2 mM and 0.8 mM, respectively.

Appendix 3E

Variation of initial velocity of *A. aeolicus* Δ19PD reaction as a function of the concentration of prephenate (A) and NAD^+ (B). In **(A)** Prephenate was varied from 72-396 μM at fixed concentrations of NAD^+ of: 57 (▲), 115 and (x) 140 (■) μM. In **(B)** NAD^+ was varied from 54-430 μM at fixed concentrations of prephenate of: 43 (x), 108 (♦) and 216 (▲) μM. The data were fit to the equation describing a sequential kinetic mechanism, $v = VAB/(K_{ia}K_b + K_aB + K_bA + AB)$, to generate the lines shown in the figure. v is the initial velocity, V is the maximum velocity, A and B are concentrations of reactants, Ka and Kb are Michaelis constants for A and B, and Kia is the dissociation constant from the binary complex. The following kinetic parameters when prephenate was the variable, were calculated as 12.1 s^{-1} (V), 146.3 ± 11.5 (K_a), 82.3 ± 7.1 μM (K_b), 137.8 ± 22.1 μM (K_{ia}).

Appendix 3E (continued)

A

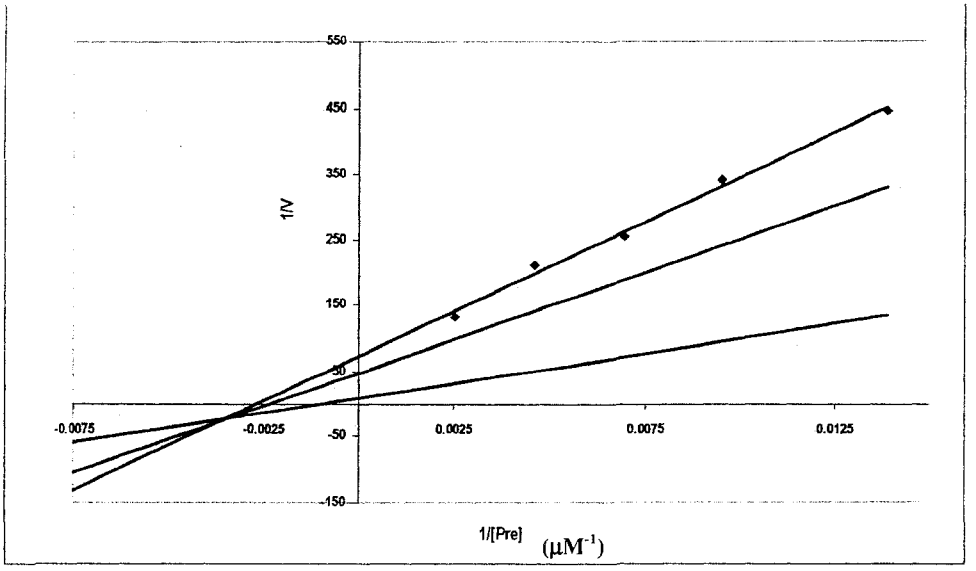

B

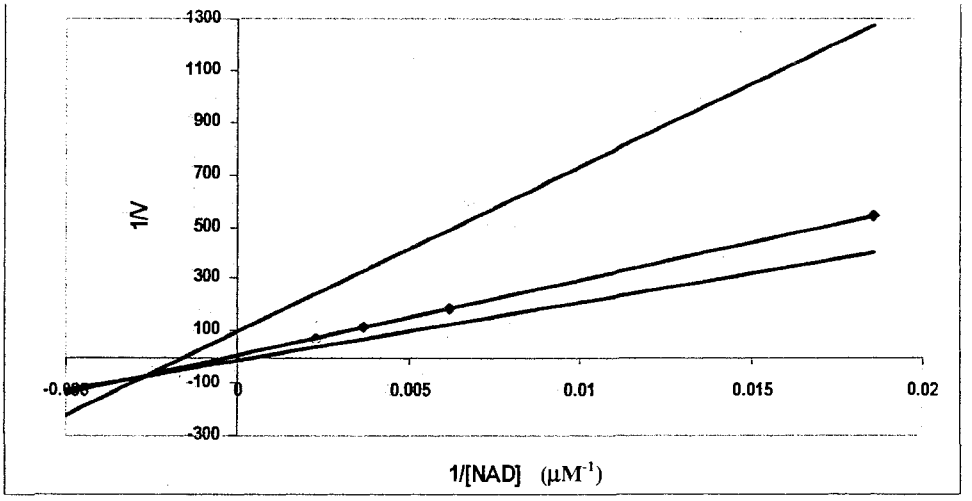

Appendix 3F

		HPP	HPpropionate
Δ19PD	K (μM)	99 ± 10	110 ± 9
	K_{is} (μM)	118 ± 14	485 ± 67

Appendix 4A

Comparison between the architecture of *H. influenzae* and the modeled *E. coli* PD portion of CM-PD. (**A**) Cartoon representation of the monomer of the PD portion of CM-PD from *H. influenzae* in complex with its cosubstrate NAD^+ (blue sticks) and L-Tyr (yellow stick) (PDB access code, 2pv7). The monomer consists of 12 α-helices and β-sheets. The N-terminal domain contains a Rossman fold characteristic of nucleotide binding site. The C-terminal is highly α-helical and participates in the dimerization domain. (**B**) Three-dimensional structure representation of PD domain of *E. coli* CM-PD modeled against *H. influenzae* CM-PD. The loop between β5 and β6 in the model is positioned differently than in the *H. influenzae* PD enzyme, preventing modeling of the dimer. Model and pictures were generated using Modeller 9v3 and PyMOL, respectively.

A

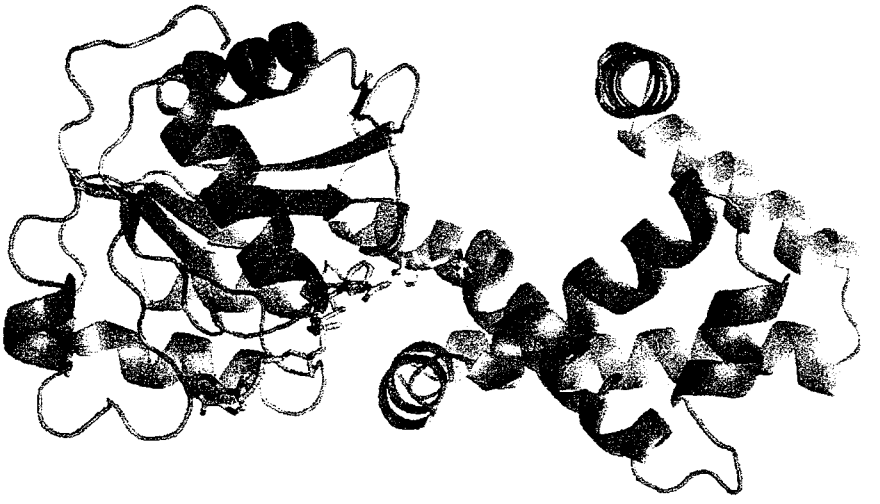

B